MONITORING SOIL WATER AND SNOW WATER EQUIVALENT WITH THE COSMIC-RAY SOIL MOISTURE PROBE AT HETEROGENEOUS SITES

A Thesis Submitted to the College of Graduate Studies and Research

in Partial Fulfillment of the Requirements

for the Degree of Master of Science

in the Department of Soil Science

University of Saskatchewan

Saskatoon

By

Mark James Patrick Sigouin

PERMISSION TO USE

In presenting this thesis in partial fulfillment of the requirements for a Postgraduate degree from the University of Saskatchewan, I agree that the Libraries of this University may make it freely available for inspection. I further agree that permission for copying of this thesis in any manner, in whole or in part, for scholarly purposes may be granted by the professor or professors who supervised my thesis work or, in their absence, by the Head of the Department or the Dean of the College in which my thesis work was done. It is understood that any copying or publication or use of this thesis or parts thereof for financial gain shall not be allowed without my written permission. It is also understood that due recognition shall be given to me and to the University of Saskatchewan in any scholarly use that may be made of any material in my thesis. Requests for permission to copy or make other uses of materials in this thesis in whole or part should be addressed to:

Head of the Department of Soil Science

University of Saskatchewan

51 Campus Drive Saskatoon

Saskatchewan S7N 5A8 Canada

DISCLAIMER

Reference in this thesis to any specific commercial products, process, or service by trade name, trademark, manufacturer, or otherwise, does not constitute or imply its endorsement, recommendation, or favouring by the University of Saskatchewan. The views and opinions of the author expressed herein do not state or reflect those of the University of Saskatchewan, and shall not be used for advertising or product endorsement purposes.

ABSTRACT

Soil water content (SWC) measurements are crucial worldwide for hydrological predictions, agricultural activities, and monitoring the progress of reclamation on disturbed land from industrial activities. In colder climates, snow water equivalent (SWE) measurements are equally important, and directly contribute to improved spring water supply forecasting. Both these variables, SWC and SWE, are commonly measured with either point-scale (e.g. soil cores for SWC and snow tubes for SWE) or large-scale (remote sensing) methods. The cosmic-ray soil moisture probe (CRP) was recently developed to fill this gap between small- and large-scale measurements. The CRP provides an average SWC reading in a landscape-scale measurement footprint (300 m radius) by taking advantage of the relationship between aboveground neutrons and soil water. Although the CRP has proved accurate in relatively homogenous sites, it has not been validated at highly heterogeneous sites. Since snow is simply frozen water, the CRP also has the potential for monitoring SWE at the landscape-scale. However, no calibration has been developed for measuring SWE with the CRP. This thesis aimed to further validate the use of a CRP for measuring SWC at a highly heterogeneous site, and calibrate a CRP for monitoring landscape-scale SWE at an agriculture field. The heterogeneous site used to validate the CRP for SWC measurement was an oil sand reclamation site made up of multiple test plots of varying soil layer treatments. Despite the clear differences in soil texture at the site, the CRP-monitored SWC compared accurately to sampled soil water content and a network of soil moisture probes. With the use of modeling, it was also possible to downscale the CRP measurement to the plot scale. For calibrating the CRP for monitoring SWE, an empirical calibration function was developed based on the relationship between the CRP-measured neutrons and SWE from snow surveys with snow tubes. Using the calibration equation, CRP-estimated SWE closely matched SWE measured from snow surveys. Differences were attributed to mid winter and spring melting of the snowpack along with varying soil water content in the top of the soil profile. This research demonstrates the usefulness of the CRP for monitoring SWC at unique sites and its ability to monitor SWE at the landscape-scale.

ACKNOWLEDGEMENTS

I would like to sincerely thank my supervisor Dr. Bing Si for his support, mentorship, and encouragement throughout my research. My gratitude is also extended to my advisory committee, Drs. Andrew Ireson and Derek Peak, and Marty Yarmuch, for their guidance and valuable input.

This research would not have been possible without funding support from NSERC, COSIA, and the University of Saskatchewan. I am also extremely grateful for the support from the Martin Pedersen and Family Postgraduate, S.N. Horner Postgraduate, John Wickhorst Memorial, and Maurice Hanson Sr. Postgraduate Scholarships, and the John Baerg Research Fund and Scholarship Trust.

A special thanks to:

- The Soil Physics Crew: Eric Neil, Trent Pernitsky, Ivanna Faucher, Min Li, Henry Chau, and Thian Wittayawarkul, as well as Carolyn Murray and Brianna Zoerb, for their much appreciated tireless help with fieldwork. You all made snow surveying in the freezing winter so much more enjoyable.
- Wei Hu, for help with modeling and fieldwork, and the invaluable input in my research.
- Bing Si, for sending me to China to learn so much more than soil science.
- My parents, Margaret and Maurice Sigouin, and sister, Renée Sigouin, for their love and support.
- And my girlfriend Stephanie, for her support and putting up with an at times stressed graduate student.

TABLE OF CONTENTS

LIST OF TABLES

LIST OF FIGURES

LIST OF ABBREVIATIONS

ASCS	Aurora Soil Capping Study
CFoC	Cumulative fraction of neutron counts
COSMIC	Cosmic-ray Soil Moisture Interaction Code
COSMOS	Cosmic-ray Soil Moisture Observing System
CRP	Cosmic-ray soil moisture probe
HLSL	High latitude sea level
hmf	Hydrogen molar fraction
LOS	Lean oil sand
MCNPX	Monte Carlo Neutron-Particle eXtended model
MSC	Meteorological Service of Canada
RCS	Reference Climate Station
SOC	Soil organic carbon
sph	Stems per hectare
SSM	Surface soil material
SWC	Soil water content
SWE	Snow water equivalent
TDT	Time-domain transmission

1. INTRODUCTION

1.1 General Introduction

The need for reliable spatially relevant soil water content (SWC) measurements is becoming increasingly important. SWC is an important variable in terms of (1) climate and weather predictions at both the regional and global scale, (2) agricultural production and management practices, and (3) the overall organization and distribution of biodiversity in natural ecosystems (Vereecken et al., 2008). SWC is also a significant variable with regards to man-made ecosystems such as those created during the reclamation process of surface mining activity (Leatherdale et al., 2012). Point scale (~1 dm^3) and large scale (>10 km^2) measurements have generally been the focus for SWC monitoring, with technologies such as time domain reflectometry (TDR) being a commonly used point scale tool, and new remote sensing tools for large scale monitoring (Robinson et al., 2008). Focusing on small and large-scale data leads to a lack of landscape-scale SWC measurements. This focus on point and large scale measurements leads to issues with the validity of upscaling point scale and downscaling large scale SWC measurements for use in modeling of water balance and surface exchange processes (Robinson et al., 2008; Vereecken et al., 2008).

In cold climates, snow water equivalent (SWE), the amount of water stored in snow, becomes more important than soil water during the winter months. Measurements of SWE are essential for water supply management for agricultural purposes and flood control in areas of seasonal snow cover such as the Canadian Prairies (Jacobson, 2012). The Canadian Prairies receive around one third of their precipitation in the form of snow (Gray and Landine, 1988). While one third may not seem very significant, snow in the Canadian Prairies produces around 80% of the yearly surface runoff making snow vital to the Prairies spring water budget.

Snowmelt water is a critical resource for domestic/livestock water supplies and soil moisture reserves for grain agriculture purposes (Gray and Landine, 1988). Snow is also a key contributor in keeping Prairie wetlands hydrated, which are important for wildlife habitat and have high runoff retention capacities (Fang and Pomeroy, 2009). Similar to the measurement scale issue of SWC, the focus of SWE measurements are either point scale through manual snow surveying with snow tubes (Jacobson, 2012), or large scale via remote sensing with a resolution generally peaking at 12.5 km (Clifford, 2010). The Cosmic-ray soil moisture probe (CRP) (Zreda et al., 2008) has the potential to fill the SWE and soil water measurement gap between the point scale and large scale. The CRP measures the natural aboveground cloud of neutron in a specific energy range, which is inversely related to the amount of hydrogen (i.e. water) in the soil since hydrogen is very efficient at reducing the energy of neutrons. The CRP records neutrons originating from a wide area (~300 m radius) thus it provides a non-invasive landscape-scale areal average SWC reading. The CRP has been shown to provide accurate SWC measurements in many locations (e.g. Zreda et al., 2008; Franz et al., 2012, Bogena et al., 2013), but only in relatively homogeneous study sites. Therefore the need to validate the CRP at very heterogeneous sites still exists. The relationship between aboveground neutrons and hydrogen can also be applied for monitoring SWE. Kodama et al. (1979) showed that it was possible to measure SWE with a cosmic-ray neutron sensing tube buried beneath a snowpack. Desilets et al. (2010) briefly showed the potential of the CRP for monitoring SWE when the probe was placed above the snowpack, but did not provide a calibration function. Thus, there is a need for calibrating and validating the CRP for monitoring landscape-scale SWE.

1.2 Research Objectives

There were two main goals of this research. The first main objective was to evaluate the SWC measurement accuracy of a CRP at a highly heterogeneous site. The specific objectives of the first study were:

- to evaluate CRP accuracy when compared to soil sampled water content and a network of soil moisture probes;
- to evaluate the potential of downscaling or "unweighting" a CRP measurement with the use of modeling.

The second main objective was to assess the potential for using a CRP to monitor SWE at the landscape-scale. The specific objectives of the second study were:

- to develop a calibration equation for monitoring SWE with a CRP;
- to assess the accuracy of monitoring SWE with a CRP compared to snow surveys from snow tube measurements;
- to identify if there is an amount of SWE where the CRP reading becomes saturated.

1.3 Organization of Thesis

This thesis is written in manuscript format with a collection of articles for submission to peer-reviewed journals. Chapter 2, following this introduction, is the Literature Review, which discusses the importance and uses of SWC and SWE measurements along with common methods of measurement. The Literature Review also discusses the theory of the cosmic-ray soil moisture probe, its measurement theory, and present uses. In Chapter 3, which addresses the first main objective, the SWC measurement accuracy of a CRP was evaluated at a very heterogeneous reclamation site in the Alberta oil sands consisting of various soil layer treatments within the CRP measurement footprint.

The second research study, Chapter 4, addresses the second main objective. In Chapter 4, a CRP was calibrated for monitoring SWE over a wide-area (300 m radius) by creating an empirical relationship between CRP-measured neutrons and manually sampled SWE from snow surveys with snow tubes in an agriculture field in Saskatoon, SK. The Summary and Conclusions section, Chapter 5, synthesizes Chapters 3 and 4 and recommends directions for future research. Due to the manuscript format, the thesis does contain some redundant information. In order to limit the redundancy, the references for all chapters were combined into a single list in Chapter 6.

2. LITERATURE REVIEW

2.1 Soil water content and landscape scale measurements

2.1.1 Importance of soil water content measurements

The data provided by soil water content (SWC) measurements has numerous practical applications as well as allows for the improved understanding of many ecological and hydrological processes at various scales. Common methods of measuring SWC such as the gravimetric method from soil sampling or measurement via in-situ probes (e.g. Time Domain Reflectometry) can provide useful information for small or local scales (<1 m^2), but at times larger scale measurements of SWC are wanted. Developments in large scale or landscape scale (>10 m^2) SWC measurement methods have provided the opportunity to better understand the role and effects of soil water on water, energy, and carbon fluxes between the soil and the atmosphere (Ochsner et al., 2013). This improved knowledge of fluxes between land and atmosphere can lead to advances in meteorological forecasts and climate projections. Landscape scale SWC measurements are also vital for assessing and predicting flooding as well as monitoring droughts. Furthermore, ecological modeling can be enhanced with better landscape SWC measurements.

The soil water present in the root zone and near the soil surface can strongly influence the atmospheric boundary layer by controlling energy and moisture fluxes from Earth's surface (Ochsner et al., 2013). Thus, soil water in the root zone and near the soil surface can also influence weather forecasts. If SWC is not adequately constrained or predicated within an atmospheric model, the model will deviate from the actual climate leading to inaccurate weather forecasts as was found by Drusch and Viterbo (2007). Often, however, soil water data

is not directly used in numerical weather predictions and forecasting but rather indirectly constrained by reducing the errors between model predicted humidity and temperature and measured data (Manhouf et al., 2009). This method reduces the forecasting error of the atmospheric boundary layer, but does not produce relevant soil water values (Drusch and Viterbo, 2007; Hess, 2001). Therefore over the long term, the forecast models will become inaccurate based on soil water values that are not realistic. Thus to improve the forecasting accuracy of weather models, remote sensing has been used to collect large-scale soil water measurements of the first 5 cm of the soil (Hoeben and Troch, 2000). However, including actual soil water measurements into a weather model does not always lead to a model improvement (Seuffert et al., 2004), meaning that the physics in the weather models need development. With accurate landscape scale soil water measurements, the flaws in weather models can be exposed.

Improving the accuracy of hydrological models and flood forecasting is another application for landscape scale size soil water measurements. Obvious social and economic benefits can be gained from improving flood predication and mitigating flood damage. Numerous studies have shown that the inclusion of large-scale soil water measurements improve streamflow and discharge predictions (e.g. Pauwels et al., 2001; Aubert et al., 2003; Brocca et al., 2010). The majority of the research and applications of soil water measurements to improving flood forecasting has come from remotely sensing soil water. Other in-situ SWC measurement methods have potential to further improve hydrological modeling and flood forecasting at large scales. Landscape and large scale soil water measurements can also lead to improvements in ecological models. Ecological models (generally predicting vegetation growth) often incorporate an estimate of soil water from the bucket method or water balance

model (Oscher et al., 2013). Ecological model accuracy can be improved by comparing the soil water estimates from ecological models to actual measurements at relevant scales.

An additional important use for landscape and large-scale soil water measurements is the monitoring of droughts. There are multiple classifications of droughts including meteorological (lack of precipitation), agriculture (reduced agriculture production), and hydrological (reduced streamflow for end uses such as hydroelectric power) (Mishra and Singh, 2010) all of which are directly related to soil water. Recent drought indicators based on soil water have been developed (Oscher et al., 2013) and include Plant Available Water and Soil Water Deficit indices. These indicators are often calculated from in-situ soil water measurements and could be expanded with larger scales of soil water measurements. It is still not clear how these relate to the more popular indicators that are based on precipitation such as the Standardized Precipitation Index (Quiring and Papkryiakou, 2003).

2.1.2 Measurement methods for landscape scale soil water content

A few common methods exist for obtaining SWC measurements at a scale larger than point scale, often referred to as field or landscape scale (> 10 m^2 spatial extent). Landscape scale SWC methods include large scale soil moisture networks of point scale measurements, benchmark/representative point sampling, distributed temperature sensing (DTS), and cosmic-ray soil moisture probes. The cosmic-ray soil moisture probe will be discussed thoroughly in a later section since it is the main focus of this thesis.

Taking multiple point measurements within a landscape or catchment is one method of measuring the average SWC at larger scale. Instead of simply taking multiple point measurements by hand throughout a field, a soil moisture network of in-situ probes (e.g. TDR probes) can be installed for more continuous measurements. New development in large-scale

soil moisture networks can be seen in the work of Bogena et al. (2010). They developed a method of utilizing wireless SWC sensors to create a wireless sensor network named SoilNet. SoilNet uses many wireless point measurement sensors that produce a SWC measurement using the well-established capacitance method (Blonquist et al., 2005). SoilNet allows wireless retrieval of SWC data from each probe through the communication of routers placed intermittently throughout the soil moisture network. Large soil moisture network such as SoilNet provide acceptable area average SWC measurements of large scales and allow the variability of SWC to be assessed. However, the installation of large soil moisture networks can be quite invasive and at times not practical. Also, proper contact between the SWC probes and the soil can be an issue.

Another method of estimating the area average SWC in large area from point measurements involves using the concept of time-stability. The idea of a time-stable location in a field, in terms of soil water content, means that the location can consistently represent the area average SWC. Vachaud et al. (1985) first introduced the concept of time stability to SWC measurements. Hu et al. (2010) introduced a simple method of finding a time-stable location in a field to represent the average SWC based on the differences between multiple SWC sampling locations and the measured mean SWC. The method provides the identification of a single sampling point for estimation of the area average SWC and does not involve complex calculations. A clear disadvantage of finding a time-stable location is that need for multiple sets of sampling data over time in order to identify the area representative location.

Distributed Temperature Sensing (DTS) systems were evidently developed for measuring temperature, but researchers have been able to apply their use to measuring soil water over transects. Temperature is measured from a DTS system with the concept of Raman scattering by observing the reaction of light travelling along a fiber-optic cable (Selker et al.,

2006). Measurement points along the fiber-optic cable are determined based on the time required for the light to travel within the cable. Distributed Temperature Sensing systems have been shown to also monitor soil water from empirical equations built from the change in temperature recorded when a pulse of heat is applied to metal sheaths surrounding the cables (Ochsner et al., 2013). A DTS system has the potential to provide attractive spatial resolution (<1 m) for soil water monitoring along transects that are >100 m. However, the method is quite invasive (installation of cable in the soil) and much more research is still needed to improve the soil water monitoring technique.

2.2 Importance of snow measurements

2.2.1 Snow Water Equivalent

Depth, density, and water equivalent are the three most important physical properties of a snowpack (Pomeroy and Gray, 1995). Snow depth at a point scale can be easily measured with the use of a ruler or rod where the measuring device is pushed into the snowpack to the ground and the depth directly observed (Goodison et al., 1981). Snow markers can be used in remote locations with the depth of snow observed from ground locations or via aircraft with binoculars or telescopes. Snow depth can also be measured using sonar (Gubler, 1981; Goodison et al., 1984; Goodison et al., 1988). With the sonar method, an ultrasonic pulse is sent towards the snowpack from a downward facing horn at some known fixed distance above the ground. The time it takes for the echo to be recorded along with the air temperature to determine the relevant speed of sound provides the depth of snow. At larger scales, snow depth can be measured using remote sensing techniques (Dietz et al., 2012).

At point scales, the standard method for measuring the density of a snowpack is the gravimetric method with the aid of snow pit (Pomeroy and Gray, 1995). Snow samples are

collected with scoops of a known volume and weighed to find the density. Many samples are collected vertically in a snow pit to find the average snow density.

Snow water equivalent (SWE) is the equivalent depth of liquid water in a snowpack. SWE is a function of the snow depth and density. SWE is sometimes calculated based on the fact that 1 mm deep of water covering a 1 m^2 area weighs 1 kg, producing the following equation (Pomeroy and Gray, 1995):

$$SWE = 0.01 d_s \cdot \rho_s \tag{2.1}$$

where SWE is in mm, d_s (snow depth) is in cm, and ρ_s (snow density) is in kg m^{-3}. Worldwide, it is the norm by weather and water data collection agencies to express SWE and snow depth in mm and cm, respectively. SWE is also generally calculated based on the density of water (ρ_w):

$$SWE = d_s \cdot \frac{\rho_s}{\rho_w} \tag{2.2}$$

where SWE again is in mm, d_s is in cm, and both ρ_s and ρ_w are in g cm^{-3}. When calculating SWE, the density of water is assumed to be 1 g cm^{-3}. If calculating SWE based on snow depth, the average density of 0.1 g cm^{-3} (100 kg m^{-3}) is often used for fresh snowfall. Thus, SWE is often assumed as 10% of the snow depth (Pomeroy and Gray, 1995). This assumption is often not true because the density of fresh snow is affected by the amount of air within the lattice structure of the snow crystals. The density of freshly fallen snow and a snowpack is greatly dependent on air temperature and wind (McKay and Gray, 1981). Fresh fallen snow can in fact vary in density from 50 to 120 kg m^{-3}, and average density of a snowpack can be greater than 280 kg m^{-3} if subject to harsh wind conditions. Common ways of measuring SWE on a point

scale include snow pits, snow tubes, and snow pillows. At larger scales, snow surveys and remote sensing are used to obtain area average SWE measurements.

2.2.2 Importance of snow in the Canadian prairies and globally

Snow is an important hydrological, ecological, and economical resource in most cold regions around the world. It is estimated that 5% of the precipitation reaching Earth's surface is snow with the percentage increasing in cold dominated regions (Hoinkes, 1967). Snow is crucial as a water supply for a large portion of the world's population. Roughly one-sixth of Earth's population relies on glacier and seasonal snow pack melt for their water supply (Barnett et al., 2005). Snow is specifically important in the Canadian Prairies (central and southern Alberta, Saskatchewan, and Manitoba), where five months of the year the average temperature is below 0˚C (Government of Canada, 2015). One third of the precipitation received on the Canadian Prairies is in the form of snow (Gray and Landine, 1988). While one third may not seem very significant, it produces around 80% of the yearly surface runoff making snow vital to the Prairies spring water budget. Snowmelt water in the Prairies is a critical resource for domestic/livestock water supplies and soil moisture reserves for grain agriculture purposes (Gray and Landine, 1988). With snow being of such an important resource for many areas and a large portion of Earth's population, naturally the collection and analysis of snow data is of equal importance.

2.2.3 Applications of snow data

Snow data is useful for a variety of applications including stream flow and flood modeling/forecasting, water resource planning and management, irrigation and agriculture activities, wildlife management, and building design. One of the most important uses of snow

cover and SWE data is stream flow and flood forecasting. Excess stream flow and flooding from snowmelt runoff can result in damage to property and livelihood causing many areas in the world to adopt flood forecasting systems (De Roo et al., 2003; Government of Canada, 2014). Numerous models are used to predict streamflow and flooding from snowmelt (e.g. Bloschl et al., 2008, Roy et al., 2010; Nester et al., 2012). The streamflow/flood forecast models incorporate a snowmelt process component that is based on snow cover and/or SWE measurements or estimates. Often, estimates of SWE are made from snow cover data obtained from remote sensing (Seidel and Matinec, 2004). Since streamflow and flooding prediction relies on the quality and accuracy of input data, it is key to measure and estimate SWE as best as possible to improve predictions (Nester et al., 2012). Often, the accuracy limitation of streamflow simulations is caused by errors in overestimation or underestimation of SWE (Turcotte et al., 2010).

Snowmelt and streamflow modeling from snow data is applicable to more than simply flood forecasts. Streamflow modeling that incorporates a snowmelt component is also important for the management of many hydroelectric dams to avoid flooding and ensure proper reservoir levels during summer months (Turcotte et al., 2004). In many parts of the world, irrigation water supplies are replenished from the melting of winter snowpacks. Snow survey measurements and observations of snow cover provide streamflow estimates for farmers who rely on irrigation and estimates of irrigation water supplies for the growing season (Steppuhn, 1981). Snow data, specifically depth and SWE measurements are also useful for engineering purposes. The measurement and recording of snow depth and SWE to establish average seasonal values in cities aid with establishing guidelines for snow load requirements for building designs (Boyd et al., 1981).

2.2.4 Snow tubes and snow surveys

One of the most common methods for measuring SWE is the gravimetric method with the use of a snow tube (Goodison et al., 1981). The snow tube, composed of a graduated hollow tube with sharp cutting teeth is used to collect a snow core. The snow core is then weighed or melted to obtain the water equivalent. Snow tube measurements provide a point measurement of SWE. Snow cores can be taken along snow courses (transects established for reoccurring measurements) or in grid patterns to obtain a snow survey of a landscape or field, i.e. a large scale measurement (Dixon and Boon, 2012). Since snow surveys are less destructive to the snowpack, they are generally preferred for measuring spatially distributed SWE in larger areas over snow pit measurements (Church, 1933; Goodison et al., 1987). Snow pits can be used to measure SWE by taking snow samples throughout the profile of a pit (Elder et al., 1998). Snow surveys are also more suited for shallow snowpacks and are less time consuming than snow pit measurements.

In Canada, the commonly used snow tubes types are Standard Federal, Snow Hydro, and Meteorological Service of Canada (MSC). The Standard Federal is the most commonly used sampler in North America and the oldest, first used in the early 1930s (Clyde, 1932; Goodison et al., 1981). It was primarily designed for alpine snowpacks with its relatively small diameter aluminum sampler tube with depth measurement slots. With all of the attachments, it is capable of taking a sample up to 5 m deep. The Standard Federal snow sampler kit is accompanied by a calibrated spring scale that allows for the reading of SWE at the location of sampling (Clyde, 1932). However, the scale is known to be quite inaccurate if in the presence of windy conditions, thus it is better practice to weigh samples indoors on a stationary calibrated balance.

The SnowHydro and MSC snow tubes are shorter and wider sampling tubes than the Standard Federal. The SnowHydro is unique in that it is constructed out of solid clear Lexan (Dixon and Boon, 2012). The clear Lexan design was implemented to avoid the need for observation slots, which are usually found in aluminum snow tubes. The MSC was specifically designed for use in shallow snowpacks in the Canadian prairies and Eastern Canada (Goodison et al., 1981). The MSC tube is constructed of aluminum, has a 16-tooth steel cutter tool, and can measure up to 1.1 m. The MSC tube also has observation slots to observe the snow sample.

Numerous studies have examined the accuracy and error involved with measuring SWE with snow tubes (Dixon and Boon, 2012; Farnes et al., 1982; Goodison, 1978; Sturm et al., 2010; Work et al., 1965). In general, snow tubes have been found to overestimate SWE when compared to snow pit measurements. Work et al. (1965) found that the Standard Federal overestimated SWE by 8.2%. Farnes et al. (1982) assessed both the Standard Federal and MSC and found that both had positive biases of SWE of 10% and 7%, respectively. Sturm et al. (2010) witnessed overestimation of SWE with the Standard Federal by up 11%, but found that the SnowHydro both over and underestimated SWE from -9 to 10% measurement error. Goodison (1978) compared snow tube SWE measurements on small plots where the total weight of snow was known and observed over measurement by the Standard Federal (4.6%) and MSC (6%). In contrast to most studies, Dixon and Boon (2012) observed underestimation by the Standard Federal, MSC, and SnowHydro compared to snow pit measurements in the Canadian Prairies. Dixon and Boon (2012) observed the SnowHydro underestimating SWE the most compared to the Standard Federal and MSC.

Some of the main causes of measurement error for snow tubes include the presence of slots along the tube, cutting tooth design, maintenance, and the inability to hold snow. Over and under estimation of SWE can occur when a snow tube has slots present. The majority of snow

tubes have narrow slots along the tube to allow the measurement of snow depth while taking a snow sample and to allow cleaning tools inside the tube. However, repeated twisting of the snow tube can cause the slots to "shave" very dense snowpacks, allowing excess snow to enter the tube (Goodison et al., 1981). The observation slots can also result in a loss of snow when weighing the snow tube or when transferring the snow sample to a container for post snow survey weighing. Cutting teeth design of the snow sampler can also be a cause of overestimation. Work et al. (1965) tested the Standard Federal in Alaska and did not witness gain or loss of snow from the observation slots on the tube, but did find that the cutting teeth tended to force additional snow into the tube. Lack of maintenance of the cutting teeth is an additional source of overestimation. Sharp cutting teeth provide a clean separation of the snow sample from the snowpack, resulting in lower SWE overestimation. In some cases, sharpening the cutting teeth caused a 50% reduction in overestimation (Beaumont, 1967). Thus, it is important to ensure that the cutting teeth of the snow tube are sharpened before performing any snow survey, especially when performing multiple surveys at the same locations throughout a winter season.

The most common source of error for underestimation of SWE is the loss of snow from the bottom of the tube. Ideally, the operator of the snow tube should aim to retain a plug of soil, vegetation, and/or ice in order to contain the snow core inside the tube when removing it from the snowpack. If a plug is not obtained while taking a snow core, significant loss of snow can occur (Turcan and Loijens, 1975). For the present thesis, the MSC snow tube was used for all of the snow surveys and a flat shovel was placed under the cutter of the MSC snow tube before removing the tube from the snowpack to minimize snow loss if a plug was not retained. The MSC snow tube was chosen over the Standard Federal because the snowpacks to be measured were relatively shallow prairie snowpacks.

Snow tube measurements and snow surveys can compare accurately to SWE measurements from snow pits (Fassnacht et al., 2010). There are, however, a few general disadvantages involved with snow surveys besides the above-mentioned causes of measurement error involved with snow tubes. First, snow surveys are quite labour and time intensive. Performing snow surveys in deep snow can obviously be difficult physically, and cold temperatures can increase the difficulty leading to reduced accuracy of measurements. Snow can freeze to the inside of the snow tube if the air temperature is warmer than the snow temperature (Goodison et al., 1981). This can lead to longer measurement time since the snow must be removed prior to any additional measurements. Also, consistent snow surveys can be challenging or unfeasible in remote locations causing gaps in continuous SWE data throughout seasons.

2.2.5 Snow pillows

Snow pillows are another method for measuring SWE at a point scale (Pomeroy and Gray, 1995). A snow pillow resembles a large octagonal, circular, or rectangular mattress and is filled with an antifreeze fluid. Installed below the snowpack (generally before snowfall), they record the change in weight of accumulated snow above the pillow often by a pressure transducer. The recorded change in accumulated snow weight is then converted to SWE. It can be difficult to fully interpret snow pillow measurements when wet and draining snow accumulates on top of the pillow, as well as when bridging of snow from ice or hard snow occurs. Snow pillows work well monitoring deep snowpacks and can be advantageous for use in remote locations for monitoring SWE since they require little maintenance and provide a continuous measurement. Generally snow pillow SWE readings compare well with snow tube

measurements (Goodison et al., 1981). When snow pillow readings do differ from snow tube readings, snow bridging is often the cause.

2.2.6 Remote sensing measurements of snow

In recent years, remote sensing has become a popular tool for measuring SWE because of its ability to collect measurements at large scales. However, many limitations and disadvantages are involved with remote sensing methods for measuring SWE. The use of passive microwave radiation emitted from Earth is likely the most common remote sensing method used for measuring SWE (Dietz et al., 2012). The basic theory regarding the use of microwave radiation for SWE measurements is well explained by Pomeroy and Gray (1995). Microwave radiation is emitted from Earth's surface and is largely dependent on the surface temperature of Earth. This radiation can be detected from space with the use of passive microwave sensors. Since snow is a porous medium, the radiation emitted from Earth's surface is scattered and attenuated. Essentially, the more snow present above Earth's surface, the less radiation is emitted. Thus, the radiation emitted is related to the mass of snow covering an area (Chang et al., 1987). Dietz et al., (2012) provides a review of the most common passive microwave methods for measuring SWE with four methods being the most commonly used. All four of the popular passive microwave methods have a spatial resolution of 25 km i.e. a pixel size of 625 km^2. This relatively coarse resolution is at times not ideal for use in hydrology modeling (Thirel et al., 2013) and can cause uncertainties from mixed pixel effects (Dietz et al., 2012). The presence of water bodies can also affect the SWE reading (Dong et al., 2005). Also, the SWE reading generally saturates at values greater than 120 mm (Derksen, 2008). Another limitation of passive microwave SWE reading is vegetation cover, which often reduces the

accuracy of the SWE measurements (Dietz et al., 2012). And finally, it is difficult to validate SWE readings from remote sensing since they are measured over such large distances.

2.3 Cosmic-ray soil moisture probe

2.3.1 Cosmic-rays and the creation of fast neutrons

The Cosmic-ray soil moisture probe (CRP) (Figure 2.1) was developed to improve soil moisture measurements at the field scale (Zreda et al., 2008). The CRP uses proportional counters to measure neutrons in the fast to epithermal range, referred to as moderated neutrons (energy >1 MeV), emitted from soil which are inversely related to soil moisture due to the neutron moderating characteristic of hydrogen (Zreda et al., 2008). The production of moderated neutrons begins with primary cosmic rays, either of galactic or solar origin, entering Earth's upper atmosphere (Zreda et al., 2012). These primary cosmic rays interact with nuclei in the atmosphere causing cascades of secondary cosmic rays often in the form of high-energy neutrons with energies in the GeV range. A high-energy neutron can cause the disintegration of nuclei leading to the production of more high-energy neutrons. Alternatively, high-energy neutrons can cause the creation of fast neutrons through a process called "evaporation." If the high-energy neutron does not possess the required energy to disintegrate a nucleus, it can enter and excite the nucleus to an energy level that is unstable. In order to return to a stable energy level, the nucleus releases a fast neutron with the processes being named evaporation. After being released in air, fast neutrons travel in all directions. Fast/epithermal neutrons travel in and between air and soil, and form near instant equilibrium concentrations above and below ground since the velocity of the neutrons is in the range of 10^4 km per second (Zreda et al., 2012).

Figure 2.1. Image of the Cosmic-ray soil moisture probe (CRP) installed in an agriculture field.

2.3.2 Theory of Cosmic-ray probe measurement: how hydrogen affects fast/moderated neutrons

The equilibrium concentration of moderated neutrons above ground is measured by the CRP (neutrons per unit time) and is a factor of the moderation efficiency of the soil. The moderation of fast neutrons is simply the loss of energy from collisions with nuclei, often termed "slowing down" or "stopping." Moderation causes fast neutrons to become moderate neutrons with increased moderation leading to slow (lower energy) neutrons. The elemental chemistry affects the soil's moderating efficiency with hydrogen atoms having a significant effect (Zreda et al., 2012). The stopping power of hydrogen is far greater than other elements commonly found in soil due to the energy decrement per collision, which is the amount of energy lost per collision by the fast neutron. The energy decrement per collision is inversely

proportional to the atomic mass of the nucleus (Bethe et al., 1940). Since Hydrogen has a small atomic mass, it takes fewer collisions with hydrogen molecules to convert a fast neutron into a slow neutron. The high slowing down power of hydrogen causes it to be the dominant moderator of fast neutrons in soil, thus an important factor controlling the concentration of moderated neutrons above soil. The dominant slowing down power of hydrogen and the fact that water is largely made up of hydrogen molecules, allows for the relation of moderated neutrons above soil to the moisture content within soil. The influence of soil water content on the moderated neutron intensity above the soil surface has in fact been known for several decades (Hendrick and Edge, 1966). Only more recently has a method been developed to estimate soil water content from moderated neutron readings.

2.3.3 Methods of estimating soil water content from moderated neutrons

Currently three methods exist to measure soil water content with a CRP. These methods include a site-specific calibration function often called the N_0-method (Desilets et al., 2010), a universal calibration function called the hmf-method (Franz et al., 2013a), and a Cosmic-ray Soil Moisture Interaction Code referred to as COSMIC operator (Shuttleworth et al., 2013). All three of the above methods were initially developed and calibrated with the use of the Monte Carlo Neutron-Particle eXtended model (MCNPX) (Pelowitz, 2005). The MCNPX model allows for the simulation and tracking of neutron particles and is considered to be a state-of-the-art particle transport model. The N_0-method is the simplest method out of the three computationally, and only requires the calibration of one parameter in order to measure soil water content. The N_0-method developed by Desilets et al., (2010) uses the following site-specific calibration function to measure soil water content:

$$\theta_v = \frac{a_0 \times \rho_{bd}}{\left(\frac{N}{N_0}\right) - a_1} - a_2 \times \rho_{bd} \quad (2.3)$$

where θ_v is volumetric soil water content ($cm^3\ cm^{-3}$) , N is the measured moderated neutron intensity (neutron counts per hour), N_0 is the calibrated moderated neutron intensity (neutron counts per hour), and a_0, a_1, and a_2 are unitless fitting parameters. The parameters a_0, a_1, and a_2 are fitting parameters found by Desilets et al., (2010) and are considered to be constant in all soil types and over time. The average bulk density (ρ_{bd}) of the site is needed to obtain volumetric soil moisture content. To calibrate the CRP and find N_0, the average θ_v within the CRP footprint is measured from soil samples (0-30 cm) taken along radials 25, 75, and 200 m away from the CRP.

The hmf-method, developed by Franz et al. (2013a), is deemed a universal calibration function and was created to use when site-specific in-situ calibration soil water content measurements cannot be obtained. The hmf-method is based on an assumed monotonic relationship between the total hydrogen inside the CRP measurement footprint and the moderated neutron flux. The amount of hydrogen inside the CRP footprint is calculated from summing the hydrogen moles from pore water, lattice water, soil organic matter, and vegetation based on a small amount of soil samples or estimates. The total hydrogen moles is then divided by the sum of all moles of all elements in the CRP footprint including air, dry above ground biomass, water, and dry soil to obtain the hydrogen molar fraction (hmf). The total air and soil elements considered are nitrogen, oxygen, silicate, hydrogen, and carbon to simplify the process. The measured/estimated hydrogen molar fraction is then used with the measured moderated neutron flux to calibrate the CRP using the following equation:

$$\frac{N}{N_s} = 4.486\exp(-48.1\times hmf) + 4.195\exp(-6.181\times hmf) \quad (2.4)$$

where N_s is a time-constant and site-specific calibration parameter. Once N_s is found from calibration with the measured hydrogen molar fraction, the soil water content can be estimated from subsequently calculated hmf values.

The Cosmic-ray Soil Moisture Interaction Code (COSMIC) is a model developed by Shuttleworth et al. (2013) to simplify the interactions of cosmic-rays with the soil surfaces to use in data assimilation. Three main processes are represented in the COSMIC model and include: 1) the exponential decrease of high energy neutrons with soil depth, 2) the creation of fast neutrons from high energy neutrons as a function of soil depth, and 3) the scattering of the created fast neutrons as they reach the soil surface. Three of the model parameters were found to be constant for all locations when calibrated by Shuttleworth et al. (2013) with the MCNPX code. Two parameters require a measurement of bulk density from 0-30 cm. Also the calibration parameter N_{COSMIC}, which is site-specific and time-constant, needs to be optimized using the measured moderated neutron flux.

Each method has its advantages and disadvantages. The N_0-method is quite straightforward and involves simple calculations, but it requires relatively intense sampling campaigns for calibration. The hmf-method does not require large sampling campaigns, however, it still requires site-specific parameters such as bulk density, lattice water, and aboveground biomass to be either measured or estimated from maps. The COSMIC model again does not need extensive sampling campaigns, but still requires a few site-specific measured parameters. Also the COSMIC model is relatively more complex than the N_0- and hmf-method in terms of calculations. Baatz et al. (2014) compared the performance of all three methods for estimating soil water content. They found that all three methods performed relatively similar

with all three producing estimates of water content within the acceptable error range. It was found that the hmf-method and the COSMIC model performed the most similar to each other. For this thesis, we used the N_0-method for calibrating and estimating soil water content with the CRP because it is the most commonly used method and allows for the collection of numerous soil samples for lattice water and soil organic carbon analysis, which are both, useful for estimating the vertical measurement footprint of the CRP.

2.3.4 Horizontal measurement footprint

Probably the most attractive attribute of measuring soil water content with a CRP is the landscape scale measurement footprint provided by the CRP. The CRP delivers a circular average soil water content reading with a measurement radius generally agreed upon of ~300-330 m (~35 ha) at sea level (Zreda et al., 2008). Thus, the CRP aids in filling the measurement gap between small and large scale soil moisture instruments. This measurement footprint was first explained by Desilets and Zreda (2013) and found from the use of the MCNPX code. The horizontal measurement footprint is defined as the area where 86% (two e-folding lengths or $[1 - e^{-2}]$) of the measured neutrons originate, with more neutrons originating closer to the CRP than further away. Soil water content is not believed to significantly affect the size of horizontal footprint, however, atmospheric density and humidity do have slight affects (Desilets and Zreda, 2013). The horizontal footprint increases with decreasing atmospheric density. This is because as the atmospheric density decreases, fewer nuclei are present for collision, thus fast neutrons have an increased probability of travelling further before becoming slow neutrons. Small changes in atmospheric density do not result in significant differences, but an overall increase in horizontal footprint of roughly 25% occurs from sea level to 3000 m altitude since air density is related to altitude (Zreda et al., 2012). Humidity also affects the horizontal

footprint similar to the effect of air density. The horizontal footprint is expected to decrease around 10% from dry air to saturated air (Zreda et al., 2012). Since water vapor (hydrogen molecules) directly affects the collision path of fast neutrons, the horizontal footprint decreases as the partial pressure of water vapor increases.

Recently, new ideas on the size of the horizontal footprint of the CRP have been proposed. Köhli et al. (2015) developed a new model to only model the transport of neutrons in order to better understand their origins and subsequent measurement by a CRP. Their model results showed that only a small amount of neutrons contributed to the CRP reading from further than 200 m away, and around 50% of neutrons originated from within 50 m of the CRP. These model results contrast those by Zreda et al. (2008) and Desilets and Zreda (2013) who observed that 50% of neutrons originated from within roughly 150 m of the CRP. Köhli et al. (2015) propose that the footprint radius is 240 m for a completely bare soil with no soil water, but can be as small as 130 m if soil water is high and large amounts of vegetation is present. The proposed CRP footprint sizes by Köhli et al. (2015) have only been modeled and have not yet been independently validated in the field. All of the published field studies validating the performance of the CRP have assumed a horizontal footprint of ~300 m and have obtained satisfying results. Thus, we still assumed a horizontal footprint of 300 m in this study when comparing to other measurements sources of soil water content, but kept in mind that discrepancies between soil water content from the CRP and other sources could be due to the horizontal footprint size.

2.3.5 Vertical measurement footprint

The vertical depth of measurement is considerably affected by soil water content, unlike what is generally considered for the horizontal footprint. Again, the effective measurement

depth of the CRP is the depth of soil from where 86% ($1 - e^{-2}$) of the measured neutrons originate. Also, the amount of neutrons originating from the soil decreases with increasing soil depth. Modeling of a pure quartz (SiO_2) soil by Franz et al. (2012a) using MCNPX code provides an estimate of the maximum and minimum measurement depths to be ~70 cm and ~12 cm. The maximum depth of ~70 cm occurs in dry soils with no water. The minimum depth of ~12 cm occurs in saturated soils (assuming saturation at 0.40 $m^3\ m^{-3}$). The decrease in measurement depth as water content increases is non linear and is also affected by soil bulk density and the water bound in organic matter and mineral or lattice water (Zreda et al., 2012). Franz et al. (2012a) also found that the depth of surface water from which 86% of the measured neutrons originate is 5.8 cm. This depth of surface water is likely related to the effective depth of measurement for snow cover and SWE. Franz et al. (2012a) defined the relationship for finding the effective CRP sensor depth (z*) based on water content, bulk density, and lattice water to be:

$$z^*(cm) = \frac{5.8}{\rho_{bd}(\tau + SOC) + \theta + 0.0829} \tag{2.5}$$

where τ and SOC are the weight fractions of lattice water and soil organic carbon, respectively, in soil. This equation assumes that bulk density, soil water content, lattice water, and soil organic carbon are uniformly distributed within the soil profile.

2.3.6 Current CRP applications and developments

Currently, CRPs are being used globally as can be seen from the COsmic-ray Soil Moisture Observing System (COSMOS) (Zreda et al., 2012). According to the COSMOS web app (http://cosmos.hwr.arizona.edu/), there are CRPs mainly installed at various locations in the

United Sates, with a few probes also installed in Europe, southern Africa, Brazil, and Australia. Initial validation studies have shown that the CRP can produce fairly reliable average soil water content measurements at the 300 m radius scale (Zreda et al., 2008; Desilets et al., 2010; Franz et al., 2012b; Coopersmith et al., 2014; Zhu et al., 2015). These studies all examined the performance of a CRP permanently installed at one location at a fairly homogeneous site in terms of soil and vegetation. One study (Bogena et al., 2013) validated a stationary CRP at a forested site with some heterogeneity in the soils, but year-to-year vegetation seemed consistent since the site was mature forest.

Chrisman and Zreda (2013) assessed the performance of a moving CRP installed on a truck rather than being installed stationary on the ground. The CRP installed on the truck, named the cosmic-ray rover, was tested in Tucson Basin, Arizona, and produce soil water content maps for a 25 km x 40 km survey area. Although there appeared to be potential for using the cosmic-ray rover for creating soil water content maps, the length of neutron count time used caused large variations in soil water content measurement of the CRP. The common neutron count time when using a CRP is one hour, but for the cosmic-ray rover the measurement time was shortened to 1-7 minutes.

Other applications of the CRP, beyond measuring average soil water content at a landscape scale, include attempting to measure snow water equivalent (Desilets et al., 2010) and aboveground biomass (Franz et al., 2013b). Desilets et al. (2010) briefly examined the use of a CRP to measure snow water equivalent at a landscape scale showing that there is potential for accurate estimates with further investigation. Franz et al. (2013b) attempted to use a CRP to estimate the aboveground biomass in a forest site and a maize field. The estimates of biomass were acceptable in the forest site compared to manual measurements, but in the maize field the below ground root biomass caused poor estimates of aboveground biomass.

3. MONITORING SOIL WATER CONTENT AT A HETEROGENEOUS OIL SAND RECLAMATION SITE USING A COSMIC-RAY SOIL MOISTURE PROBE

3.1 Preface

Many applications, such as weather prediction and irrigation agriculture, benefit from landscape-scale measurements of soil water content (SWC). Wide-area SWC measurements are also useful for monitoring the progress of reclaiming land disturbed by industrial activities such as oil sand mining. Soil water is a crucial variable that affects what type of ecosystem re-vegetates reclaimed land in the oil sand region of Northern Alberta, CAN. Therefore, an accurate method for measuring SWC at the landscape-scale is required. The cosmic-ray soil moisture probe (CRP) has shown to provide accurate wide-area measurements (300 m radius) of SWC from the inverse relationship between aboveground neutrons and soil water at relatively homogeneous sites. The purpose of this study was to assess the accuracy of the CRP at a very heterogeneous oil sand reclamation site in the Alberta oil sands by comparing to soil sampled water content and a network of soil moisture probes. The reclamation site was composed of various test plots of differing soil layer treatments within the measurement footprint of the CRP. Another goal of this study was to downscale or "unweight" the CRP measurement to the plot scale. This downscaling was accomplished by modeling SWC at the study site.

3.2 Abstract

Soil water content (SWC) measurements are important for numerous applications including climate and weather prediction, agriculture and irrigation activities, and monitoring the progress of reclamation on land disturbed by mining or other industrial activities. We

assessed the SWC measurement accuracy of a cosmic-ray soil moisture probe (CRP) and explored the possibility of downscaling the CRP measurement to the plot scale. The experiments were conducted at a highly heterogeneous reclamation site in the Alberta Oil Sands near Fort McMurray, Alberta, Canada. The study site is unique because it consists of 36 one hectare plots composed of 12 different reclamation covers made up of various layering schemes of peat and coarse-textured soil. The one-hectare plots also contain different vegetation (species and density). A CRP was installed in the center of the reclamation study site and calibrated using soil core samples. CRP-measured SWC was compared to weighted average SWC measured from soil cores and a network of soil moisture probes within the CRP footprint over two summers. The CRP responded clearly to precipitation events with peaks in the measured SWC and the CRP estimates of SWC were very close to SWC estimated with soil cores and in-situ soil moisture probes with a RMSE of 0.031 $cm^3\ cm^{-3}$ and 0.024 $cm^3\ cm^{-3}$, respectively, over the two summers. We also attempted to downscale the CRP measurements from the 2014 season to the plot scale using HYDRUS-1D modeling and the known soil texture in order to unweight the CRP-measured SWC. The modeled SWC (optimized with the CRP measurements) within the CRP footprint was relatively close to the CRP-measured SWC with a RMSE of 0.039 $cm^3\ cm^{-3}$. Overall, the CRP provided accurate average SWC measurements at the reclamation site despite the soil and vegetation heterogeneity.

3.3 Introduction

Soil water content (SWC) is required for a better understanding of and predicting hydrological processes below and above the soil surface (Vereecken et al., 2008). It also affects the magnitude of energy transfer and water infiltration at the soil surface - thus it is crucial for predicting climate and weather at local and global scales (Ochsner et al., 2013). SWC

measurements are also important for agricultural production and irrigation management, where accurate knowledge of water content can have economic benefits by limiting over-use of water (Fares and Alva, 2000). In addition, SWC affects land and ecosystem restoration success, especially in water-limited environments (Alberta Environment, 2010).

Methods of measuring SWC at small scales (cm^2) with various *in situ* probes and large scales (km^2) with remote sensing are common and generally reliable (Robinson et al., 2008). Until recently, there remained a measurement scale gap for SWC between point and large scale measurements. The Cosmic-ray soil moisture probe (CRP) was developed in recent years to address the lack of field or landscape scale SWC measurement tools (Zreda et al., 2008). The CRP has been an instrument of great interest because it provides an estimate of average SWC within a ~300 m radius of the instrument. It does not measure SWC directly, but rather measures neutrons above ground. These neutrons, referred to as moderated neutrons in this study, are in the fast to epithermal range and have energies generally <1 MeV (Hess et al., 1961). The neutrons are formed from primary and secondary cosmic rays entering Earth's atmosphere. Moderated neutrons travel at high velocities, and when they collide with other particles or matter, they lose energy (Zreda et al., 2012). Collisions with hydrogen atoms cause the greatest velocity decreases for moderated neutrons compared to all other collisions. This means that fewer collisions with hydrogen molecules are needed to greatly reduce the energy of moderated neutrons compared to other atoms. Thus, hydrogen in water near the soil surface is one of the main controls over the amount of moderated neutrons above the soil surface.

There are a few advantages associated with the CRP (Desilets et al., 2010). The CRP is non-invasive, passive, and not sensitive to differences in soil texture. CRPs can be easily transported and installed in remote locations and data can be remotely obtained from a CRP via satellite telemetry. The CRP provides a time-continuous measurement of SWC and can

operate year-round with little maintenance. Most importantly, the CRP has a landscape scale measurement footprint. The CRP also shows promise for the use of monitoring snow water equivalent (SWE) at a similar landscape scale (Desilets et al., 2010; Sigouin and Si, unpublished).

CRPs are quite widely used globally as can be seen from the COsmic-ray Soil Moisture Observing System (COSMOS) probe map (cosmos.hwr.arizona.edu). There also have been a handful of studies validating the method at various sites in the USA and Europe. However, these studies generally involved using the CRP at relatively homogeneous study sites. Desilets et al. (2010) studied the use of a CRP in Arizona, USA at Mt. Lemmon Cosmic Ray Laboratory and Lewis Springs. Franz et al. (2012b) applied the CRP at a desert site in Tucson, AZ, USA. Again, this site appeared quite homogenous. Bogena et al. (2013) examined the use of a CRP in a humid forest in Germany. Their site did show clear heterogeneity in terms of soil types, but was mainly dominated by older Norway spruce (*Picea abis L.*, planted in 1946) which covered 90% of the studied catchment. The main objective of this study is to assess the performance of a CRP for estimating SWC at a study site that possesses strong heterogeneity in soil and some variation in vegetation within the CRP footprint. The study site is a mining reclamation site consisting of various test plots composed of different soil layer and tree planting treatments. An additional objective is to explore the possibility of downscaling the CRP measurements to the plot scale.

3.4 Materials and methods

3.4.1 Study site description

The study site for this research was the Aurora Soil Capping Study (ASCS) site (57.3346 °N, -111.5351 °W) situated at Syncrude Canada Ltd.'s Aurora North mine. The Aurora North

mine is one of several oil sand mining operations located north of Fort McMurray, AB, Canada. The ASCS site is a large experimental reclamation site composed of 36 one-hectare plots of varying soil layer and tree planting treatments (Figure 3.1). It is located on an out-of-pit overburden disposal area that is composed of lean oil sand (LOS) material removed during mining to expose the oil sand ore body. LOS generally ranges from loamy sand to sandy loam and contains an oil content less than 7%. The soil reclamation treatments of the study are surface soil materials salvaged during mining within the disturbance footprint. The surface soil (topsoil) materials of the study include peat and surface salvage material (SSM). Subsoil materials of the study include a variety of coarse-textured (loamy sand to sand) materials, including Bm horizons salvaged from approximately 0.15 to 0.5 m below the pre-disturbance surface, B/C horizon salvaged from approximately 0.5 to 1.0 m, and a deep subsoil salvage from approximately 0.15 m to 2.5 m. The peat is high in organic matter content and was salvaged from bogs and fens in the mine footprint. The SSM is forest floor material and the underlying coarse textured surface A horizon material to approximately 0.15 m. Beyond the southern and northern borders of the ASCS, but within the CRP footprint, the area consists of lean oil sand overburden awaiting soil reclamation placement. Twelve soil layer treatments are triplicated in a completely randomized design at the ASCS site providing a total of 36 plots. Figure 3.2 shows the 12 different layer profiles at the ASCS site. The sampling footprint of the CRP included all of 15 plots and a portion of an additional 10 plots with at least one of each of the 12 profile treatments.

In May 2012 each plot was planted with a mix of aspen (*Populus tremuloides*), jackpine (*Pinus banksiana*), white spruce (*Picea glauca*) at approximately 1,800 stems per hectare (sph). For other research purposes 25 x 25 m sub-plots have also been constructed, consisting of the individual tree species above and a mix tree species plot. The planted density of the sub-plots

is 2,000 or 10,000 sph. This results in each one-hectare treatment plot containing at least four tree sub-plots with a density of 10,000 sph, with some four additional sub-plots with a density of 2,000 sph. Understory species including green alder (*Alnus crispa*), pin cherry (*Prunus pensylvanica*), and saskatoon (*Amelanchier alnifolia*) were planted within the plots, but outside the sub-plots, at a total density of approximately 575 sph. Additional volunteer species from the soil seedbank have emerged, consisting of native herbaceous species such as fireweed (*Chamerion angustifolium*), pin cherry and blueberry (*Vaccinium Spp.*) and weed species such as Russian thistle (*Salsola kali*).

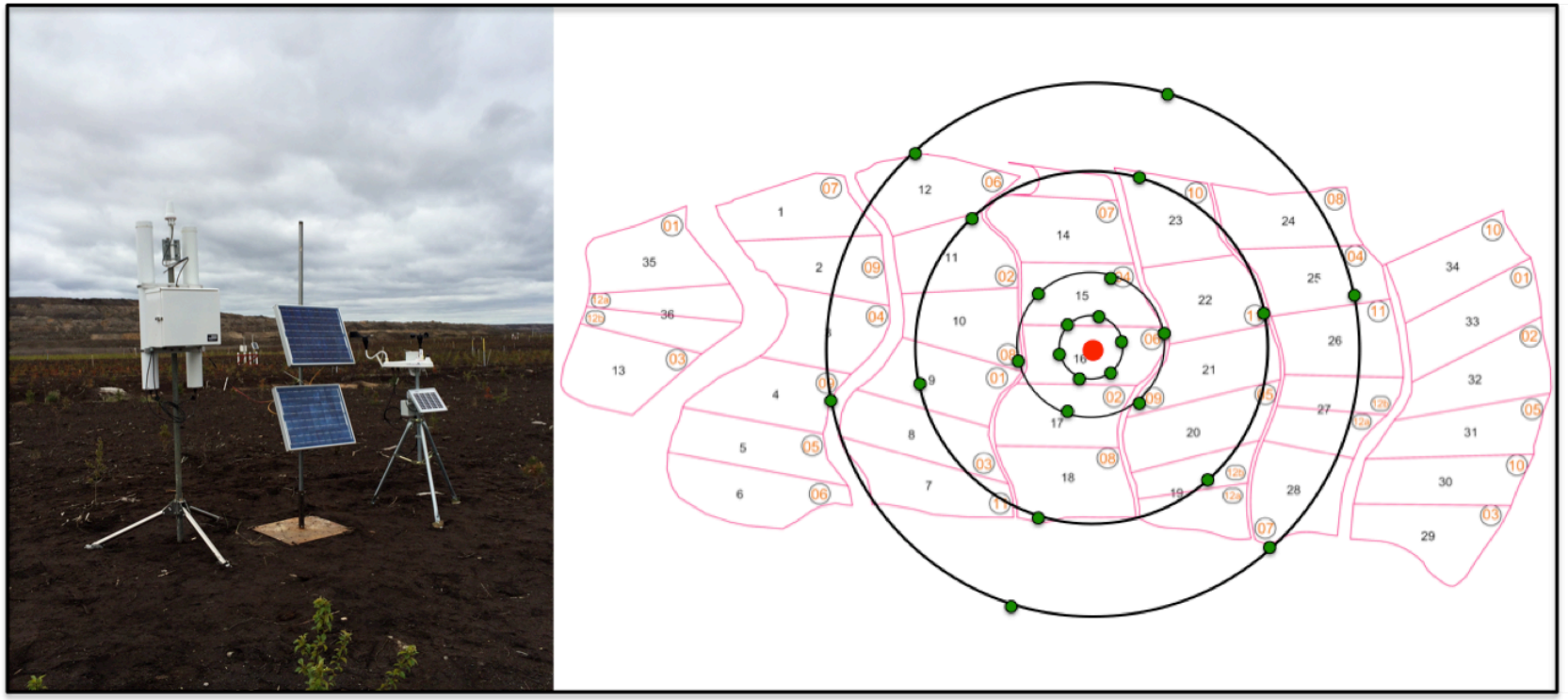

Figure 3.1. Image of CRP and weather station installed at the ASCS site (left) and an areal view of the location of the CRP (red dot) at the study site (right). The black circles around the CRP location represent the 25, 75, 200, and 300 m radials used for soil sampling and calibration. The green dots represent the soil sampling locations. The red polygons in the image on the right represent the one-hectare soil cover plots with the red numbers representing which layer treatment was used in the plot.

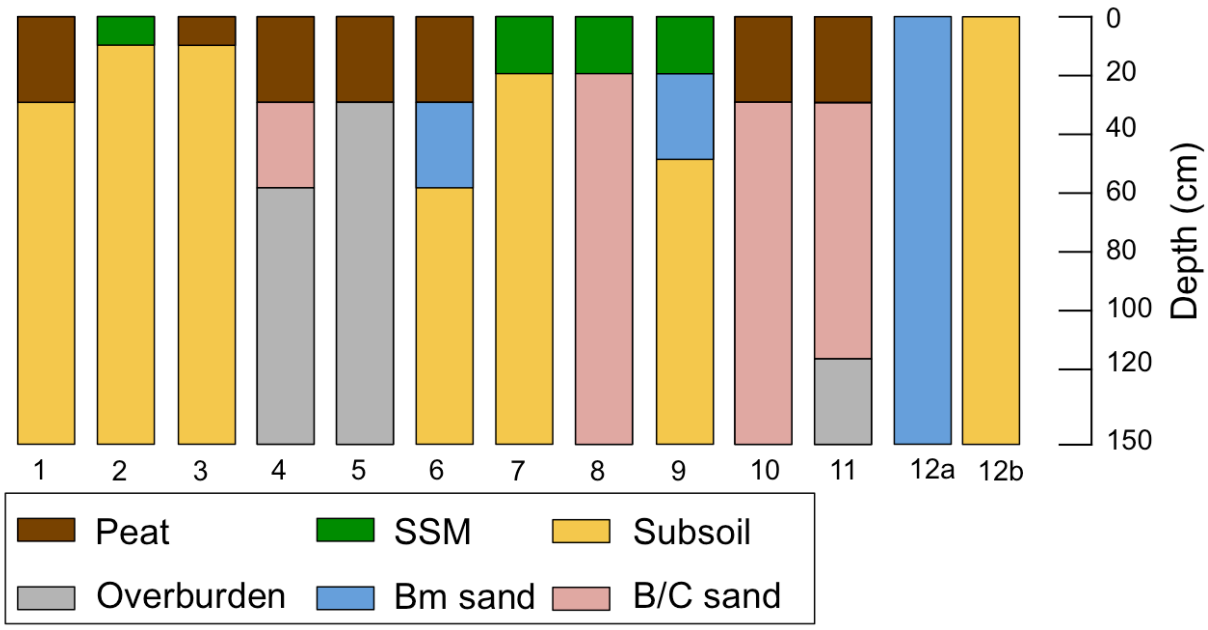

Figure 3.2. Layer treatments of the 12 soil covers at the ASCS site.

3.4.2 CRP and moderated neutron intensity correction

The CRP utilized in this study was a CRS-1000/B (Hydroinnova, NM, USA). This CRP is comprised of two neutron counter tubes and a component box that stores an iridium modem data logger (remote data access) and a 12V battery capable of solar recharging needed to create an electrical potential inside the counter tubes. The neutron counter tubes are filled with a gas that has significant neutron-slowing properties that releases electrons following collisions with neutrons that have entered the tubes. The data logger records the electrical pulse created by the electrons and the strength of this pulse is proportional to the number of

neutrons that have entered the tube. The CRP has both a slow neutron (lower energy) counter tube and a moderated neutron counter tube. The moderated neutron counter tube measures the moderated neutron intensity during a specific time interval, which is used for calculating SWC.

The CRP was installed in the center of the ASCS site, near the center of plot 16, at the beginning of summer in 2014 and 2015. The CRP collected moderated neutron intensity (neutron counts per hour) from the end of May to the end of October in 2014, and from the beginning of June to the end of October in 2015. Moderated neutron intensity above the soil surface is affected by atmospheric pressure, air humidity, and the time-varying incoming cosmic ray flux. Thus, the raw moderated neutron intensity values must be corrected for these three variables before estimating SWC from the moderated neutron counts. Correcting the moderated neutron intensity values is accomplished by multiplying the raw moderated neutron counts by a final correction factor composed of correction factors for atmospheric pressure, air humidity, and temporal variation of incoming cosmic ray flux. The final correction factor (F_{final}) has the following equation (Zreda et al., 2012):

$$F_{final} = F_p \cdot F_w \cdot F_i \tag{3.1}$$

where F_p, F_w, and F_i are the correction factors for air pressure, humidity, and variations of incoming cosmic ray flux, respectively. F_p is calculated using the following equation:

$$F_p = e^{(\frac{P-P_{ref}}{L})} \tag{3.2}$$

where P and P_{ref}, both in hPa, are air pressure at the CRP location during the time of neutron intensity measurement and reference air pressure. L is the mass attenuation length and is a function of the average air pressure, atmospheric depth, and effective vertical cutoff rigidity (Desilets and Zreda, 2003). For the ASCS site, L is 129.73. The CRP records air pressure readings with every neutron count, but additional air pressure measurements were obtained from a WeatherHawk Weather Station (WeatherHawk, UT, USA) installed at the study site. The reference air pressure can be either the average air pressure at sea level, or the average air pressure at the site where the CRP is located (Zreda et al., 2012). We chose to use the average air pressure at the ASCS site for the air pressure correction (972 hPa).

F_w, the air humidity or water vapor correction factor is estimated with the following equation (Rosolem et al., 2013):

$$F_w = 1 + 0.0054 \cdot (p_v - p_{vRef}) \tag{3.3}$$

where p_v (g m^{-3}) is the absolute humidity at the time of moderated neutron measurement, and p_{vRef} is the reference absolute humidity chosen to be the value at the time of CRP calibration. The WeatherHawk was used to measure relative humidity and air temperature for calculating absolute humidity (see Appendix C for absolute humidity calculation).

Since the incoming cosmic ray flux varies with time, a correction must be applied to the moderated neutron data in order to compare CRP readings. The temporal variation of cosmic ray flux is found with data from neutron monitors and the following equation:

$$F_i = \frac{I_{avg}}{I_{nm}} \tag{3.4}$$

where I_{avg} is the average neutron count over the study period and I_{nm} is the neutron count for the time of measurement. The neutron monitor at Fort Smith (60.02 ˚N, -111.93 ˚W), NWT, Canada, was chosen for the correction because it is the closest monitor to the ASCS site. Neutron monitor data is freely available from the Neutron Monitor Database (NMDB) online.

Once all of the individual correction factors are calculated, the raw moderated neutron intensity can be corrected with the following formula:

$$N_{Cor} = N_{Raw} \cdot F_{final} \tag{3.5}$$

where N_{Cor} and N_{Raw} are the corrected and raw moderated neutron intensity (Neutron counts h^{-1}) values, respectively.

3.4.3 CRP calibration soil sampling and CRP water content measuring

On-site calibration of the CRP was performed following installation at the study site in 2014. Six locations were sampled with equal arc lengths along each of the four radials 25, 75, 200, and 300 m away from the CRP (Franz et al., 2012b). At each sampling location, soil cores in 0.05 m increments were collected to a depth of 0.3 m using a manual coring device with a diameter of 0.045 m, and subsequently stored in airtight bags and refrigerated until analysis. Gravimetric water content (θ_g) of each sample was determined by the oven-dry method and was converted to volumetric water content (θ_v) from the bulk density of the soil cores. The average θ_v of the calibration samples taken at the end of May 2014 was quite high (0.39 cm^3 cm^{-3}). Zreda et al. (2008) indicated that the measurement depth of the CRP at that water content was only ~12 cm in pure silica sand. Therefore, only the average θ_v estimates from 0 –

15 cm depth were used to calibrate the CRP in summer, 2014. The following CRP calibration equation from Desilets et al. (2010) was used:

$$\theta_v = \frac{a_0 \times \rho_{bd}}{\left(\frac{N}{N_0}\right) - a_1} - (a_2 \times \rho_{bd}) \quad (3.6)$$

where N is the corrected moderated neutron intensity (Neutron counts h^{-1}), N_0 is the calibrated moderated neutron intensity value (Neutron counts h^{-1}), and ρ_{bd} (g cm^{-3}) is bulk density. a_0, a_1, and a_2 are fitting parameters with values of 0.0808, 0.372, and 0.115, respectively. Since θ_v is known from the soil cores, simple rearranging of Eq. 3.6 can allow N_0 to be solved. Once N_0 is obtained, Eq. 3.6 is used for estimating SWC from CRP moderated neutron intensity readings. Soil sampling campaigns were performed with the same coring device four additional times (July 3, 2014; August 26, 2014; September 30, 2014; October 21, 2014) after calibration in 2014 at the same 24 locations as the initial calibration. The locations of the sampling points were kept consistent with the use of a GPS. In 2015, four sampling campaigns (June 4, 2015; July 17, 2015; August 10, 2015; October 2015) were executed at the same 24 sampling locations for CRP comparison.

3.4.4 CS616 sensor network

The CRP estimated SWC was also compared to the soil moisture network at the ASCS site. CS616 Water content Reflectometers (Campbell Scientific Inc., Edmonton, AB) were installed in each plot at the time of construction of the site. The CS616 probes measure volumetric water content and operate similar to Time Domain Reflectometry (TDR) probes using the sensitivity of soil dielectric permittivity to soil water content (Campbell Scientific Inc.,

2015). Multiple CS616 probes were placed within the soil profile at multiple depths (5 to >200 cm) at one location in each plot, with probes near the soil surface at 5, 15, and 25 cm. Each probe was connected to a data logger and volumetric ($cm^3\ cm^{-3}$) SWC was measured every 3 hours. A different calibration curve was used for the probes in each separate cover soil material. To obtain the calibration curves, probes were placed in the different cover materials prepared to known water contents and bulk densities. A minimum of four known water contents was used for each material type covering a range from below permanent wilting point to above field capacity. The sensor response from the CS616 probes for each water content was recorded and calibration curves for each cover soil were developed. The CS616 probes in 23 of the 25 plots inside the CRP footprint were used for comparison. The probes in plots 1 and 4 were not included because only small portions of these plots were in the CRP footprint. The cluster of CS616 probes in the soil profile were installed at different locations from plot to plot. Because the CS616 probes were not evenly placed in the ASCS site and thus not evenly placed around the installed CRP, horizontal weighting (see Sec. 3.4.6) was needed for comparing the CS616 measured SWC to the CRP estimated SWC.

3.4.5 Estimation of CRP measurement depth

While the horizontal measurement footprint of the CRP does not vary significantly in size with changing environmental conditions (Desilets and Zreda, 2013), the measurement depth is affected greatly by varying SWC. To estimate the depth of measurement of the CRP, the equation given by Franz et al. (2012a) was used:

$$z^* = \frac{5.8}{\rho_{bd}(\tau+SOC)+\theta_v+0.0829} \tag{3.7}$$

where z^* is the estimated CRP measurement depth, τ is the weight fraction of lattice water in the soil, SOC is the weight fraction of soil organic carbon, and θ_v is the water content estimated from the CRP. The average ρ_{bd} and SOC from the 0 – 15 cm soil samples was used.

Lattice water refers to the water in the mineral grains and bound water (Franz et al., 2012a). To measure lattice water, composite samples were created from all of the samples of similar material type (peat, SSM, Bm sand, B/C sand, and subsoil). The composite samples were pretreated with H_2O_2 to remove organics then analyzed for lattice water at an Activation Laboratories LTD. commercial laboratory in Ancaster, Ontario Canada. Lattice water was obtained by measuring the amount of water released from decomposing the samples at 1000˚C after already drying them at 105˚C. The average lattice water value for the measurement area of the CRP was calculated by taking a weighted average based on the area of cover of the various surface materials within the CRP footprint (Table 3.1). Only the materials that were present in the top 15 cm of the ASCS plots were incorporated for the lattice water average. The organic carbon content of the soil samples was measured using a LECO C632 dry combustion carbonator (LECO Corp., St. Joseph, MI, USA). The average SOC was found using the soil samples from 0 – 15 cm. The hydrogen in organic matter (SOC) is assumed to be similar to the weight percent of organic carbon due to the complex nature of organic matter (Franz et al., 2013a).

Table 3.1 Weighted fraction of lattice water in each soil material type within the CRP footprint.

Material type	Average lattice water (wt %)	Area cover weight	Weighted fraction
Peat	5.47	0.37	0.0203
SSM	1.13	0.32	0.0036
Bm	0.17	0.04	0.0001
Sub soil	0.73	0.08	0.0006
B/C	0.20	0.00	0.000
Overburden	1.87	0.19	0.0036

3.4.6 Horizontal weighting of soil moisture network measurements

The horizontal sensitivity of the CRP must be taken into account when comparing SWC measurements from soil samples or soil sensors to CRP-estimated SWC. The SWC measured from the soil samples in this study did not need horizontal weighting because the sampling pattern employed already incorporates the necessary weighting (Franz et al., 2012b). There were an equal number of sampling points (six) evenly spaced along each of the four radials meaning there was the least distance between points along the 25 m radial and increasing distance between points on the 75, 200, and 300 m radials. Therefore a simple arithmetic mean was used for calculating the average SWC from the soil samples before applying vertical weighting.

The CS616 probes, however, did need horizontal weighting since they were not positioned in the same manner as the soil sampling locations. To compare sensor estimate of SWC to the CRP estimates, the horizontal weighting method presented by Bogena et al. (2013) was used. Bogena et al. (2013) fitted a polynomial curve to the relationship between CRP measurement footprint radius and cumulative fraction of neutron counts (*CFoC*). The fitted polynomial to calculate *CFoC* based on the CRP footprint radius is:

$$CFoC = a_1 r^5 - a_2 r^4 + a_3 r^3 - a_4 r^2 + a_5 r + a_6 \quad (3.8)$$

where r is the measurement footprint diameter (m). The fitted parameters, a_1- a_6, are presented in Table 2 of Bogena et al. (2013). Since the CS616 probes were not evenly distributed throughout the CRP footprint, the footprint area was divided into six circular segments of 50 m (0-50, 50-100, 100-150, 150-200, 200-250, and 250-300 m) with each segment given a horizontal weight (wt_h) from the following formula:

$$wt_{h,i} = CFoC_i - CFoC_{i-1} \quad (3.9)$$

The weights were rescaled after the initial calculation so the sum of all the weights was equal to 1. Table 3.2 displays the rescaled weights for each segment. The average water content from the CS616 probes was found for each segment and then the horizontally weighted average CS616 water content inside the CRP footprint was obtained by averaging the segments based on their weights.

Table 3.2 Rescaled horizontal weights (wt_h) and Cumulative Fraction of Counts (CFoC) for six radial segments for horizontal weighting of average soil water content.

CRP Footprint radius *r* (m)	**CfoC**	**Segment (m)**	**wt_h**
50	0.298	0-50	0.364
100	0.471	50-100	0.211
150	0.594	100-150	0.150
200	0.692	150-200	0.121
250	0.767	200-250	0.092
300	0.818	250-300	0.062

3.4.7 Vertical weighting of manually measured and soil moisture network water content measurements

The vertical sensitivity also decreases with increasing distance (i.e. soil depth) away from the CRP (Franz et al., 2012a), thus vertical weighting must also be applied to the sampled soil water measurements and horizontally weighted CS616 measurements. The linear vertical weighting approach proposed by Franz et al. (2012b) was adopted in this study. Their depth weighting function is based on the effective measurement depth of the CRP (z^*) and the depth of soil (z). For $0 \leq z \leq$, the vertical weight for a given z is:

$$wt_v = a\left[1 - \left(\frac{z}{z^*}\right)\right] \tag{3.10}$$

where wt_v is the vertical weight and a is a constant needed to conserve the weights and is found by the following equation:

$$a = \frac{1}{z^* - \frac{z^{*2}}{2z^*}} \tag{3.11}$$

Despite the simplicity of the presented depth weighting function, Franz et al. (2012b) observed very comparable results when using the weighting function to compare soil water measurements to CRP measurements. When applying Eq. 3.10 in this study, the calculated weights at each depth were combined to correspond to the soil sampling depths and the depths of the CS616 probes. The weights for the sampled water contents were combined from 0 to 4 cm, 5 to 9 cm, and 10 to z^*cm. For the CS616 probes, the weights were combined for 0 to 6 cm

and 7 to z^* cm and applied to the horizontally weighted values to find the weighted average within the CRP footprint.

3.4.8 Simulating water content in the CRP footprint with HYDRUS-1D

CRP-estimated SWC is a horizontally and vertically weighted average of the actual SWC within the 300 m radius measurement footprint. At times it might be useful to have a non-weighted average water content estimate at the site where a CRP is installed. We developed a simulation method in order to demonstrate CRP SWC measurements can, in principle, be "unweighted" by modeling the horizontally and vertically weighted average water content in the top of the soil profile of the contrasting capping soils inside the 300 m radius footprint at the ASCS site. The HYDRUS-1D software (Šimůnek et al., 2008), which uses a numerical solution of the 1-D Richards equation, was used to model the moisture dynamics within the measurement depth of the CRP (See Tables D.1 and D.2 for detailed parameter set up). Peat and SSM were the only top cover materials simulated because the majority of the CRP footprint consisted of those two materials. Two soil columns were simulated in the HYDRUS-1D software: 1) a column with a 30 cm cover of peat, and 2) a column with a 20 cm cover of SSM. Below the cover material in each column was a layer of subsoil to a depth of 100 cm. Simulated SWCs of these two columns were weighted according to the area occupied by each capping material and distance away from the CRP for comparison to the CRP SWC estimates. Hydraulic parameters for the different materials were optimized by minimizing the difference between average simulated SWC and CRP-measured SWC. The soil hydraulic properties in the peat and SSM were obtained using the van Genuchten-Mualem model within the HYDRUS-1D software:

$$\theta(h) = \begin{cases} \theta_r + \frac{\theta_s - \theta_r}{[1+|\alpha h|^n]^m} & h < 0 \\ \theta_s & h \geq 0 \end{cases} \quad (3.12)$$

$$K(h) = K_s S_e^{0.5} \left[1 - \left(1 - S_e^{0.5/m}\right)^m\right]^2 \quad (3.13)$$

$$S_e = \frac{\theta - \theta_r}{\theta_s - \theta_r} \quad (3.14)$$

$$m = 1 - \frac{1}{n} \qquad n > 1 \quad (3.15)$$

where, θ_s and θ_r are saturated and residual water contents ($cm^3\ cm^{-3}$), h is pressure head (cm), α is the inverse of the air-entry value (cm^{-1}), n is a pore-size distribution index, and K_s is saturated hydraulic conductivity ($cm\ h^{-1}$). The parameters used during the simulations are shown in Table 3.3. The parameters θ_s, θ_r, and K_s, although different between peat and SSM, were kept constant during all simulations. Only the α and n parameters were optimized for the peat and SSM using the CRP-estimated water content reading. The θ_r, θ_s, and K_s parameters for the peat were estimated based on findings by Letts et al. (1999) on peat soils. Peat soils can have θ_s values as high as 0.9 $cm^3\ cm^{-3}$, but since the peat has a mineral soil component a value of 0.7 $cm^3\ cm^{-3}$ was assumed. The θ_r, θ_s, and K_s parameters for the SSM were estimated from the texture of the sandy material and the Neural Network Prediction within the HYDRUS-1D software. The HYDRUS-1D Neural Network Prediction was also used to obtain the van Genuchten-Mualem parameters for the underlying sub soil sand.

Table 3.3 Parameters used in HYDRUS-1D modeling and optimized parameters (bold letters).

Soil Material	α	n	θ_r	θ_s	K_s (cm h^{-1})
Peat	**0.042**	**1.8**	0.095	0.7	0.92
SSM	**0.043**	**3.03**	0.05	0.38	8.3
Subsoil	0.034	3.98	0.052	0.38	20.83

To simplify the simulations, daily water content was modeled in the peat and SSM columns. Simulations were performed only for the 2014 field season, thus a total simulation time of 147 days (May 28 to October 21). The initial water content conditions in the different materials of the columns were acquired from the CS616 data at the beginning of May 28, 2014. The initial water contents were set to 0.45 cm^3 cm^{-3} for the peat layer, 0.15 cm^3 cm^{-3} for the LFH layer, and 0.13 cm^3 cm^{-3} for the subsoil. Daily precipitation measured by the WeatherHawk was used for the upper boundary conditions of the columns and free drainage was assumed as the lower boundary conditions. The daily potential soil surface evaporation (E_p) was calculated in HYDRUS-1D using the Hargreaves method (Jensen et al., 1990):

$$E_P = 0.0023 R_a (T_m + 17.8)\sqrt{TR} \tag{3.16}$$

where R_a is the extraterrestrial radiation (J m^{-2} s^{-1}), T_m is the daily mean air temperature calculated as the average of the maximum and minimum air temperatures (˚C), and TR is the range between the daily maximum and minimum air temperatures (˚C). The R_a is calculated in HYDRUS-1D based on the latitude of the site. The WeatherHawk weather station provided temperature data for calculating E_p.

The simulated water contents for the peat and SSM columns were weighted based on their percentage of cover of the peat and SSM within the CRP footprint and distance away from

the probe. This weighted average was needed to compare to the CRP reading in order to optimize the α and n parameters for peat and SSM. The percent cover of peat and SSM in each 50 m circular segment around the CRP was estimated. A weight for peat and SSM was obtained for each 50 m segment from the product of the percent cover and the associated horizontal weight. Finally the sum of all weights for each segment provided a single weight coefficient (percent cover and horizontal) for each material. Since more area closer to the CRP was covered in peat, the peat weight coefficient was 0.692 and the SSM weight coefficient was 0.307. Average weighted water content was calculated from the simulated water contents and the weight coefficients and compared to the daily average CRP reading during the 2014 field season. Initial estimates of α and n parameters were made for the peat and SSM. The results of Letts et al. (1999) and the Neural Network Prediction tool were used to estimate α and n for the peat and SSM, respectively. Numerous combinations of α and n parameters deviating stepwise from the initially estimated parameters were obtained for the two cover materials by using MatLab (The MathWorks Inc.) and then used in simulations in HYDRUS-1D. The two combinations of α and n parameters for peat and SSM that produced the average water content with the lowest RMSE when comparing to the CRP reading were considered the optimized parameters.

3.5 Results and discussions

3.5.1 CRP estimation of water content: measurement depth and rainfall response

The initial calibration of the CRP (May 2014) included the soil samples up to 30 cm in depth. The CRP-estimated θ_v from the initial calibration was relatively high causing the estimated measurement depth from Eq. 3.7 to be just over 10 cm. The CRP was recalibrated using the soil samples from 0 – 15 cm in order to better represent the CRP footprint. The 0 – 15

cm calibration and subsequent N_0 was then used for the remainder of the CRP reading period of summer 2014 and all of summer 2015. For summer 2014, the average CRP-θ_v was 0.29 cm^3 cm^{-3} with many occasions where the θ_v was above 0.30 cm^3 cm^{-3} (Figure 3.3). 2015 was a slightly drier summer, with the average estimated CRP θ_v being 0.21 cm^3 cm^{-3}. June and July 2015, according to the CRP, were drier than 2014, which caused the difference in average CRP θ_v between both study seasons.

The average estimated measurement depths for both 2014 and 2015 were fairly shallow (Figure 3.3). For 2014 the average measurement depth was 12.07 cm, with the estimated depth reaching greater than 15 cm only a few occasions near the end of August. In 2015 the average measurement depth was 14.33 cm. The deeper estimated measurement depth for 2015 is due to the drier soil conditions compared to the 2014 season. The overall shallow measurement depth of the CRP in 2014 and 2015 is caused by relatively high water contents from the peat coversoil, as well as the organic matter (SOC) and lattice water contents. Bogena et al. (2013), who also observed shallow CRP measurement depths, found that the effective measurement depth in a forested area was primarily controlled by SWC in wet conditions (>0.3 cm^3 cm^{-3}). In drier conditions, they concluded that hydrogen found in organic matter and lattice water was more important for reducing the sensor depth. In contrast, Franz et al. (2012b) observed lower SWC values (0.05-0.15 cm^3 cm^{-3}) and disregarded SOC, resulting in deeper calculated measurement depths (20-35 cm). The average SOC in the top 15 cm of the ASCS site found from the calibration soil samples was 11.68% (weight fraction = 0.12). This level of SOC is caused by the peat coversoil, which is largely composed of organic matter. The peat contained the highest lattice water percentage (5.47%; Table 3.1) and also covered the most area within the 300 m horizontal footprint of the CRP in the 0 - 15 cm depths. Thus, the

soil water content, the high SOC levels, and the lattice water all caused the estimated measurement depth of the CRP to be relatively shallow throughout both summers.

Total precipitation from the end of May 2014 until the end of October 2014 was 294 mm and 209 mm from the beginning of June 2015 until the middle of October 2015. Overall, the CRP readings clearly responded to the rainfall events captured by the WeatherHawk in both years (Figure 3.4). A clear example of CRP response to the precipitation can be seen at the end of May 2014 (soon after installation of CRP) when a large rainfall event took place and the CRP-estimated θ_v increased from 0.35 to 0.46 $cm^3\ cm^{-3}$ over the span of one day. Another example during the 2015 season can be seen during the middle of July 2015. On July 12, 2015 the CRP-estimated θ_v was near 0.15 $cm^3\ cm^{-3}$, but following rainfall events during the next few days the CRP θ_v fluctuated closely around 0.26 $cm^3\ cm^{-3}$.

3.5.2 Soil sampled and CRP-estimated water content

In general, the CRP estimated water content compared closely to the average θ_v measured on soil samples from 0-15 cm (Figure 3.4). The variability of the soil sampled water content measurements can be seen in Appendix A. Root Mean Square Error (RMSE) and Mean Bias Error (MBE) were calculated to assess the error between the CRP-estimated and soil sampled θ_v with the following equations:

$$RMSE = \sqrt{\frac{1}{n}\sum_{i=1}^{n} e_i^2} \tag{3.17}$$

$$MBE = \frac{1}{n}\sum_{i=1}^{n} e_i \tag{3.18}$$

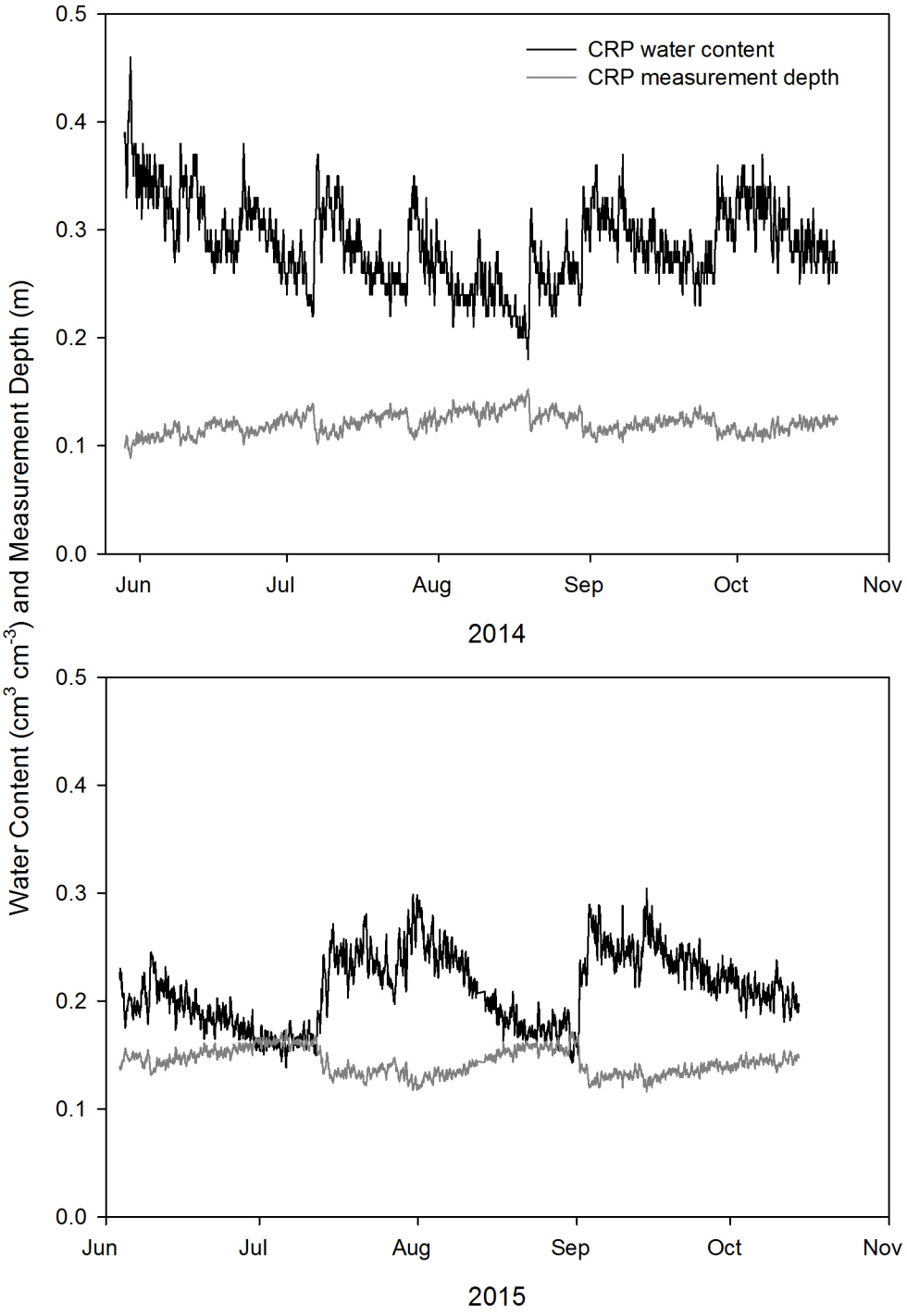

Figure 3.3. The CRP-estimated soil water content and estimated measurement depth for 2014 (top) and 2015 (bottom).

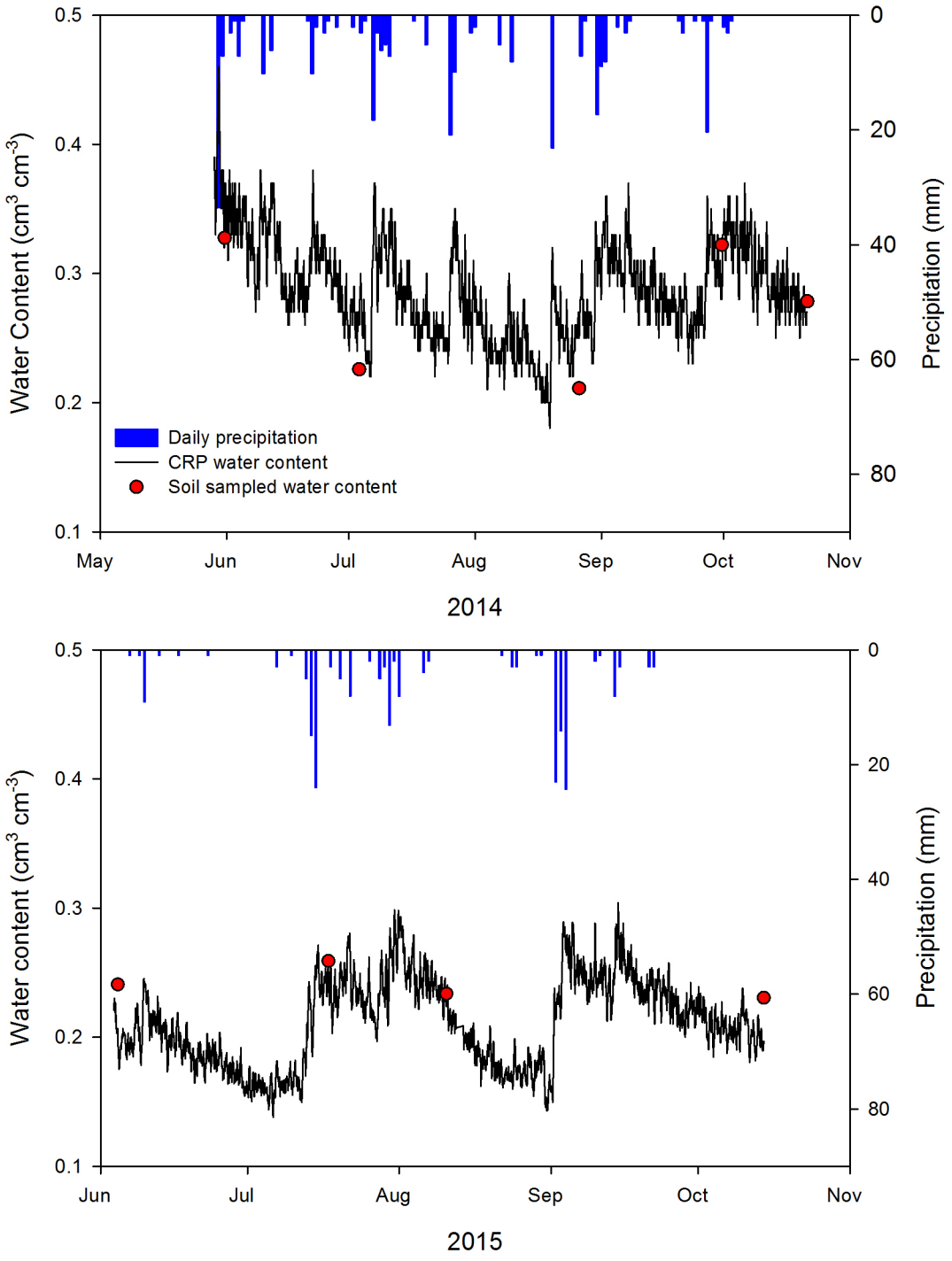

Figure 3.4. CRP-estimated water content and the vertically weighted average water content from manually sampled soil cores for 2014 (top) and 2015 (bottom). Precipitation events represent daily precipitation.

where *n* is the number of samples and *e* is the error between predicted and observed values (*e = predicted – observed*). The manually sampled θ_v was the observed measurement, and the CRP-estimated θ_v was the predicted measurement. MBE provides an indication of the average over- or under-prediction of the CRP-estimated θ_v. For 2014, the RMSE and MBE were 0.034 and 0.012 $cm^3\ cm^{-3}$, respectively for 2014, 0.026 and -0.018 $cm^3\ cm^{-3}$, for 2015 and 0.031 and -0.001 $cm^3\ cm^{-3}$ for the combined dataset. Therefore, the CRP performed quite well in terms of estimated θ_v – estimates slightly lower than the soil samples - considering the large footprint, temporal and spatial variability of soil water, and uncertainty from the calibration of the CRP being from one sampling campaign only (May 2014).

It has been shown that vegetation biomass can affect the calibration relationship for a site (Bogena et al. 2013). From visual observations, it appeared that more vegetation was present on the study site in year two (2015) compared to year one (2014). Changes in biomass between the two years were quite apparent because the vegetation began re-establishing a few years prior to this study (2012), thus the trees and understory species were less than 2 m in height. Despite differences in vegetation between study years, the calibration from 2014 proved to be just as accurate for the 2015 study season. Perhaps the drier 2015 study season allowed less overall vegetation growth than would have occurred if the site received similar precipitation amounts as 2014.

The level of agreement of the CRP estimated water content with the measurements on soil samples is similar to the results found by Zreda et al. (2008) in a fairly homogeneous site, although they only sampled the area average soil water content two separate times within the CRP footprint - once when the site was dry and once when the site was wet, and they did not report RMSE. Franz et al., (2012b) also found satisfactory agreement when comparing CRP-

estimated θ_v to soil sample vertically weighted θ_v (five separate sampling campaigns), with an RMSE of 0.0095 cm^3 cm^{-3}. However, the lower RMSE found by Franz et al. (2012b) compared to that reported in this paper may be partially explained by the comparatively lower soil heterogeneity at the site of Franz et al. (2012b) and that they used all five sampling campaigns to find an average calibration function. Using all five sampling campaigns from 2014 to calibrate the CRP at the ASCS site only slightly improves the 2014 RMSE to 0.031 cm^3 cm^{-3}. For both of the above-mentioned studies (Zreda et al., 2008; Franz et al., 2012b), the average soil sample water content was obtained from samples along three radials (25m, 75m, and 175-200m) around the CRP. For this study, four radials were sampled – 25 m, 75 m, 200 m, and 300 m away from the CRP. Our results show good agreement with average water content inside an assumed CRP footprint of 300 m, despite new thoughts by Köhli et al. (2015) that the CRP footprint ranges from only 130 to 240 m depending on the soil water content.

We observed greater errors (RMSE) between CRP-estimated and soil sample measured water contents when effective measurement depth (z^*) was not used to weight the soil sample measured water contents (Figure A.4 in Appendix A). Thus depth-weighting is critical for validating the CRP. Bogena et al. (2013) proposed a slightly more complex depth weighting function than the linear function used in this study from Franz et al. (2012b). The function used by Bogena et al. (2013) is based on the cumulative fraction of neutron counts at different depths within the soil similar to the horizontal weighting function used in this study for the CS616 weighting. Both depth weighting functions were compared and produced similar average θ_v, thus the simple linear Franz et al. (2012b) function was quite satisfactory. Because of the exponential characteristics of the cumulative fraction of counts as can be seen in Figure 4 of Bogena et al. (2013), perhaps the advantage of nonlinear function of Bogena et al. (2013) would be more apparent if the water content at the study site was lower.

3.5.3 Continuously measured CS616 and CRP estimated water content

The existing CS616 SWC sensor network at the site provided an additional dataset to compare to the CRP-estimated θ_v for the summer of 2014. The CS616 probes provided a more continuous measurement of SWC (measurements every 3 hours) compared to the soil sample campaigns performed approximately once per month. Figure 3.5 displays the CRP-estimated θ_v and the CS616-θ_v before and after weighting. The CRP and CS616-θ_v follow each other quite well throughout the entire summer of 2014. Peaks in the CS616-θ_v from rainfall events occurred at similar times as the CRP-estimated θ_v. Horizontal weighting was applied to the CS616 probes because the probes were not evenly distributed throughout the CRP footprint (See Figure A.5 for mean SWC inside 50 m swaths used for horizontal weighting). Also, only the CS616 probes within the estimated CRP measurement depth (23 probes at 5 cm and 23 probes at 15 cm) were used for finding the average θ_v within the CRP footprint. Overall the horizontally and vertically weighted CS616-measured θ_v showed reasonable agreement with the CRP-estimated θ_v. It is clear from Figure 3.5 that weighting of the CS616-θ_v resulted in a closer match to the CRP-estimated θ_v, especially in terms of variance of average θ_v.

When treating the horizontally and vertically weighted CS616-θ_v values as the observed measurements and the CRP-estimated θ_v as the predicted measurements and using Eqs. 3.17 and 3.18, RMSE and MBE were 0.024 $cm^3\ cm^{-3}$ and 0.005 $cm^3\ cm^{-3}$, respectively. This RMSE is within the error of the CS616 probes, which have an accuracy of ± 2.5% or ± 0.025 $cm^3\ cm^{-3}$ (Campbell Scientific Inc., 2015). Some overestimation by the CRP compared to the weighted CS616 measured θ_v appears to occur following peaks in SWC from rainfall events throughout the middle of June and beginning of July (Figure 3.5). This might be from the CRP responding to

surface water collected after rainfall in the two man-made canals that are positioned North to South separating sections of the one hectare cover treatment plots. Zhu et al. (2015) observed an overestimation of SWC by the CRP in agricultural field when surface water was present from irrigation. They compared CRP-estimated θ_v to a network of 19 SoilNET probes within the CRP footprint. No horizontal or vertical weighting was mentioned by Zhu et al. (2015), but still an RMSE of 0.0275 $cm^3\ cm^{-3}$ was observed during non irrigated periods. During irrigation events the RMSE increased to 0.037 $cm^3\ cm^{-3}$, with the higher error attributed to surface water from irrigation not measured by the SWC sensor network.

Other studies have also observed a close correlation between CRP-estimated θ_v and SWC sensor network measurements. Franz et al. (2012b) compared CRP-measured θ_v to vertically and horizontally averaged estimates from a network of time-domain transmission (TDT) probes in a similar pattern as the common manual calibration sampling scheme over a 6 month period and found an RMSE of 0.0165 $cm^3\ cm^{-3}$. Bogena et al. (2013), who compared CRP-measured θ_v to vertically and horizontally averaged estimates from a network of SoilNET probes at a naturally heterogeneous site, found an RMSE of 0.0294 $cm^3\ cm^{-3}$ over a period of two years. Bogena et al. (2015) used horizontal and vertical depth weighting. All of these results are similar to the results obtained in this study in terms of the CS616 average θ_v, notwithstanding the distinct heterogeneity of the ASCS site.

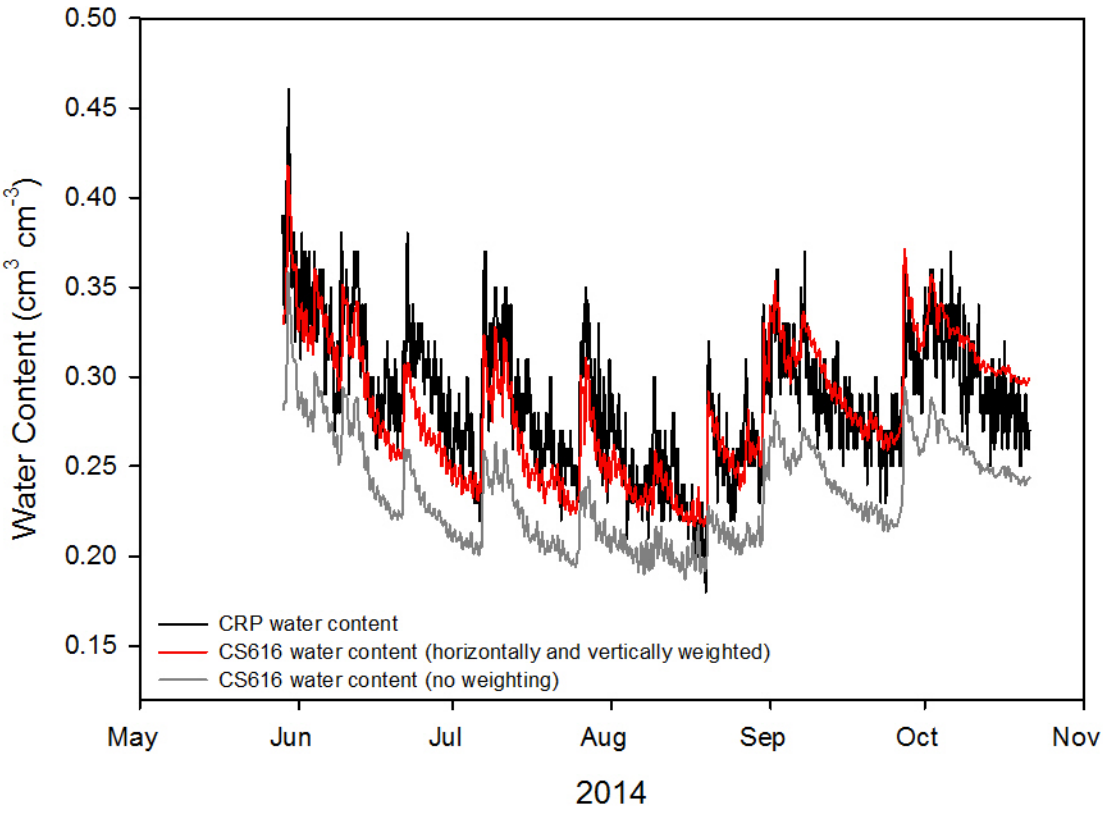

Figure 3.5. CRP-measured soil water content and the CS616 horizontally and vertically weighted average soil water content.

3.5.4 Simulated water content in CRP footprint

The spatial weighting function of the CRP may be problematic for applications where a non-weighted spatially averaged SWC estimate is desired. If the measurement area is relatively homogeneous, a non-weighted average of the actual water content is representative of CRP-estimated SWC. If the site is heterogeneous (e.g. higher SWC closer to CRP), however, the non-

weighted average water content will not agree with the spatially weighted CRP measurement. For this site, the heterogeneity in terms of soil texture was known so it was possible to model the SWC in the CRP footprint by optimizing the modeled SWC from the CRP readings.

We used the CRP-estimated SWC to optimize the α and n parameters (van Genuchten-Mualem parameters) for peat and SSM. For the peat, the optimized α and n were 0.042 and 1.8, respectively. These values fall in between the α and n parameters of relatively undecomposed Fibric (α = 0.08, n = 1.9) and somewhat decomposed Hemic (α = 0.02, n = 1.7) peat materials found by Letts et al., (1999). Thus, the optimized parameters appear reasonable since the peat material varied in decomposition. The optimized α and n for the SSM were 0.043 and 3.03, respectively. The parameter α is related to how narrow (higher α) or broad (lower α) the air-entry region is of a given material's water retention curve (Radcliffe and Simunek, 2010). We would expect the α value of the peat to be lower than SSM since soils with high water retention (e.g. clays) generally have lower α parameters. The high organic matter content of the peat should lead to high water retention. The n parameter is related to the steepness of the water retention curve (i.e., variance of the pore size distribution), with larger n values resulting in steeper curves (Radcliffe and Simunek, 2010). Sandy soils generally have steeper water retention curves (i.e., narrow pore size distributions), thus the larger n value of SSM compared to the peat is justifiable.

Figure 3.6 shows the best-fit weighted modeled daily SWC from HYDRUS-1D and the daily CRP-estimated SWC for 2014. The weighted, modeled SWC is a weighted average of the simulated SWC at 8 cm in two columns with one containing peat and one containing SSM as the cover materials. The non-weighted peat and SSM simulated water contents are also shown in Figure 3.6 (bottom) with the average soil sampled peat and SSM SWC. The average SWCs for the peat and SSM were obtained by averaging the water content of the 5-10 cm soil samples

from the corresponding capping materials for each of the five sampling campaigns in 2014. The simulated, weighted average SWC compares relatively well to the daily CRP-estimated SWC with a RMSE of 0.039 cm^3 cm^{-3}. Also, the non-weighted peat and SSM simulated water contents correlate closely with the soil sampled water contents with a RMSE of 0.038 cm^3 cm^{-3} and 0.035 cm^3 cm^{-3}, respectively. As expected, the simulated, weighted average SWC spikes with rainfall events similar to the CRP daily water content. However, there is a higher increase in SWC following rainfall events in the simulated, weighted average SWC. This may be because vegetation was not accounted for in the model and consequently there is an underestimation of evapotranspiration or overestimated soil water contents. This overestimation of simulated soil water contents is likely the cause of the difference between the simulated weighted average SWC and the CRP-estimated SWC between mid July and early September. Despite discrepancies between the CRP and modeled SWC, the non-weighted simulated peat and SSM water contents closely matched the soil sampled water contents for the respective capping soils. These results show that there is potential to downscale or "unweight" the CRP reading with the aid of simulation if the hydraulic parameters of the individual soils present inside the CRP footprint are known or optimized.

We have demonstrated that the CRP measurement can be downscaled or "unweighted" to subplots within the measurement footprint with some background knowledge of the soil at the site. This is significant, because in many parts of the world, small farms have only a few hectares of land or less causing significant heterogeneity across the landscape. It is estimated that of the approximately 570 million farms worldwide, more than 475 million have less than 2 hectares of land (Lowder et al., 2014). This can be a significant challenge for deploying a CRP if the field area is smaller than the entire sensor footprint. Also, CRP measurements can provide ground truthing of remote sensing. Often, one pixel of remotely sensed data contains two or

more polygons with different soil and/or vegetation (Charpentier and Groffman, 1992; Mohanty and Skaggs, 2001). This would require downscaling the CRP measurement before using as a ground truth measurement. Furthermore, in natural landscapes, the transition zone from one ecosite (land unit based on soil water and nutrient regime) to another, for example the transition from small wetlands to dry uplands, can result in differences in soil and vegetation over a distance of <100 m (Bauer et al., 2009; Dimitrov et al., 2014). These transition zones would also impact the interpretation of CRP measurements. Combining modeling with the unweighting or downscaling method, one may be able to obtain soil water contents for two or more ecosites within the measurement footprint.

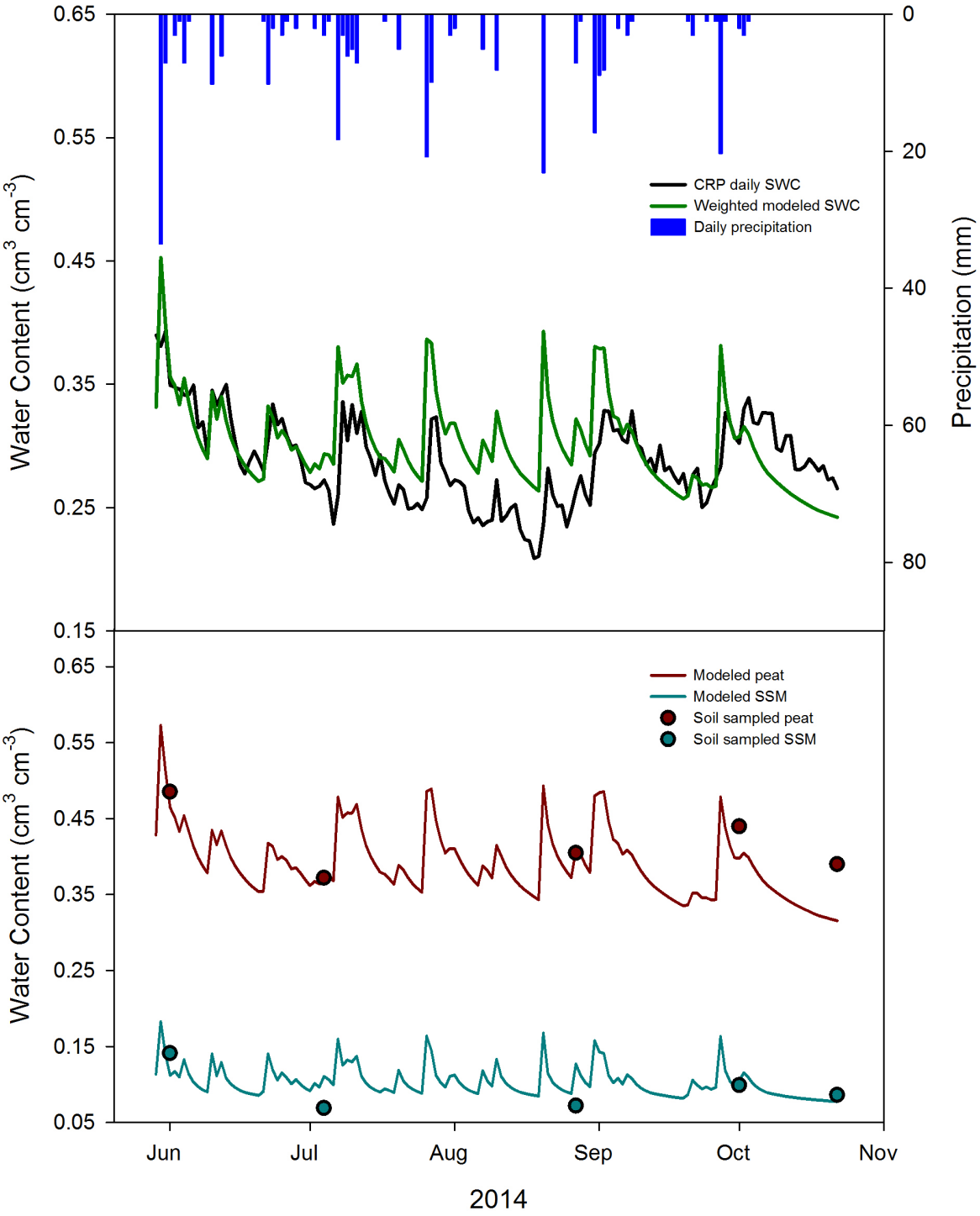

Figure 3.6. (top) Weighted, modeled soil water content (SWC) from HYDRUS-1D and daily CRP-estimated water content. The weighted, modeled SWC is a weighted average of the simulated peat and SSM soil water contents. (bottom) Modeled and soil sampled peat and SSM SWC.

3.5.5 Applications of the CRP for use in oil sand reclamation

There are some potential advantages in using a CRP to measure SWC or soil moisture in order to monitor the progress of oil sands reclamation. Oil sands mining companies are required by law to reclaim the land disturbed from mining, with a common goal being to reclaim the land so that the soil and landforms are capable of supporting a self-sustaining, locally common boreal forest, irrespective of the end land use (Poscente and Charette, 2012). In order for the mining operator to be relieved of any further reclamation responsibilities, a reclamation certificate must be issued by government regulators, indicating that the goal of reclamation has been achieved. The ultimate goal of reclamation is to re-establish key vegetation species and community assemblages to represent different ecological communities based on soil moisture and nutrient regime (Alberta Environment, 2010). Thus, soil moisture is a critical factor in recreating landscapes during reclamation. In terms of the re-establishment of woody plants from seeds and vegetation, soil water is the most important factor (Alberta Environment, 2010). In some cases, a dry spring and summer can cause over 80% mortality in vegetation that was seeded in the spring. This is why soil moisture is listed as the first "indicator" to monitor and measure guidelines and frameworks for oil sands reclamation (Poscente and Charette, 2012). Soil water content is also measured at long-term monitoring plots on natural sites and reclaimed oil sand sites to provide benchmarks for later use when monitoring reclamation progress (Johnson and Miyanishi, 2008). A CRP could be used to monitor SWC at newly established reclamation covers. The CRP can be installed in remote locations with the data accessed remotely. It can provide a confident measurement of SWC that is continuous, non-invasive (beyond the initial calibration), and landscape-scale sized. It could

replace soil moisture networks made up of numerous probes installed throughout reclamation covers. Because the CRP sits above the soil surface, uninstalling it after monitoring is simple and non-invasive.

There are also some limitations involving the use of a CRP for monitoring reclamation covers. The measurement depth of the CRP could be a limitation in some cases. With relatively high soil water and organic matter contents the measurement depth is quite low (~15 cm). This measurement depth might be too shallow in some cases as the root network of the vegetation to acquire soil water can extend well below the CRP measurement depth. Because reclamation of oil sands land involves re-vegetation, the vegetation levels within the CRP footprint could change significantly during the first years of vegetation establishment. We did not see an effect of vegetation on the calibration of the CRP after one year of growth, but over time the calibration might be affected. Baatz et al. (2015) developed a simple vegetation correction for the CRP that could be used if vegetation growth negatively affected the calibration.

3.6 Conclusions

The performance of a cosmic-ray soil moisture probe for measuring average soil water content was assessed at a highly heterogeneous oil sand reclamation area in the Alberta Oil Sands for two summers. The CRP was calibrated using soil core samples taken along radials 25, 75, 200, and 300m away from the CRP, which is slightly different than the normal calibration method. The CRP monitored volumetric SWC from the end of May to the end of October in 2014 and 2015. The accuracy of the CRP was compared to soil core samples and a soil moisture sensor network composed of CS616 probes installed at various depths in each plot. The CRP-estimated water content compared well to water content measured from soil cores

(gravimetric method) collected throughout the summer and early fall months in 2014 and 2015 at the calibration locations. The CRP-estimated SWC also compared closely to the more continuous measurement of SWC from the CS616 sensor network. Overall, low error was observed between the CRP-estimated SWC and the SWC measured from the manually sampled soil cores and soil moisture network despite the clear heterogeneity (soil texture, vegetation) of the study site with discrepancies most likely due to surface water present after rainfall events. An important step in the process of verifying the measurement of the CRP was vertically weighting the average SWC measured from the sampled cores and horizontally and vertically weighting the average soil moisture sensor-estimated SWC. Failing to do so may result in misleading results.

The advantages associated with CRP sensors (wide area and continuous measurement, satellite acquisition of data), allow CRPs to have potential use for monitoring soil water content at other more homogeneous natural and reclamation areas in the world. It is also important to acknowledge the limitations of the CRP including a relatively shallow measurement depth and possible calibration issues with growing vegetation from year to year. Despite the limitations, the CRP appears to provide an accurate estimate of SWC at very heterogeneous sites, thus it should prove to be accurate at other less distinctively heterogeneous areas.

4. CALIBRATION OF A NON-INVASIVE COSMIC-RAY PROBE FOR WIDE AREA SNOW WATER EQUIVALENT MEASUREMENT

4.1 Preface

In colder climates, such as the Canadian Prairies, snow measurements becoms equally as important as soil water during the winter months for uses such as flood prediction and estimates of upcoming water storage for agriculture. Snow water equivalent (SWE) is measured from snowpacks and, similar to soil water content measurements, is often obtained from either point-scale measurements using snow tubes or large-scale measurements from remote sensing. Since snow is simply frozen water, the cosmic-ray soil moisture probe (CRP) also can potentially measure SWE at the landscape-scale. The purpose of this study was to calibrate a CRP for measuring SWE non-invasively at the landscape-scale. This was achieved by establishing an empirical relationship between above ground neutrons measured by the CRP and SWE from snow surveys measured with snow tubes. The calibration was performed during the first study winter and its validity tested the second winter.

4.2 Abstract

Measuring snow water equivalent (SWE) is important for many hydrological purposes such as modeling and flood forecasting. Measurements of SWE are also crucial for agricultural production in areas where snowmelt runoff dominates spring soil water recharge. Typical methods for measuring SWE include point measurements (snow tubes) and large-scale measurements (remote sensing). We explored the potential of using the cosmic-ray soil

moisture probe (CRP) to measure average SWE at a measurement scale between those provided by snow tubes and remote sensing. The CRP measures above ground moderated neutron intensity within a radius of approximately 300 m. Using snow tubes, surveys were performed over two winters (2013/2014 and 2014/2015) in an area surrounding a CRP in an agricultural field in Saskatoon, Saskatchewan, CAN. The raw moderated neutron intensity counts were corrected for atmospheric pressure, water vapor, and temporal variability of incoming cosmic ray flux. The mean SWE from manually measured snow surveys was adjusted for differences in soil water storage before snowfall between both winters because the CRP reading appeared to be affected by soil water below the snowpack. The SWE from the snow surveys was negatively correlated with the CRP-measured moderated neutron intensity, giving Pearson correlation coefficients of -0.92 (2013/14) and -0.94 (2014/15). A linear regression performed on the manually measured SWE and moderated neutron intensity counts for 2013/14 yielded an r^2 of 0.84. Linear regression lines from the 2013/14 and 2014/15 manually measured SWE and moderated neutron counts were very similar, thus differences in antecedent soil water storage did not appear to affect the slope of the SWE vs. neutron relationship. The regression equation obtained from 2013/14 was used to model SWE using the moderated neutron intensity data for 2014/15. The CRP-estimated SWE for 2014/15 was similar to that of the snow survey, with a RMSE of 7.7 mm. The CRP-estimated SWE also compared well to estimates made using snow depths at meteorological sites near (<10 km) the CRP. Overall, the empirical equation presented provides acceptable estimates of average SWE using moderated neutron intensity measurements. Using a CRP to monitor SWE is attractive because it delivers a continuous reading, can be installed in remote locations, requires minimal labour, and provides a landscape-scale measurement footprint.

4.3 Introduction

Landscape-scale snow water equivalent (SWE) measurements are important for applications such as hydrological modeling, flood prediction, water resource management, and agricultural production (Goodison et al., 1987). Particularly in the Canadian Prairies, snowmelt water is a critical resource for domestic/livestock water supplies and soil water reserves for agriculture purposes (Gray and Landine, 1988). Snow is also a key contributor in recharging Canadian Prairie wetlands, which provide important wildlife habitat (Fang and Pomeroy, 2009).

Common techniques for measuring SWE include snow tubes (gravimetric method), snow pillows, and remote sensing (Pomeroy and Gray, 1995). Snow tube sampling is the most common method for determining SWE and although it provides a point measurement, can be used to survey a larger area. However, snow surveys with snow tubes are labour intensive and can be difficult to perform in remote locations. Snow pillows can provide SWE measurements in remote locations, but produce merely a point measurement of roughly 3.5 m^2 to 11.5 m^2 (Goodison et al., 1981). In addition, snow pillows do not accurately measure shallow snowpacks due to snow removal by wind transport and melting (Archer and Stewart, 1995). Remote sensing has the capability of measuring SWE at large scales based on the attenuation of microwave radiation emitted from Earth's surface by overlying dry snow (Dietz et al., 2012). The applicability of remote sensing techniques for SWE monitoring is limited by their coarse measurement resolutions (~625 km^2), their inability to accurately measure wet snow, and their shortcomings in measuring forested landscapes. One remote sensing method that allows for a finer resolution utilizes the natural gamma radiation emitted from Earth's surface that is detected by a spectrometer placed on an airplane (Pomeroy and Gray, 1995). Although the natural gamma radiation method provides improved resolution compared to most remote

sensing techniques, it is not a practical method since it requires multiple flights for multiple measurements.

A measurement scale between that of the point measurements and the large scale remote sensing is desirable due to the high variability in SWE that can occur even over small distances (Pomeroy and Gray, 1995). Shook and Gray (1996) found high variability in snow depth and water equivalent when performing snow surveys with samples every 1 m along transects in shallow snow covers in the Canadian Prairies. Variability of SWE at this small scale was attributed to differences in wind redistribution and transport, along with variations in surface roughness and micro topography. The high variability of SWE at smaller scales can lead to difficulty when trying to estimate average SWE in a field or catchment from a few point measurements. Instead, labour intensive snow surveys are generally required. At larger scales, spatial variability of SWE is generally a function of the differences in snowfall and accumulation from varying vegetation and topography (Pomeroy and Goodison, 1997). The autocorrelation of SWE and snow depth can also cause issues when trying to obtain mean SWE estimates with point measurements (Pomeroy and Gray, 1995). Landscape-scale measurements of SWE can help to avoid issues with spatial autocorrelation of SWE and snow depth by sampling over a large enough area.

The cosmic-ray soil moisture probe (CRP) is a relatively new instrument that was primarily developed for measuring average soil water content at the landscape scale (Zreda et al., 2008), but also has the potential to be a useful tool for measuring SWE. The CRP measures neutrons in the fast to epithermal range, which are emitted from soil and inversely related to soil water content due to the neutron moderating characteristic of hydrogen (H). The CRP is an appealing soil water content measurement tool for several reasons. Firstly, it has a measurement area of ~300 m radius, which helps to fill the gap in scales between that of the

point measurements and landscape-scale remote sensing. Secondly, it measures soil water content passively (non-radioactive) and non-invasively (CRP sits above the soil surface). Thirdly, the CRP can be deployed easily in remote areas. Lastly, it provides a continuous measurement of average soil water content, often with a temporal resolution of one hour. The CRP measurement is based on the moderation of neutrons by hydrogen in water, therefore it is also capable of measuring neutrons moderated by the hydrogen in snow, i.e. frozen water.

The possibility of measuring SWE from the moderation of neutrons by snow has been known since the late 1970s (Kodama et al., 1979), but studies have been limited. Kodama et al. (1979) used a cosmic-ray moderated neutron sensor buried beneath the snow to measure SWE. Although their results showed a promising relationship between moderated neutron counts and SWE, the fact that the moderated neutron measuring tube was installed beneath the snowpack resulted in merely a point measurement. Others have successfully used cosmic-ray probes buried under snowpacks to measure SWE, including a network of buried probes in France (Paquet et al., 2008). Desilets et al. (2010) compared SWE values measured with a CRP installed above-ground to that of SWE values measured manually with a snow tube at the Mt. Lemmon Cosmic Ray Laboratory, Arizona. However, the CRP was installed within a laboratory, and Desilets et al. (2010) provided limited details of their study and did not include the relationship they utilized for deriving SWE from measured moderated neutron counts. Using a CRP to monitor SWE was also tested at the Marshall Field Site, Colorado, USA (Rasmussen et al., 2012). Again, limited details were given on the methods of the study and the empirical relationship used to predict SWE from moderated neutron intensity.

The purpose of this study was to establish a simple empirical relationship between SWE and moderated neutrons measured above a snowpack using a CRP. Average SWE in an agricultural field was predicted from CRP moderated neutron measurements using relationship

developed in this study between SWE and moderated neutrons. Predicted SWE from CRP measurements was compared to manual snow surveys and snow precipitation data from multiple locations around the study site, providing the ensuing results discussed herein.

4.4 Methods

4.4.1 Site description

This work was performed at an agricultural field (52.1326 ˚N, -106.6168 ˚W) located near the University of Saskatchewan in Saskatoon, Saskatchewan, Canada. The field covers roughly 46 ha and is approximately rectangular in shape. This study site was primarily chosen because the estimated measurement footprint of the CRP would fall within the boundaries of the field. The topography of the site is relatively flat. The field is mostly free from trees and vegetation except for a small cluster at its south edge and the crop stubble that was left after harvest in the fall of each study year. The same study site was used for both (2013/14 and 2014/15) winter field seasons. Wheat stubble (height ~20 cm) was present on the field for the 2013/14 winter, and canola stubble (height ~25 cm) for the 2014/15 winter. Also, a set-move wheeled irrigation line was located across the center of the field during the 2013/14 winter causing increased snow accumulation, but the irrigation line was removed before the 2014/15 winter.

4.4.2 CRP and background water content

The model of CRP used in this study was a CRS-1000/B (Hydroinnova, NM, USA). This model consists of two neutron detector tubes and an Iridium modem data logger for remote data access. One of the detector tubes is shielded (or moderated) to measured neutrons of slightly higher energy (epithermal to fast range) and one tube is unshielded to measure lower

energy neutrons (slow neutrons). The neutrons detected by the moderated tube in the epithermal to fast range are referred to as moderated neutrons. Slow neutrons are affected by H, but also other neutron absorbing elements in soil such as B, Cl, and K (Desilets et al., 2010), thus only the moderated neutron count was used in this study. An in-depth description of how the CRP measures neutrons can be found in Zreda et al. (2012). The CRP was installed in the center of the field site (Figure 4.1) from the end of October 2013 until after snowmelt in the spring of 2014 (2013/14 winter). Similarly, for the 2014/15 winter, the CRP was installed in the same location and again collected data until snowmelt in spring of 2015. After installation of the CRP and before the first snowfall event of both winters, average soil water content within the CRP measurement footprint was measured manually from soil cores of known volume. The soil sampling scheme was as follows: 18 total sampling locations comprised of 6 locations evenly spaced along each of 3 radials spanning outward of the CRP (25 m, 75 m, and 200 m). Each location was sampled in 5 cm increments to a depth of 30 cm. This sampling scheme follows the typical method for calibrating CRPs for measuring soil water content (Franz et al., 2012b). Volumetric water content was measured from the cores via the oven-drying method (Gardner, 1986).

The soil water storage in the top 10 cm of the soil profile, prior to snowfall, was estimated for both winters from the measured average soil water content and precipitation data. Precipitation data was collected from a Saskatchewan Research Council (SRC) climate station (52.1539 ˚N, -106.6075 ˚W) located near the study site. Rainfall events recorded after soil sampling, but before the appearance of the snowpack, were added to the antecedent soil water storage. It was assumed that all of the water from rain events before snowfall entered the soil and evapotranspiration was negligible due to the low air temperatures. The soil water storage in the top 10 cm of the soil profile was 2.15 cm in 2013 and 4.53 cm in 2014, creating a

difference of 2.38 cm in water storage between the beginnings of the 2013 and 2014 winters. We assumed that the water content in the top 10 cm of the soil profile did not change drastically over the winter. We acknowledge that this assumption is prone to errors since soil water content can change throughout the winter months from mid-winter melt infiltration and migration of water to the freezing front leading to soil water moving upwards in the soil profile (Gray and Granger, 1985).

Figure 4.1. Location of CRP and estimated 300 m radius measurement footprint (black radial). The red lines represent the sampling radials. Image from Google Maps.

4.4.3 Raw moderated neutron correction

Before further analysis of the hourly neutron count rates from the CRP, the raw neutron counts must be corrected for differences in air pressure, atmospheric water vapor, and the temporal variation of incoming cosmic ray flux. Corrected neutron counts are attained from multiplying the raw counts by correction factors:

$$N_{COR} = N_{RAW} \cdot F_p \cdot F_w \cdot F_i \tag{4.1}$$

where N_{COR} is the corrected moderated neutron count, N_{RAW} is the raw moderated neutron count, F_p is the air pressure correction factor, F_w is the atmospheric water vapor correction factor, and F_i is the variation of incoming cosmic-ray flux correction factor.

Correcting for differences in air pressure is important since the incoming cosmic-ray flux is attenuated with increasing nuclei present in the atmosphere i.e. as air pressure increases (Desilets and Zreda, 2003). F_p is calculated with the following equation:

$$F_p = e^{(\frac{P-P_0}{L})} \tag{4.2}$$

where e is the natural exponential. P is the measured air pressure (hPa) at the site during the moderated neutron count time. Air pressure was measured near the CRP using a WeatherHawk 232 Direct Connect Weather Station (WeatherHawk, UT, USA). P_0 is a reference air pressure chosen to be 1013 hPa (average sea-level air pressure). L represents the mass attenuation length (g cm^{-2}), which is a function of latitude and atmospheric depth (Desilets and Zreda, 2003). The mass attenuation length for Saskatoon was found to be 130.24 g cm^{-2}.

Since neutron counts are mainly related to the amount of hydrogen molecules in an area, raw moderated neutron counts must also be corrected for differences in atmospheric

water vapor. Rosolem et al. (2013) found the following correction function for atmospheric water vapor:

$$F_w = 1 + 0.0054 \cdot (p_{v0} - p_{v0}^{ref}) \tag{4.3}$$

where p_{v0} is the absolute humidity (g m^{-3}) at the site during the measurement time. The parameter p_{v0}^{ref} is the reference absolute humidity and was set to that of dry air (0 g m^{-3}). Relative humidity and air temperature, which are both used to calculate absolute humidity, were measured at the site using the WeatherHawk weather station. See Appendix C for calculation of absolute humidity.

Correcting for the temporal variation of the cosmic-ray flux is the final correction for the raw neutron counts. This correction is performed using counts from neutron monitors along with the following equation:

$$F_i = \frac{N_{avg}}{N_{nm}} \tag{4.4}$$

where N_{avg} is the average neutron monitor count rate during the study period and N_{nm} is the specific hourly neutron monitor count rate at the time of interest. Data from the neutron monitor at Fort Smith (60.02 ˚N, -111.93 ˚W), NWT, Canada, was used in this study. The Fort Smith data was obtained from the NMDB database (www.nmdb.eu). Finally, since neutron fluxes vary with geographic location, the corrected moderated neutron data was scaled relative to high latitude sea level (HLSL). A publically accessible online neutron flux scaling calculator (http://www.seutest.com/cgi-bin/FluxCalculator.cgi) was used to scale the Saskatoon site based on the latitude, longitude, and elevation. The calculated scaling factor for the study

location was 1.59. The corrected moderated neutron counts were then multiplied by the scaling factor and averaged over 7 hours. A seven-hour running average was used for the moderated neutron intensity counts in order to reduce the inherent noise of the hourly moderated neutron data and reduce measurement uncertainty, yet still allow responses to precipitation events to be observed (Zreda et al., 2008).

4.4.4 Snow surveys

Snow surveys were performed periodically in the field each winter within the estimated CRP measurement footprint. During the 2013/14 winter, seven surveys consisting of 18 sampling points were completed. Throughout the 2014/15 winter, eleven surveys composed of 36 sampling points were performed. The SWE sampling points were evenly spaced along each of the individual soil sampling radials, 25 m, 75 m, and 200 m, away from the CRP. The sampling radials are unevenly spaced away from the CRP to allow for the calculation of a simple arithmetic mean of SWE based on the non-linear decreasing sensitivity of the CRP with increasing distance away from the probe (Zreda et al., 2008). Snow cores were collected for SWE using a Meteorological Service of Canada (MSC) snow tube with an inner diameter of 7.04 cm. The cores were carefully transferred to plastic bags, sealed, and transported to the lab for processing. The depth of snow was measured in situ at each sampling location during the snow survey.

4.4.5 Snow depth data

Snow depth data from two reference sites were used for comparison to the snow surveys and CRP data. These were the SRC site and Saskatoon Airport Reference Climate Station (RCS) site (52.1736˚, -106.7189˚), located approximately 2.4 and 8.2 km from the CRP.

At both reference sites, snow depths were measured using a SR50 Sonic Ranging Sensor (Campbell Scientific, Canada). Manual readings with measuring sticks were also performed occasionally at the SRC site.

The snow depth data were converted to SWE values in order to compare to the snow surveys and CRP data. Shook and Gray (1994) studied shallow snow covers (less than 60 cm) in the province of Saskatchewan over 6 years and found the following linear relationship for predicting SWE from snow depth:

$$SWE = 2.39D + 2.05 \quad (4.5)$$

where D is snow depth in cm and SWE is in mm. Equation 4.5 was used to estimate SWE using the snow depth data from the two reference sites. Although the SRC and Saskatoon Airport RCS sites are located a few kilometers away from the study site, comparing estimated SWE from these reference sites to SWE estimated from the CRP is still useful if we look only at the overall trend of snow accumulation.

4.5 Results and Discussion

4.5.1 Snow surveys and moderated neutron intensity

Moderated neutron intensity recorded by the CRP and SWE from snow surveys are shown in Figure 4.2. According to the field snow surveys from both winters (2013/14 and 2014/15), the measured mean SWE peaked at 64.7 mm in 2013/14 and 53.7 mm in 2014/15. The SWE varied significantly throughout the field between individual sampling locations, despite the study site being relatively homogeneous. Box plots of the snow surveys from both winters can be seen in Appendix B. The standard deviation (STD) of SWE for the snow surveys ranged from 5.7 to 18.1 mm in 2013/14 and 2.5 to 10.7 mm in 2014/15. It should be noted that the final five mean SWE values for 2014/15 include the addition of a shallow basal ice layer

that was observed along the soil surface, below the entire snowpack. The ice layer formed after a warm period near the end of January 2015 and was present at each SWE sampling location. The ice layer was too dense for the teeth of the snow tube to cut through, thus the depth of ice was recorded. An average ice layer depth of 1 cm was observed during the last 5 snow surveys. The ice water equivalent was calculated from an assumed density of 0.916 g cm^{-3}, found by Hobbs (1974) to be the average density of ice. A value of 9.2 mm was then added to the mean SWE measured during the final 5 snow surveys of 2014/15.

Early in both winters (early November), the moderated neutron intensity decreased quite drastically in response to the first snow events of the season. These results are consistent with Desilets et al. (2010) who, although did not have precipitation data, found that observed snowfall events caused quick decreases in moderated neutron intensity. The first cluster of precipitation events and first significant decrease in moderated neutron intensity in 2014/15 (Figure 4.2) represent rainfall events. The second distinct decrease in moderated neutron intensity, in late November 2014/15, was caused by snowfall events. In Figure 4.2, all of the precipitation events for 2013/14 were snowfall events.

In general, moderated neutron intensity shows an expected negative relationship with both precipitation events and SWE, resulting in decreased moderated neutron intensity and increased mean SWE in response to precipitation. A relatively strong negative correlation between mean SWE and the moderated neutron intensity at the time of snow survey can be seen from the Pearson's correlation coefficients -0.92 and -0.94 for 2013/14 and 2014/15, respectively. These correlations show there is potential for predicting SWE from moderated neutron intensity measured above the snowpack.

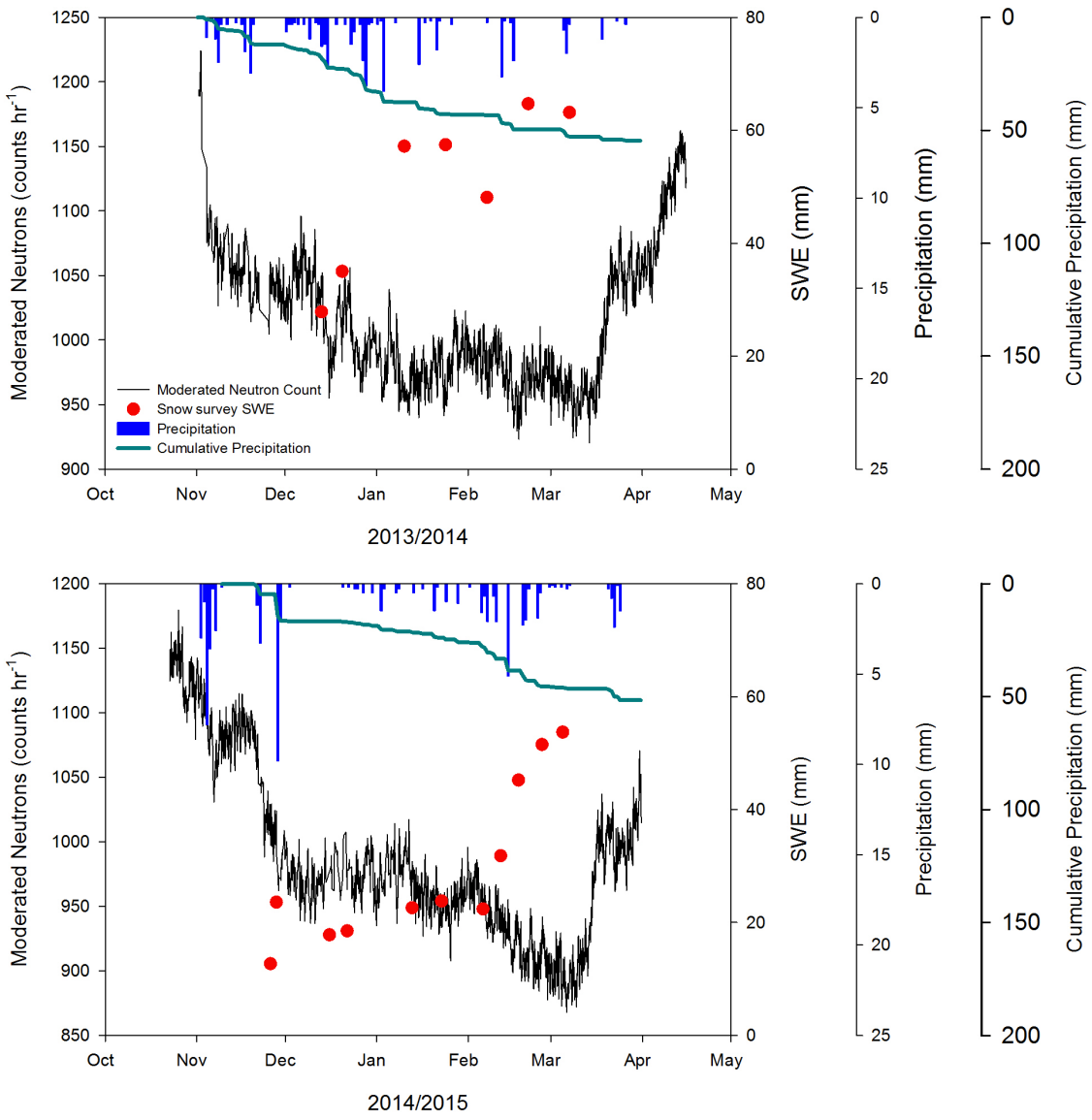

Figure 4.2. Moderated neutron intensity and snow survey SWE for 2013/14 (top) and 2014/15 (bottom). Precipitation sourced from SRC site and represents daily precipitation.

4.5.2 Regression of moderated neutron intensity and SWE

Simple linear regression was performed on the manually measured SWE values and the corresponding moderated neutron intensity during the snow survey. Initial regressions showed that both 2013/14 and 2014/15 had similar regression slopes but quite different intercepts (Figure B.2 in Appendix B). The difference in intercepts was attributed to the differences in soil water storage in the upper soil profile prior to snowfall. The previously mentioned calculated difference in soil water storage in the top 10 cm of the soil profile of 23.8 mm was added to the SWE values of 2014/15 and linear regression was repeated. The added soil water storage caused the 2014/15 linear regression line to match more closely with the regression line for 2013/14. This result indicates that the CRP reading is still being affected by water present in the upper soil profile despite the presence of a snowpack. Thus, knowledge of the initial or background soil water storage in the top of the soil profile before each winter is important for predicting SWE from moderated neutron intensity from year to year. However, the combined measurement depth of the CRP in the snowpack and underlying soil is not fully known. With no standing water covering the soil surface, the CRP measurement depth is thought to range from 70 cm (dry soil) to 12 cm (saturated soil) (Zreda et al., 2008). In pure water, Franz et al. (2012a) found the effective measurement depth to be ~58 mm, i.e. the CRP measurement becomes saturated when more than 58 mm of water is above the soil surface. The effective measurement depth is considered the depth at which 86% (two e-folds) of the measured neutrons originate assuming an exponential decrease in neutron intensity with depth. In our case, we observed a CRP response to SWE values of greater than 70 mm, when including antecedent soil water in the upper soil profile, during the 2014/15 winter. Since snow is substantially more porous and has a lower density than liquid water, neutrons may be

able to penetrate deeper in snow packs (> 58 mm) and interact with the water near the soil surface when the snow pack is shallow.

After correcting for soil water storage, the 2013/14 and 2014/15 manually measured SWE and moderated neutron intensity values were combined to form one dataset and simple linear regression was completed. Figure 4.3 displays the 2013/14 and 2014/15 combined data and regression, along with the separate linear regression lines for 2013/14 and 2014/15. The r^2 of the 2013/14 and 2014/15 combined regression is 0.80. The linear regression and relationship of the SWE and moderated neutron intensity data differs from the exponential relationship that Kodama et al. (1979) found and employed for estimating SWE from moderated neutron intensity. An exponential curve was fit to the 2013/14 and 2014/15 combined data, but the r^2 was not improved drastically compared to the linear regression, thus the simpler linear regression was used for modeling SWE from moderated neutrons. The error bars in Figure 4.3, representing standard deviation of manually measured SWE, generally overlap their associated regression line. This indicates that the linear regression captures the variability revealed by the manual snow surveys.

The individual regression curve for the 2013/14 data is shown in Figure 4.4. The best-fit linear regression equation for the 2013/14 data is $y = -0.3374x + 380.86$ with an r^2 of 0.84. The similarity of the 2013/14 regression curve (Figure 4.4) to the 2013/14 and 2014/15 combined regression curve can also be seen from Figure 4.3. Due to the similarity between the two curves, the 2013/14 curve was used for estimating SWE in 2014/15. This similarity between the regression lines indicates that the slope of the model is not affected by differences in soil water storage near the soil surface.

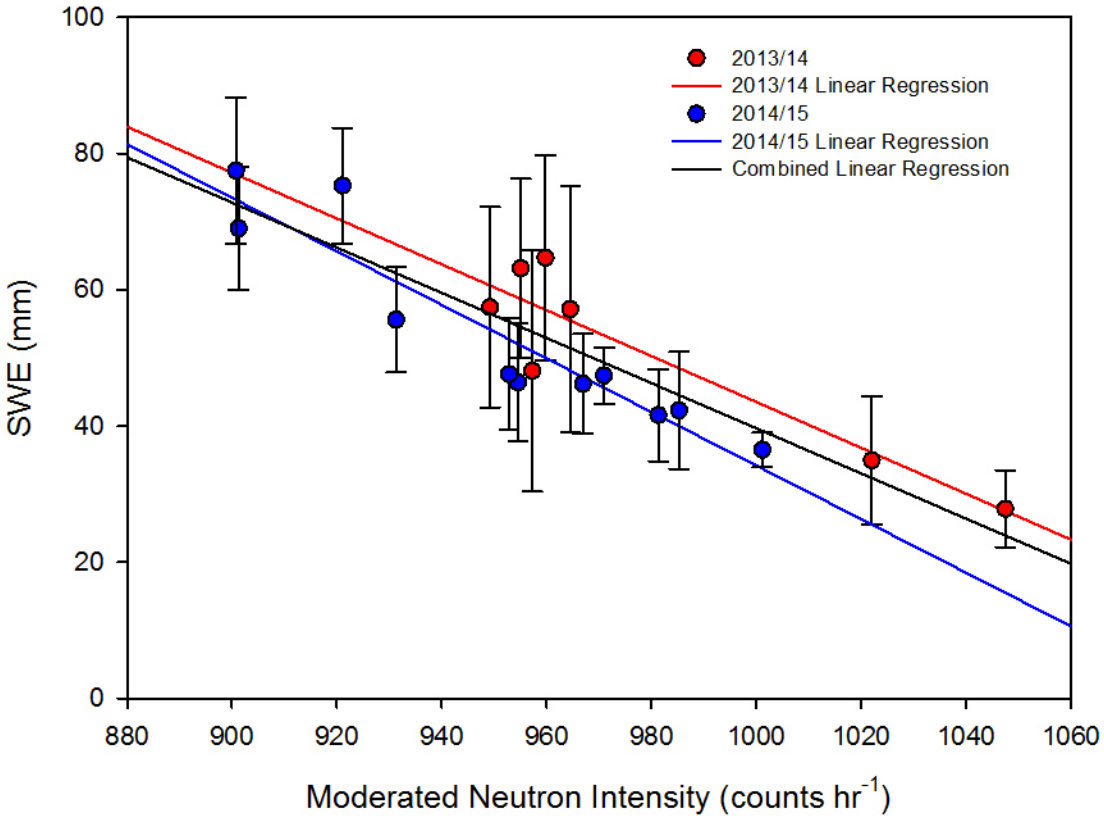

Figure 4.3. Linear regression of 2013/14, 2014/15, and combined measured SWE and corresponding moderation neutron intensity. SWE for 2014/15 is adjusted for soil water storage in top of the soil profile and error bars represent standard deviation of SWE.

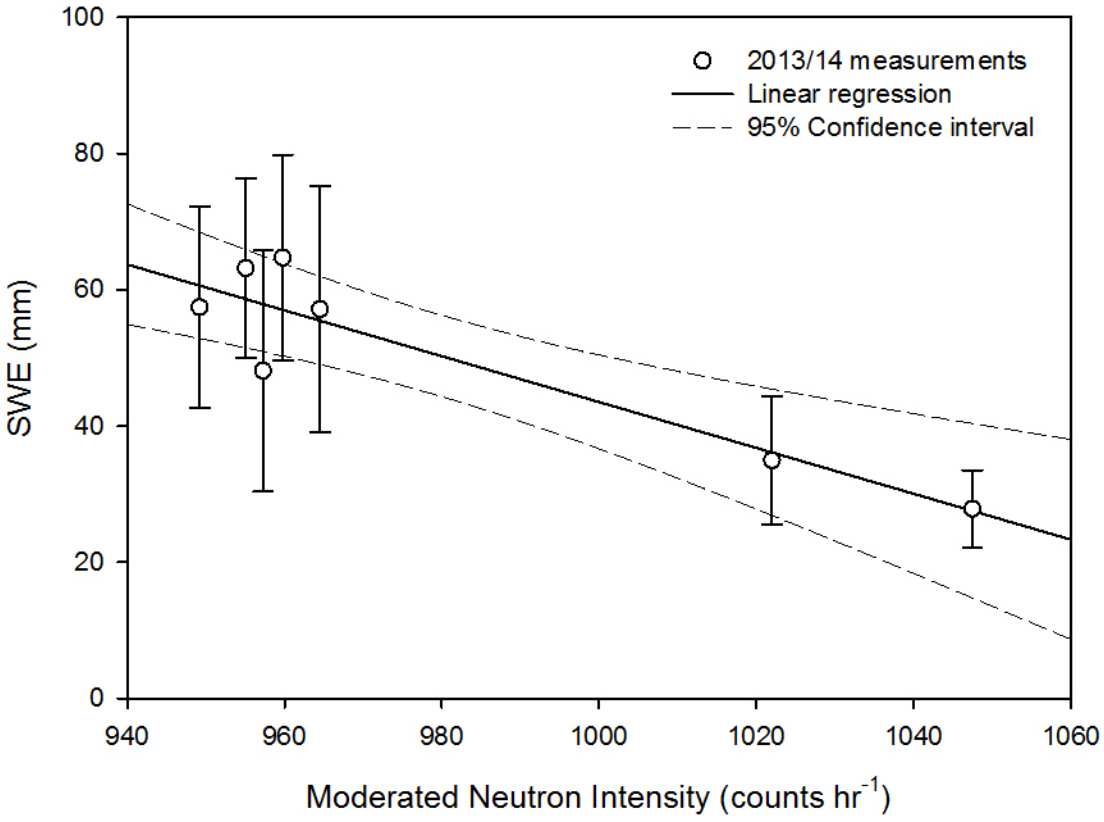

Figure 4.4. Linear regression of 2013/14 measured SWE and corresponding moderated neutron intensity. Error bars represent standard deviation of SWE.

4.5.3 Estimating SWE from moderated neutron intensity above snowpack

The CRP estimated SWE from moderated neutron intensity measurements for both 2013/14 and 2014/15 winters are shown in Figure 4.5. The 2013/14 regression equation was used to estimate SWE based on the moderated neutron intensity in the form of:

$$SWE_{CRP} = -0.3374(N_{COR}) + 380.86 \quad (4.6)$$

where SWE_{CRP} is in mm and N_{COR} is the corrected and scaled moderated neutron intensity. A correction for the difference in soil water storage between 2013/14 and 2014/15 was applied when estimating SWE for 2014/15 by subtracting 23.8 mm from the calculated SWE_{CRP}.

For both winters, the CRP-estimated SWE matched the manually measured SWE well. Of course for 2013/14 the manually measured SWE corresponds nicely to the CRP-estimated SWE since the regression equation from 2013/14 was used for SWE prediction. Nevertheless, the CRP-estimated SWE in 2013/14 display good responses to precipitation, with an increase or peak in estimated SWE occurring at approximately the same time as snowfall events. CRP-estimated SWE for 2014/15 agrees with the manually measured SWE, but not as well as 2013/14. Again, snowfall events in 2014/15 resulted in an increase in SWE estimated from the CRP. In particular, the snowfall event in later March 2015 caused a clear response from the CRP-estimated SWE after the majority of the snowpack in the field was melted in mid-March. The root-mean-squared error (RMSE) and mean absolute error for the 2014/15 CRP-estimated SWE is 7.7 and 6.7 mm, respectively. These error results are comparable to Rasmussen et al. (2012), who found an RMSE of 5.1 mm between SWE estimated from snow depth and from a CRP.

Snowpack melt occurred during both winters, brought about by warmer temperatures and consistent solar radiation, with significant melts occurring in February 2014 and January 2015. The CRP-estimated SWE responded to the melt in February 2014 with a noticeable decrease at the end of January and early February (Figure 4.5). However, the CRP overestimated SWE during the melt period in January 2015 (Figure 4.5). In January 2015 the manually measured SWE was approximately 20mm, while the CRP-estimated SWE was generally between 30 and 40 mm. In late January 2015 the CRP-estimated SWE did finally decrease with a corresponding decrease in manually measured SWE. This overestimation of SWE by the CRP during snowpack melt periods is likely caused by a significant portion of snowmelt water that is removed from the snowpack and infiltrated to the upper soil profile. Any snowmelt water that infiltrated the very top portion of the soil profile would affect the moderated neutron intensity, thus causing the CRP to estimate greater amounts of SWE.

Desilets et al. (2010) also witnessed an overestimation of SWE by the CRP following a snowmelt period. Nearly all of the snowpacks they studied appeared to have melted close to the end of their winter study season followed by a large snowfall event causing a rapid increase in CRP-predicted SWE. Manual measurements of SWE around the CRP location gave a mean of roughly 25 mm, while the CRP-estimated SWE was around 55 mm (Figure 2 in Desilets et al., 2010). This CRP overestimation of SWE could also be attributed to snowmelt water remaining in the top of the soil profile and decreasing the moderated neutron intensity.

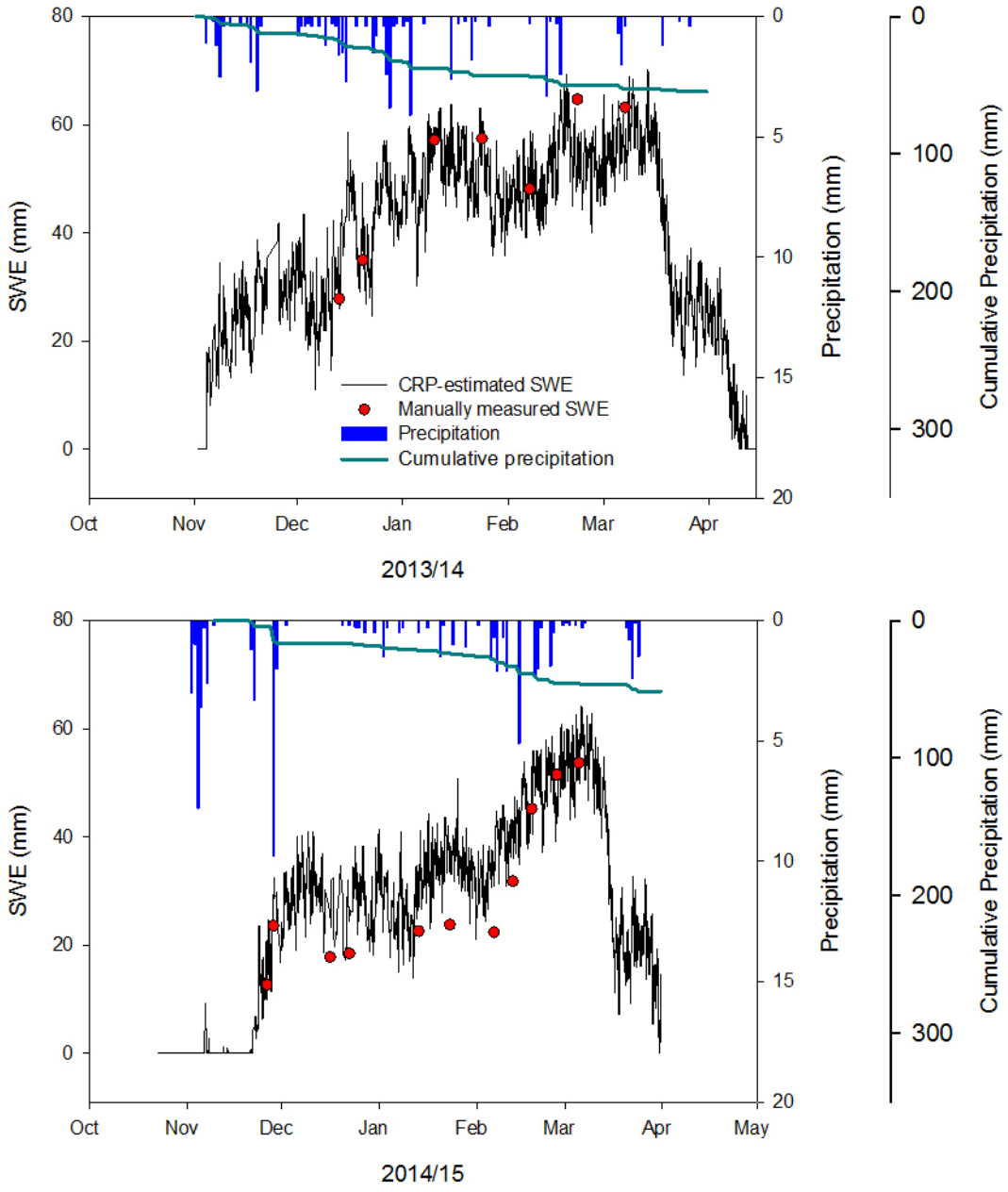

Figure 4.5. 2013/14 (top) and 2014/15 (bottom) CRP-estimated SWE and manually measured SWE.

4.5.4 CRP and snow depth estimated SWE

The CRP-estimated SWE was also compared to estimated SWE from snow depth measurements at two different reference sites near the study site. Figure 4.6 contains the CRP-estimated SWE along with SWE estimated from the SRC and Saskatoon Airport RCS sites. As mentioned earlier, the SRC site is roughly 2 km away from the study site and the Saskatoon Airport RCS site is approximately 8 km away. The reference sites are similar to the study site in the way that all three are open areas containing little to no trees. The SRC site, located in the middle of an agricultural field and nearest to the study site, is very similar to the CRP location in terms of topography and the surrounding area. It is difficult to fully compare the snow depth results to the CRP-modeled SWE since the two measurement sites are located some distance from the CRP and only a single point measurement was made at each of these reference sites. Thus, the snow depth measurements might not be accurate or spatially representative for SWE, but they do allow the examination of the snowpack dynamics in this region.

Looking at Figure 4.6, it can be seen that the overall trend SWE for both winters at the SRC and Saskatoon Airport RCS sites is quite close to the CRP-estimated SWE. At the beginning of each winter SWE appears at very similar times at all three sites. Increases in SWE also appear at comparable times at all sites. The aforementioned melt periods in January and February of each winter appear more noticeable in the SRC and Saskatoon Airport RCS estimates than in the CRP estimates. In February 2014 it can be seen that the SRC-estimated SWE is consistently lower than the CRP-estimated SWE. Higher SWE at the study site could be attributed to increased accumulation of snow along the irrigation line in the center of the CRP study site possibly caused by wind redistribution.

It is also interesting to note the late accumulation of snow near the end of March 2015. All three sites show an increase in SWE from the final snowfall event at the end of the winter in

2015. Despite all three sites being over 2 km away from each other and the strong spatial variability of SWE, the general trend is comparable signifying that the CRP is performing well in terms of estimating SWE.

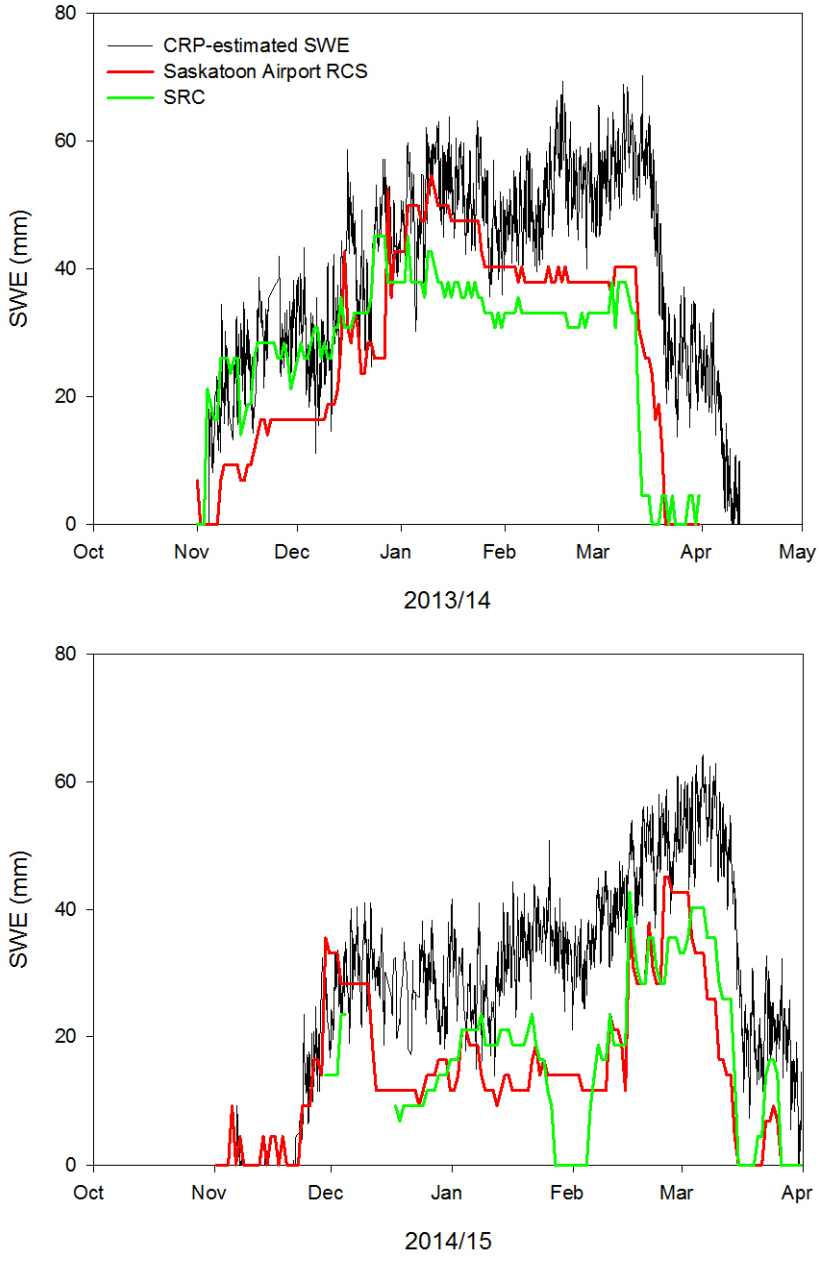

Figure 4.6. 2013/14 (top) and 2014/15 (bottom) CRP-estimated SWE and SWE estimated from snow depth.

4.6 Conclusions

A simple empirical equation for estimating SWE with the use of a cosmic-ray soil moisture probe was presented. It was found that the relationship between above-ground moderated neutron intensity and manually measured field SWE was well represented by a negative linear function. CRP-estimated SWE corresponded well with snow surveys performed inside the CRP's measurement footprint. SWE estimates based on snow depth measurements at two sites near the study site were also in accordance with the CRP-estimated SWE. Overall, the presented equation performed favourable with regards to providing an estimate of average field SWE at this agricultural study site.

There are several advantages associated with measuring SWE using a CRP. The measurement footprint of the CRP (~300 m radius) is appealing since it provides a measurement scale between that of the point scale (snow tubes, snow pillows) and large scale (remote sensing). The CRP can be installed in remote locations where consistent snow surveys are not possible. It is far less laborious to estimate SWE passively using the CRP than to conduct field-scale snow surveys. Also, the CRP can provide a continuous estimate of SWE throughout the winter season.

One apparent limitation with using the CRP to estimate SWE arises from the occurrence of considerable snowmelt during the winter months. Significant snowmelt occurred in both of the studied winter seasons and both situations caused the CRP to overestimate SWE. Hydrogen molecules affect moderated neutron intensity, thus any melted snow is still recognized by the CRP despite not actually representing snow (SWE) in the field. Thus, monitoring SWE with the CRP might be limited to cold, pre-melt SWE. However, it appears that it requires substantial snowpack melt in order for the CRP to overestimate SWE.

Similar to the way the moderated neutron intensity is affected by snowmelt water, the CRP measurement is also influenced by the soil water storage in the top of the soil profile beneath the snowpack being measured. CRPs may overestimate SWE by measuring water in soil just below the snow cover. This overestimation of SWE can cause issues with estimating snowmelt infiltration and runoff. Significant overestimation of snowmelt infiltration can occur when SWE is overestimated and soil water is underestimated (Gray et al., 2001). Knowing the soil water storage in the upper soil profile is important when applying the presented empirical function at other sites. Differences in soil water storage in the top 10 cm of the soil profile between the two winter seasons in this study clearly showed the effect that water near the soil surface has on the CRP measurement. Therefore, it is important to have a measurement or estimate of the soil water storage in the upper soil profile before snowfall accumulation occurs. This measurement of soil water storage could be measured by the CRP if installed and calibrated before snowfall or in-situ soil moisture probes could be used at the soil surface until freezing. Better understanding the depth to which water within the top of the soil profile affects the CRP reading when a snowpack is present should be looked at in future studies. Other future research should focus on assessing the performance of the empirical relationship at other sites similar to this agricultural study site as well as other forested sites with increased vegetation and snowfall interception.

5. SUMMARY AND CONCLUSIONS

5.1 Summary of findings

Accurate SWC and SWE data are clearly needed to increase the accuracy of climate and flood predictions, improve agriculture productivity, and monitor reclamation progress on industry disturbed land. The need for this data increases when trying to predict changes in weather patterns and extreme weather events from climate change which in turn has potential detrimental effects on agriculture production and food security worldwide (Wheeler and Braun, 2013). Additionally to accurate data, spatially relevant SWC and SWE data are needed. The CRP, with its wide area measurement footprint (300 m radius), can provide SWC readings when a resolution between point- and large-scale measurements is needed. The CRP also has the potential to be a useful instrument for monitoring landscape-scale SWE. Thus, improved understanding of the accuracy and applications of the CRP in different environments can lead to more accurate and spatially relevant SWC and SWE data collection.

In Chapter 3, the SWC measurement accuracy of the CRP was evaluated at a highly heterogeneous oil sand reclamation study site. The reclamation site was composed of multiple test plots of varying soil layer treatments of peat and sand, leading to distinct soil texture heterogeneity. Despite the clear heterogeneity within the 300 m radius measurement footprint, the CRP-estimated SWC readings were close to the SWC estimated from soil samples and an in-situ network of soil moisture probes. Slight overestimation of SWC by the CRP was observed which was attributed to surface water accumulating after precipitation events. Due to high organic matter and water contents at the reclamation site, the estimated measurement depth of the CRP was relatively shallow (~15 cm). Due to the decreasing sensitivity of the CRP as distance from the prove increases, vertical (depth) and horizontal weighting of the SWC from

soil samples and in-situ soil moisture probes were required for comparing to the CRP-measured SWC. Using the CRP-measured SWC to optimize model parameters, we were able to simulate the SWC at the test plot scale within the probe's measurement footprint, essentially "unweighting" or downscaling the CRP reading.

In Chapter 4, the potential for monitoring SWE with the CRP was evaluated at an agricultural field in Saskatchewan. A negative correlation was observed between CRP-measured neutrons and manually measured SWE from snow surveys conducted over the course of one winter. An empirical linear calibration function was developed from this neutron vs. SWE relationship in order to estimate SWE from CRP-measured neutrons. During the year following calibration, CRP-estimated SWE compared closely to snow surveys. The CRP-estimated SWE also correlated well with snow depth-estimates SWE at other locations with a few kilometers of the study site. It was found that the CRP reading was affected soil water in the top of the soil profile below the snowpacks. Thus, measurement of the antecedent soil water content in the upper soil profile prior to snowpack formation was needed to adjust the calibration function for use in the second winter. Also, snowmelt during the winter led to overestimation of SWE by the CRP.

5.2 Conclusions

The results from the research in this thesis display that the CRP can be a useful instrument for monitoring SWC and SWE at a landscape-scale. The performance of the CRP at the oil sand reclamation study site shows that it can provide accurate SWC measurements at very heterogeneous sites. Inaccuracies might occur when standing water is present within the measurement footprint. The successful calibration of the CRP for monitoring SWE displays its ability to provide year-round monitoring in climate regions with seasonal snow cover.

Overestimation of SWE may occur from ice layers beneath the snowpack caused from mid-winter melting. Besides relatively accurate estimates of SWC and SWE at a landscape-scale, other advantages are associated with the CRP including a continuous and non-invasive measurement. Additionally, CRP data can be easily collected via satellite, thus installation and measurement at remote locations is achievable.

It is apparent from the research in this thesis that some limitations are involved with the use of the CRP and must be acknowledged. Although the CRP provides an area average SWC reading at a landscape-scale, the measurement is a weighted average. At certain sites with high heterogeneity, a weighted average may not represent the actual average SWC. We were able to use modeling to "unweight" the CRP-measured SWC because the heterogeneity of our study site was known. Without knowledge of the spatial heterogeneity of the soil, it would be difficult to "unweight" the CRP-measured SWC. The measurement depth can be an additional limitation. Due to the high organic and water content at the reclamation study site, the estimated CRP measurement depth was on average approximately 15 cm. In certain cases, for example when plants have deeper rooting zones, a measurement depth of >15 cm might be more relevant. When using the CRP for monitoring SWE, mid-winter melting appears to be the greatest limitation for accurate results. Because the CRP-measured neutrons are affected by all hydrogen within the footprint, ice layers formed below the snowpack influence the aboveground neutron cloud. However, the formation of ice layers below the snowpack may not be an issue if the goal is to know how much total (snow and ice) water equivalent is present above the soil surface. Despite the drawbacks involved with the use of the CRP, this research shows that it can provide, at a landscape-scale, accurate estimates of SWC at highly variable sites as well as accurately monitor SWE.

5.3 Future research

Part of the first research study (Chapter 3) in this thesis involved evaluating the potential to "unweight" the CRP-measured SWC. Downscaling or unweighting the CRP-measured SWC can be beneficial when the true total average SWC or average of a small section inside the footprint at heterogeneous sites is required. The downscaling method involving modeling proposed in this thesis should be applied and tested at other heterogeneous sites in order to see if it can be applied at sites with less knowledge of the soil distribution. In Chapter 4, it was observed that the soil water in the upper soil profile below the snowpack affected the CRP-measured neutrons. The depth to which soil water affects the CRP reading when shallow snow cover is present should be further investigated. The calibration of the CRP for monitoring SWE was performed at an agricultural field with relatively shallow snowpacks. Future studies should assess the performance of the presented calibration function at other similar agricultural fields over a longer time period than the one used in this research. The calibration equation should be tested at sites with deeper snow cover, since the maximum level of SWE that can be measured by the CRP was not apparent from this research. The study site in Chapter 4 contained limited vegetation, thus future studies should also aim to monitor SWE with the CRP in areas with greater vegetation and subsequent snowfall interception.

6. REFERENCES

Alberta Environment. 2010. Guidelines for Reclamation to Forest Vegetation in the Athabasca Oil Sands Region, 2nd Edition. Prepared by the Terrestrial Subgroup of the Reclamation Working Group of the Cumulative Environmental Management Association, Fort McMurray, AB.

Archer, D., and D. Stewart. 1995. The installation and use of a snow pillow to monitor snow water equivalent. Water Environ. J. 9(3): 221–230.

Aubert, D., C. Loumagne, and L. Oudin. 2003. Sequential assimilation of soil moisture and streamflow data in a conceptual rainfall–runoff model. J. Hydrol. 280: 145–161.

Baatz, R., H.R. Bogena, H.H. Franssen, J.A. Huisman, W. Qu, C. Montzka, and H. Vereecken. 2014. Calibration of a catchment scale cosmic-ray probe network : A comparison of three parameterization methods. J. Hydrol. 516: 231–244.

Baatz, R., H.R. Bogena, H.-J. Hendricks Franssen, J.A. Huisman, C. Montzka, and H. Vereecken. 2015. An empirical vegetation correction for soil water content quantification using cosmic ray probes. Water Resour. Res. 51(4): 2030–2046.

Barnett, T.P., J.C. Adam, and D.P. Lettenmaier. 2005. Potential impacts of a warming climate on water availability in snow-dominated regions. Nature 438(7066): 303–309.

Bauer, I.E., J.S. Bhatti, C. Swanston, R.K. Wieder, and C.M. Preston. 2009. Organic matter accumulation and community change at the peatland-upland interface: Inferences from 14C and 210Pb dated profiles. Ecosystems 12(4): 636–653.

Beaumont, R.T. 1967. Field Accuracy of Volumetric Snow Samplers at Mt. Hood, Oregon. Phys. Snow Ice Proc. 1(2): 1007–1013.

Bethe, H.A., S.A. Korff, and G. Placzek. 1940. On the interpretation of neutron measurements in cosmic radiation. Phys. Rev. 57: 573–587.

Blonquist, J.M., S.B. Jones, and D. A. Robinson. 2005. Standardizing Characterization of Electromagnetic Water Content Sensors. Vadose Zo. J. 4(4): 1059–1069.

Bloschl, G., C. Reszler, and J. Komma. 2008. A spatially distributed flash flood forecasting model. Environ. Model. Softw. 23(4): 464–478.

Bogena, H.R., M. Herbst, J. a. Huisman, U. Rosenbaum, a. Weuthen, and H. Vereecken. 2010. Potential of Wireless Sensor Networks for Measuring Soil Water Content Variability. Vadose Zo. J. 9(4): 1002-1013.

Bogena, H.R., J.A. Huisman, R. Baatz, H.H. Franssen, and H. Vereecken. 2013. Accuracy of the cosmic-ray soil water content probe in humid forest ecosystems : The worst case scenario. Water Resour. Res. 49: 1–14.

Bolton, D. 1980. The computation of equivalent potential temperature. Mon. Wea. Rev. 108: 1046-1053.

Boyd, D.W., W.R Schriever, and D.A. Taylor. 1981. Snow and buildings. In *D.M. Gray and D.H. Male (eds), Handbook of Snow: Principles, Processes, Management and Use.* Pergamon Press, Toronto, Canada, 562-579.

Brocca, L., F. Melone, T. Moramarco, W. Wagner, V. Naeimi, Z. Bartalis, and S. Hasenauer. 2010. Improving runoff prediction through the assimilation of the ASCAT soil moisture product. Hydrol. Earth Syst. Sci. 14(10): 1881–1893.

Campbell Scientific Inc. 2015. CS616 and CS625 water content reflectometers: Instruction manual [PDF]. http://s.campbellsci.com/documents/ca/manuals/cs616_625_man.pdf

Chang, A.T.C., J.L. Foster, and D.K. Hall. 1987. Nimbus-7 smmr derived global snow cover parameters. Ann. Glaciol. 9: 39–44.

Charpentier, M. A. and P.M. Groffman. 1992. Soil moisture variability within remote sensing pixels. J. Geophys. Res. 97(D17): 18987–18995.

Church, J.E. 1933. Snow surveying: Its principles and possibilities. Geogr. Rev. 23(4): 529–563.

Clifford, D. 2010. Global estimates of snow water equivalent from passive microwave instruments: history, challenges and future developments. Int. J. Remote Sens. 31(14): 3707–3726.

Clyde, G. D. 1932. Circular 99 – Utah snow sampler and scales for measuring water content of snow. Utah State Agricultural College, Utah Agricultural Experiment Station: Logan, Utah.

Coopersmith, E., M. Cosh, and C. Daughtry. 2014. Field-Scale Moisture Estimates Using COSMOS Sensors:A Validation Study with Temporary Networks and Leaf-Area-Indices. J. Hydrol. 519: 637–643.

De Roo, A.P.J., B. Gouweleeuw, J. Thielen, J. Bartholmes, P. Bongioannini-Cerlini, E. Todini, P.D. Bates, M. Horritt, N. Hunter, K. Beven, F. Pappenberger, E. Heise, G. Rivin, M. Hils, A. Hollingsworth, B. Holst, J. Kwadijk, P. Reggiani, M. Van Dijk, K. Sattler, and E. Sprokkereef. 2003. Development of a European flood forecasting system. Int. J. River Basin Manag. 1(1): 49–59.

Derksen, C. 2008. The contribution of AMSR-E 18.7 and 10.7 GHz measurements to improved boreal forest snow water equivalent retrievals. Remote Sens. Environ. 112(5): 2701–2710.

Desilets, D., and M. Zreda. 2003. Spatial and temporal distribution of secondary cosmic-ray nucleon intensities and applications to in situ cosmogenic dating. Earth Planet. Sci. Lett. 206: 21–42.

Desilets, D., M. Zreda, and T.P.A. Ferré. 2010. Nature's neutron probe: Land surface hydrology at an elusive scale with cosmic rays. Water Resour. Res. 46(11): 1-7.

Desilets, D., and M. Zreda. 2013. Footprint diameter for a cosmic-ray soil moisture probe: Theory and Monte Carlo simulations. Water Resour. Res. 49(6): 3566–3575.

Dietz, A.J., C. Kuenzer, U. Gessner, and S. Dech. 2012. Remote sensing of snow – a review of available methods. Int. J. Remote Sens. 33(13): 4094–4134.

Dimitrov, D.D., J.S. Bhatti, and R.F. Grant. 2014. The transition zones (ecotone) between boreal forests and peatlands: Modelling water table along a transition zone between upland black spruce forest and poor forested fen in central Saskatchewan. Ecol. Modell. 274: 57–70.

Dixon, D., and S. Boon. 2012. Comparison of the SnowHydro snow sampler with existing snow tube designs. Hydrol. Process. 26(17): 2555–2562.

Dong, J., J.P. Walker, and P.R. Houser. 2005. Factors affecting remotely sensed snow water equivalent uncertainty. Remote Sens. of Environ. 97: 68-82.

Drusch, M., and P. Viterbo. 2007. Assimilation of Screen-Level Variables in ECMWF's Integrated Forecast System: A Study on the Impact on the Forecast Quality and Analyzed Soil Moisture. Mon. Weather Rev. 135(2): 300–314

Elder, K., W. Rosenthal, and R.E. Davis. 1998. Estimating the spatial distribution of snow water equivalence in a montane watershed. Hydrol. Process. 12: 1793–1808.Hess, R. 2001. Assimilation of screen-level observations by variational soil moisture analysis. Meteorol. Atmos. Phys. 77(1): 145–154.

Fang, X., and J.W. Pomeroy. 2009. Modelling blowing snow redistribution to prairie wetlands. Hydrol. Process. 23: 2557–2569.

Fares, A., and A.K. Alva. 2000. Evaluation of capacitance probes for optimal irrigation of citrus through soil moisture monitoring in an entisol profile. Irrig. Sci. 19(2): 57–64.

Farnes, P.E., N.R. Peterson, B.E. Goodison, and R.P. Richards. 1982. Metrication of manual snow sampling equipment. Proc. 50th Annu. Meet. West. Snow Conf. 120–132.

Fassnacht, S.R., C.M. Heun, J.I. López-Moreno, and J. Latron. 2010. Variability of snow density measurements in the Rio Esera Valley, Pyrenees Mountains, Spain. Cuad. Investig. Geogr. 36(1): 59–72.

Franz, T.E., M. Zreda, T.P. a. Ferre, R. Rosolem, C. Zweck, S. Stillman, X. Zeng, and W.J. Shuttleworth. 2012a. Measurement depth of the cosmic ray soil moisture probe affected by hydrogen from various sources. Water Resour. Res. 48(8): 1–9.

Franz, T.E., M. Zreda, R. Rosolem, and T.P.A. Ferre. 2012b. Field validation of a cosmic-ray neutron Sensor using a distributed sensor network. Vadose Zo. J. 11(4): 1–10.

Franz, T.E., M. Zreda, R. Rosolem, and T.P.A. Ferre. 2013a. A universal calibration function for determination of soil moisture with cosmic-ray neutrons. Hydrol. Earth Syst. Sci. 17(2): 453–460.

Franz, T.E., M. Zreda, R. Rosolem, B.K. Hornbuckle, S.L. Irvin, H. Adams, T.E. Kolb, C. Zweck, and W.J. Shuttleworth. 2013b. Ecosystem-scale measurements of biomass water using cosmic ray neutrons. Geophys. Res. Lett. 40(15): 3929–3933.

Gardner, W. 1986. Water content. In *A. Klute (eds), Methods of Soil Analysis: Part 1 – Physical and Mineralogical Methods*. Soil Science Society of America, Inc., Madison, USA, 493-544.

Goodison, B. E. 1978. Accuracy of snow samplers for measuring shallow snowpacks: an update. Proc. 35th Annu. Meet. East. Snow Conf. 36-49.

Goodison, B E., H.L. Ferguson and G.A. McKay. 1981. Measurement and data analysis. In *D.M. Gray and D.H. Male (eds), Handbook of Snow: Principles, Processes, Management and Use.* Pergamon Press, Toronto, Canada, 191-274.

Goodison BE, Wilson B, Wu K, Metcalfe J. 1984. An inexpensive remote snow-depth gauge: an assessment. Proceedings of the Western Snow Conference 52: 188–191.

Goodison, B.E., J.E. Glynn, K.D. Harvey, and J.E. Slater. 1987. Snow Surveying in Canada: A Perspective. Can. Water Resour. J. 12(2): 27–42.

Goodison B.E., R.A. Metcalfe, R.A. Wilson, K. Jones. 1988. The Canadian automatic snow depth sensor: a performance upgrade. Proceedings of the Western Snow Conference 56: 178–181.

Government of Canada. 2014. Flood forecasting centres across Canada. https://www.ec.gc.ca/eau-water/default.asp?lang=En&n=7BF9B012-1. (Accessed Sept. 2, 2015)

Government of Canada. 2015. Canadian climate norms: 1981-2010 climate normal and averages. http://climate.weather.gc.ca/climate_normals/index_e.html. (Accessed Sept. 2, 2015)

Gray, M., and R.J. Granger. 1985. In situ measurements of moisture and salt movement in freezing soils. Canadian Journal of Earth Sciences. 23(5): 696-704.

Gray, M., and P.G. Landine. 1988. An energy-budget snowmelt model for the Canadian Prairies. Can. J. Earth Sci. 25: 1292–1303.

Gray, D.M., B. Toth, L. Zhao, J.W. Pomeroy, and R.J. Granger. 2001. Estimating areal snowmelt infiltration into frozen soils. Hydrol. Process. 15(16): 3095–3111.

Hendrick, L.D., and R.D. Edge. 1966. Cosmic-ray neutrons near Earth. Phys. Rev. 145(4):1023-1025.

Hess, W.N., E.H. Canfield, and R.E. Lingenfelter. 1961. Cosmic-Ray Neutron Demography. Geophys. Res. 66: 665–677.

Hoeben, R., and P. a Troch. 2000. Assimilation of active microwave observation data for soil moisture profile estimation. Water Resour. Res. 36(10): 2805-2819.

Hoinkes, H. 1967. Glaciology in the international hydrological decade. IAHS Comm. Snow Ice Reports Discuss. 79: 7–16.

Hobbs, P.V. 1974. Ice physics. Oxford University Press. Great Britain, England.

Jacobson, M.D. 2012. Snow Water Equivalent Estimation for a Snow-Covered Prairie Grass Field by GPS Interferometric Reflectometry. Positioning 3: 31–41.

Johnson, E. A. and K. Miyanishi. 2008. Creating new landscapes and ecosystems: the Alberta Oil Sands. Ann. N. Y. Acad. Sci. 1134: 120–45.

Knoll, G.F. 1989. Radiation detection and measurement. John Wiley & Sons, Inc. New York, USA.

Kodama, M., K. Nakai, S. Kawasaki, and M. Wada. 1979. An application of cosmic-ray neutron measurements to the determination of the snow-water equivalent. J. Hydrol. 41: 85–92.

Kohli, M., M. Schron, M. Zreda, U. Scmidt, P. Dietrich, and S. Zacharias. 2015. Footprint characteristics revised for field-scale soil moisture monitoring with cosmic-ray neutrons. J. Hydrol. 6(4): 1–19.

Korres, W., T.G. Reichenau, P. Fiener, C.N. Koyama, H.R. Bogena, T. Cornelissen, R. Baatz, M. Herbst, B. Diekkrüger, H. Vereecken, and K. Schneider. 2015. Spatio-temporal soil moisture patterns – A meta-analysis using plot to catchment scale data. J. Hydrol. 520: 326–341.

Leatherdale, J., D.S. Chanasyk, and S. Quideau. 2012. Soil water regimes of reclaimed upland slopes in the oil sands region of Alberta. Can. J. Soil Sci. 92: 117–129.

Lowder, S.K., Skoet, J. and Singh, S. 2014. What do we really know about the number and distribution of farms and family farms worldwide? Background paper for The State of Food and Agriculture 2014. ESA Working Paper No. 14-02. Rome, FAO.

Mahfouf, J. -F., K. Bergaoui, C. Draper, F. Bouyssel, F. Taillefer, and L. Taseva. 2009. A comparison of two off-line soil analysis schemes for assimilation of screen level observations. J. Geophys. Res. 114(D8): 1–21.

McKay, G. A. and D.M. Gray. 1981. The distribution of snowcover. In *D.M. Gray and D.H. Male (eds), Handbook of Snow: Principles, Processes, Management and Use.* Pergamon Press, Toronto, Canada, 153-190.

Mishra, A.K., and V.P. Singh. 2010. A review of drought concepts. J. Hydrol. 391(1-2): 202–216.

Mohanty, B.P., and T.H. Skaggs. 2001. Spatio-temporal evolution and time-stable characteristics of soil moisture within remote sensing footprints with varying soil, slope, and vegetation. Adv. Water Resour. 24(9-10): 1051–1067.

Nester, T., R. Kirnbauer, J. Parajka, and G. Blöschl. 2012. Evaluating the snow component of a flood forecasting model. Hydrol. Res. 43(6): 762-779.

Ochsner, T.E., M.H. Cosh, R.H. Cuenca, W.A. Dorigo, C.S. Draper, Y. Hagimoto, Y.H. Kerr, E.G. Njoku, E.E. Small, and M. Zreda. 2013. State of the Art in Large-Scale Soil Moisture Monitoring. Soil Sci. Soc. Am. J. 77(6): 1-32.

Paquet, E., M. Laval, L.M. Basalaev, A. Belov, E. Eroshenko, V. Kartyshov, A. Struminsky, and V. Yanke. 2008. An application of cosmic-ray neutron measurements to the determination of the snow-water equivalent. Proc. 30th Int. Cosm. Ray Conf. 1: 761–764.

Pauwels, V.R.N., R. Hoeben, N.E.C. Verhoest, and F.P. De Troch. 2001. The importance of the spatial patterns of remotely sensed soil moisture in the improvement of discharge predictions for small-scale basins through data assimilation. J. Hydrol. 251: 88–102.

Pelowitz, D.B. 2005. MCNPX User's Manual, Version 5. Los Alamos National Laboratory, Los Alamos.

Pomeroy, J.W. and D.M. Gray. 1995. Snowcover: Accumulation, relocation and management. NHRI Science Report No. 7.

Pomeroy, J. W. and B. E. Goodison. 1997. Winter and snow. *In W. G. Bailey, T. R. Oke, and W. R. Rouse eds. The surface climates of Canada.* McGill-Queen's University Press, Montreal, Can. 68-100.

Poscente, M. and T. Charette. 2012. Criteria and indicators framework for oil sands mine reclamation certification. CEMA Final Report. 1-160.

Quiring, S.M., and T.N. Papakryiakou. 2003. An evaluation of agricultural drought indices for the Canadian prairies. Agric. For. Meteorol. 118: 49–62.

Radcliffe, D.E. and J. Simunek. 2010. Soil physics with hydrus: modeling and applications. CRC Press, Boca Raton, U.S.A.

Rasmussen, R., B. Baker, J. Kochendorfer, T. Meyers, S. Landolt, A.P. Fischer, J. Black, J.M. Thériault, P. Kucera, D. Gochis, C. Smith, R. Nitu, M. Hall, K. Ikeda, and E. Gutmann. 2012.

How Well Are We Measuring Snow: The NOAA/FAA/NCAR Winter Precipitation Test Bed. Bull. Am. Meteorol. Soc. 93(6): 811–829.

Robinson, D.A., C.S. Campbell, J.W. Hopmans, B.K. Hornbuckle, S.B. Jones, R. Knight, F. Ogden, J. Selker, and O. Wendroth. 2008. Soil Moisture Measurement for Ecological and Hydrological Watershed-Scale Observatories: A Review. Vadose Zo. J. 7(1): 358–389.

Rosolem, R., W.J. Shuttleworth, M. Zreda, T.E. Franz, X. Zeng, and S.A. Kurc. 2013. The effect of atmospheric water vapor on neutron count in the cosmic-ray soil moisture observing system. J. Hydrometeorol. 14(5): 1659–167.

Roy, A., A. Royer, and R. Turcotte. 2010. Improvement of springtime streamflow simulations in a boreal environment by incorporating snow-covered area derived from remote sensing data. J. Hydrol. 390(1-2): 35–44.

Seidel, K. and J. Matinec. 2004. Remote Sensing in Snow Hydrology: Runoff Modelling Effect of Climate Change. Praxis Publishing, Chichester, UK.

Selker, J.S., L. Thévenaz, H. Huwald, A. Mallet, W. Luxemburg, N. Van De Giesen, M. Stejskal, J. Zeman, M. Westhoff, and M.B. Parlange. 2006. Distributed fiber-optic temperature sensing for hydrologic systems. Water Resour. Res. 42(12): 1–8.

Seuffert, G., H. Wilker, P. Viterbo, M. Drusch, and J.-F. Mahfouf. 2004. The Usage of Screen-Level Parameters and Microwave Brightness Temperature for Soil Moisture Analysis. J. Hydrometeorol. 5: 516–531.

Shook, K. and D. M. Gray. 1994. Determining the snow water equivalent of shallow prairie snowcovers. In *Proceedings of the 51st Eastern Snow Conference*.

Shook, K., and D. M. Gray. 1996. Small-scale spatial structure of shallow snowcovers. Hydrol. Process. 10: 1283–1292.

Shuttleworth, J., R. Rosolem, M. Zreda, and T. Franz. 2013. The COsmic-ray Soil Moisture Interaction Code (COSMIC) for use in data assimilation. Hydrol. Earth Syst. Sci. 17(8): 3205–3217.

Šimůnek, J., M.T. van Genuchten, and M. Šejna. 2008. Development and applications of the HYDRUS and STANMOD software packages and related codes. Vadose Zo. J. 7(2): 587–600.

Steppuhn, H. 1981. Snow and agriculture. In *D.M. Gray and D.H. Male (eds), Handbook of Snow: Principles, Processes, Management and Use.* Pergamon Press, Toronto, Canada, 60-125.

Sturm, M., B. Taras, G.E. Liston, C. Derksen, T. Jonas, and J. Lea. 2010. Estimating Snow Water Equivalent Using Snow Depth Data and Climate Classes. J. Hydrometeorol. 11(6): 1380–1394.

Thirel, G., P. Salamon, P. Burek, and M. Kalas. 2013. Assimilation of MODIS snow cover area data in a distributed hydrological model using the particle filter. Remote Sens. 5(11): 5825–5850.

Turcan, J., and J. S. Loijens. 1975. Accuracy of snow survey data and errors in snow sampler measurements. Proc. 32nd East. Snow. Conf. 2-11.

Turcotte, R., P. Lacombe, C. Dimnik, and J.-P. Villeneuve. 2004. Prévision hydrologique distribuée pour la gestion des barrages publics du Québec. Can. J. Civ. Eng. 31(2): 308–320.

Turcotte, R., T.-C. Fortier Filion, P. Lacombe, V. Fortin, A. Roy, and A. Royer. 2010. Simulation hydrologique des derniers jours de la crue de printemps: le problème de la neige manquante. Hydrol. Sci. J. 55(6): 872–882.

Vachaud, G., A. Passerat de Silans, P. Balabanis, and M. Vauclin. 1985. Temporal stability of spatially measured soil water probability density function. Soil Sci. Soc. Am. J. 49:822–828.

Vereecken, H., J. a. Huisman, H. Bogena, J. Vanderborght, J. a. Vrugt, and J.W. Hopmans. 2008. On the value of soil moisture measurements in vadose zone hydrology: A review. Water Resour. Res. 44(4): 1-21.

Wheeler, T., and J. Von Braun. 2013. Climate change impacts on global food security. Science. 341: 508–513.

Willmott, C.J., and K. Matsuura. 2005. Advantages of the mean absolute error (MAE) over the root mean square error (RMSE) in assessing average model performance. Clim. Res. 30(1): 79–82.

Work, R. A, H.J. Stockwell, T.G. Freeman, and R.T. Beaumont. 1965. Accuracy of field snow studies, western United States, including Alaska. U. S. Army Corps of Engineers, Cold Regions Research and Engineering Lab: Hanover, New Hampshire. 1-43.

Zhu, Z., L. Tan, S. Gao, and Q. Jiao. 2015. Observation on Soil Moisture of Irrigation Cropland by Cosmic-Ray Probe. IEEE Geosci. Remote Sens. Lett. 12(3): 472–476.

Zreda, M., D. Desilets, T.P.A. Ferré, and R.L. Scott. 2008. Measuring soil moisture content non-invasively at intermediate spatial scale using cosmic-ray neutrons. Geophys. Res. Lett. 35(21): 1–5.

Zreda, M., W. Shuttleworth, X. Zeng, C. Zweck, D. Desilets, T. Franz, and R. Rosolem. 2012. COSMOS: The COsmic-ray Soil Moisture Observing System. Hydrol. Earth Syst. Sci. 16(11): 4079–4099.

APPENDICES

APPENDIX A. VARIABILITY OF SOIL WATER CONTENT MEASURED AT ASCS SITE

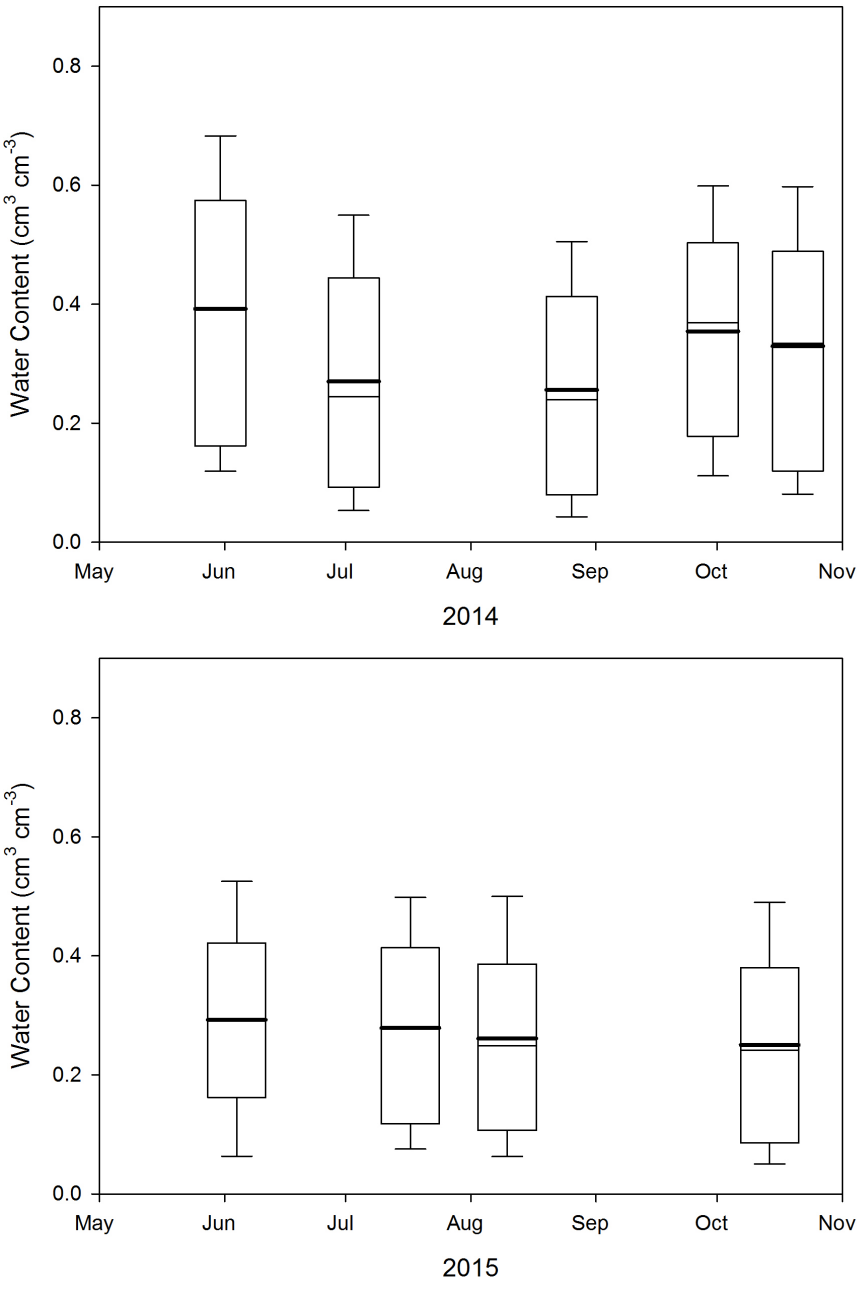

Figure A.1. Box plots displaying the variability of soil water content inside the CRP footprint for the sampling campaigns in 2014 and 2015 at the ASCS site. Soil samples were taken along radials 25, 75, 200, and 300 m away from the CRP. The bolded line represents the mean.

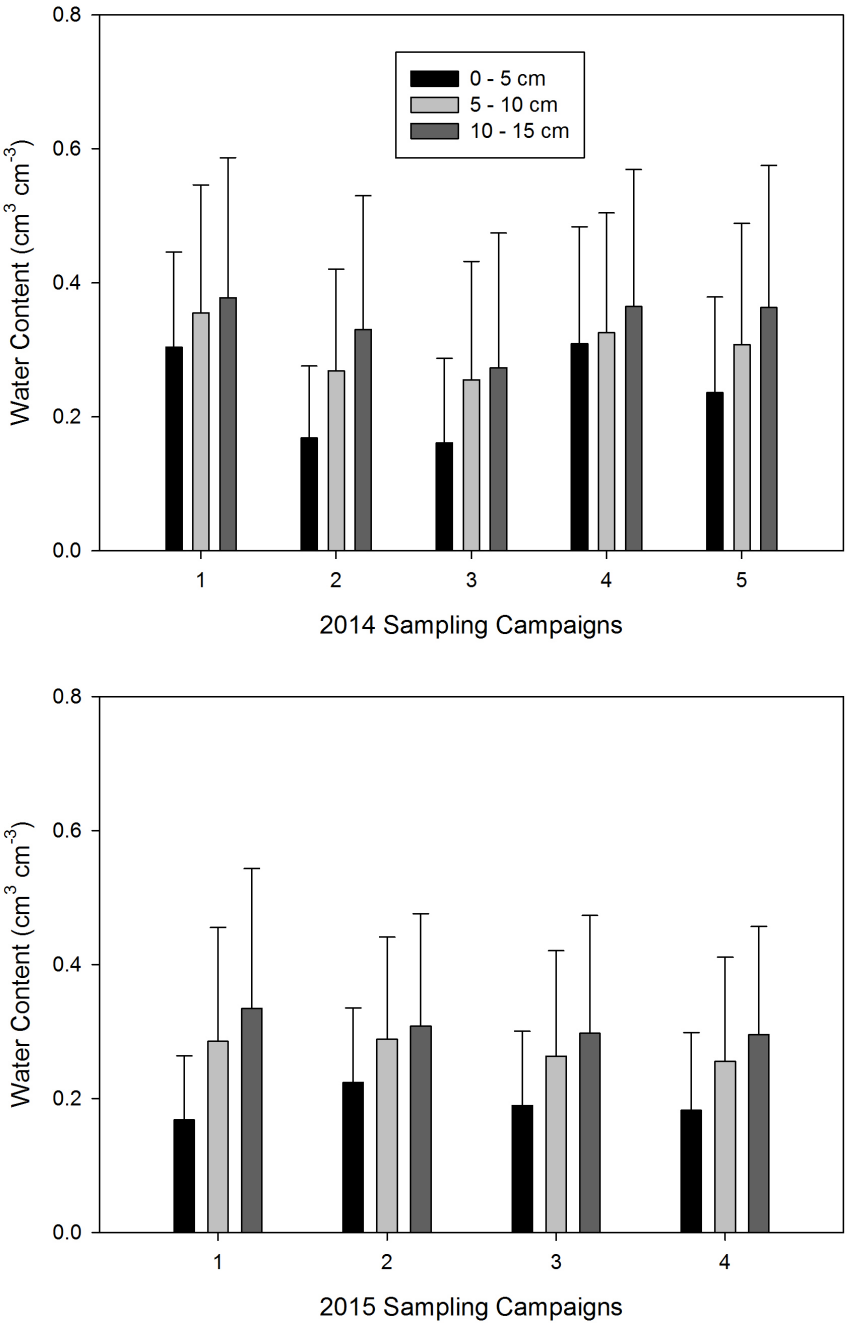

Figure A.2. Mean soil water content of three depths in the CRP footprint at the ASCS site. Only the water contents up to 15 cm are displayed since the estimated depth of the CRP for both 2014 and 2015 summers was approximately 15 cm. The 2014 sampling campaigns were: 1) May 31st, 2) July 3rd, 3) August 28th, 4) September 30th, and 5) October 10th. The 2015 sampling campaigns were: 1) June 4th, 2) July 17th, 3) August 10th, and 4) October 14th. Error bars represent standard deviation.

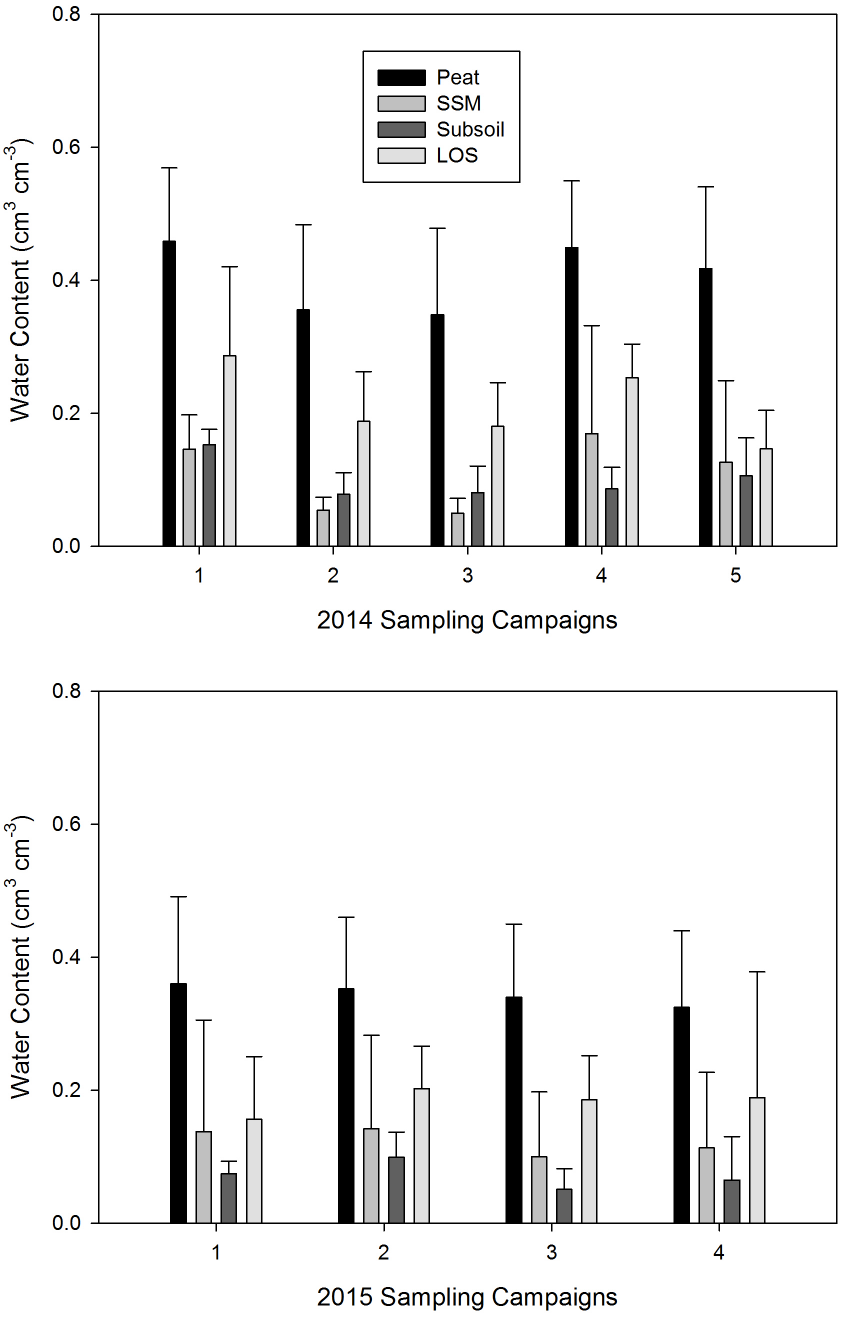

Figure A.3. Mean soil water content of the various cover materials from 0 – 15 cm inside the CRP footprint. The 2014 sampling campaigns were: 1) May 31st, 2) July 3rd, 3) August 28th, 4) September 30th, and 5) October 10th. The 2015 sampling campaigns were: 1) June 4th, 2) July 17th, 3) August 10th, and 4) October 14th. Error bars represent standard deviation.

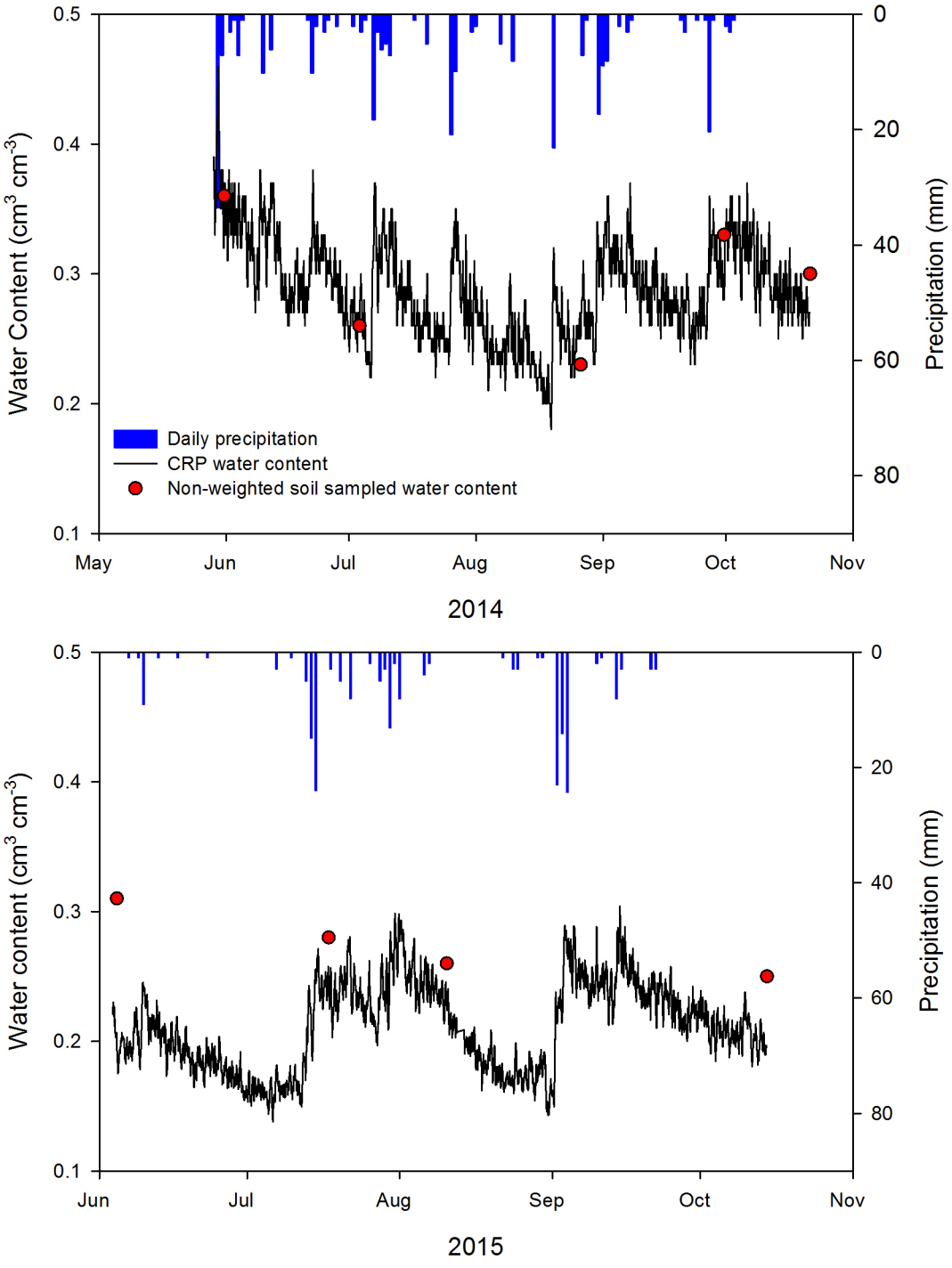

Figure A.4. CRP-measured water content and mean non-weighted soil sampled water content from 0 – 15 cm soil depth in the CRP footprint.

.

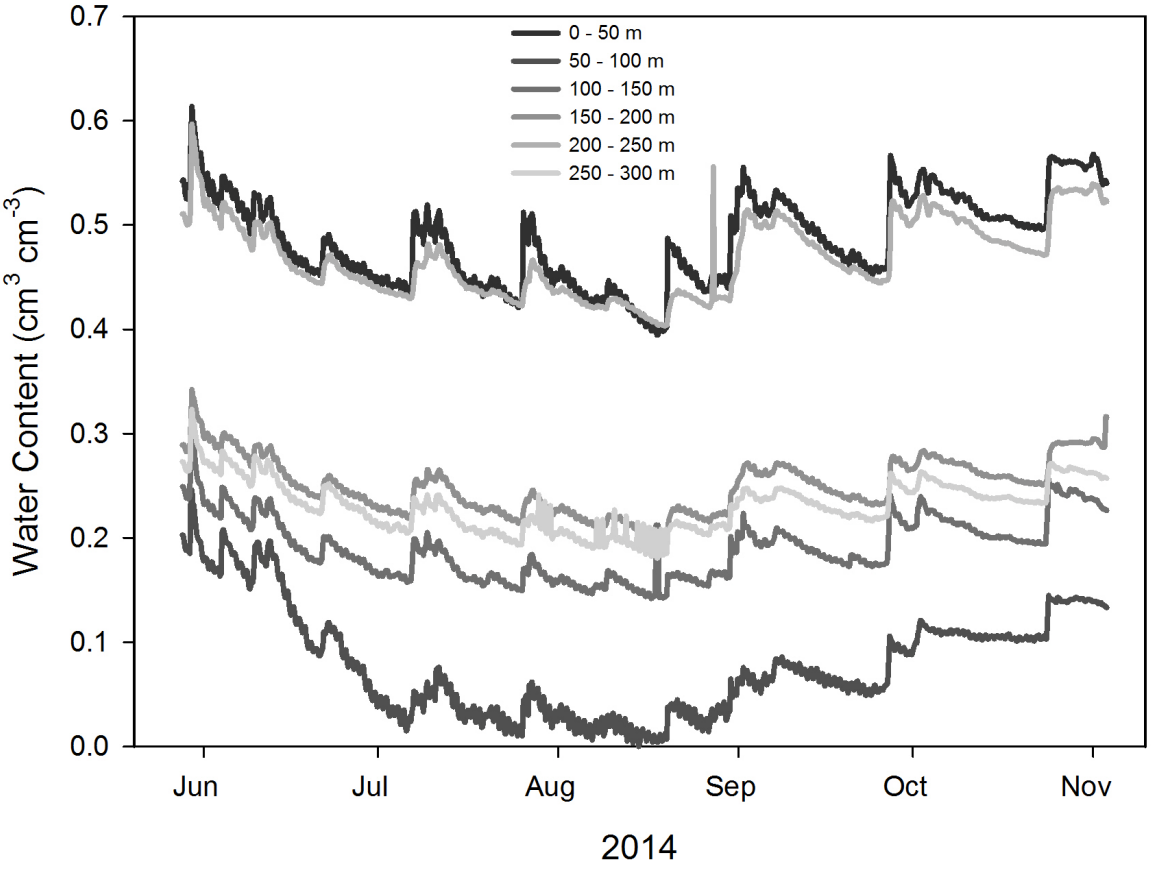

Figure A.5. Mean water content measured by CS616 soil probes inside 50 m radial swaths in the CRP footprint. The probes were installed at 15 cm within the soil profile. The mean water contents of 50 m radial swaths were used to horizontally weight the mean CS616 water content inside the CRP footprint

APPENDIX B. SNOW WATER EQUIVALENT DATA FOR 2013/14 AND 2014/15 FROM THE AGRICULTURE FIELD SITE

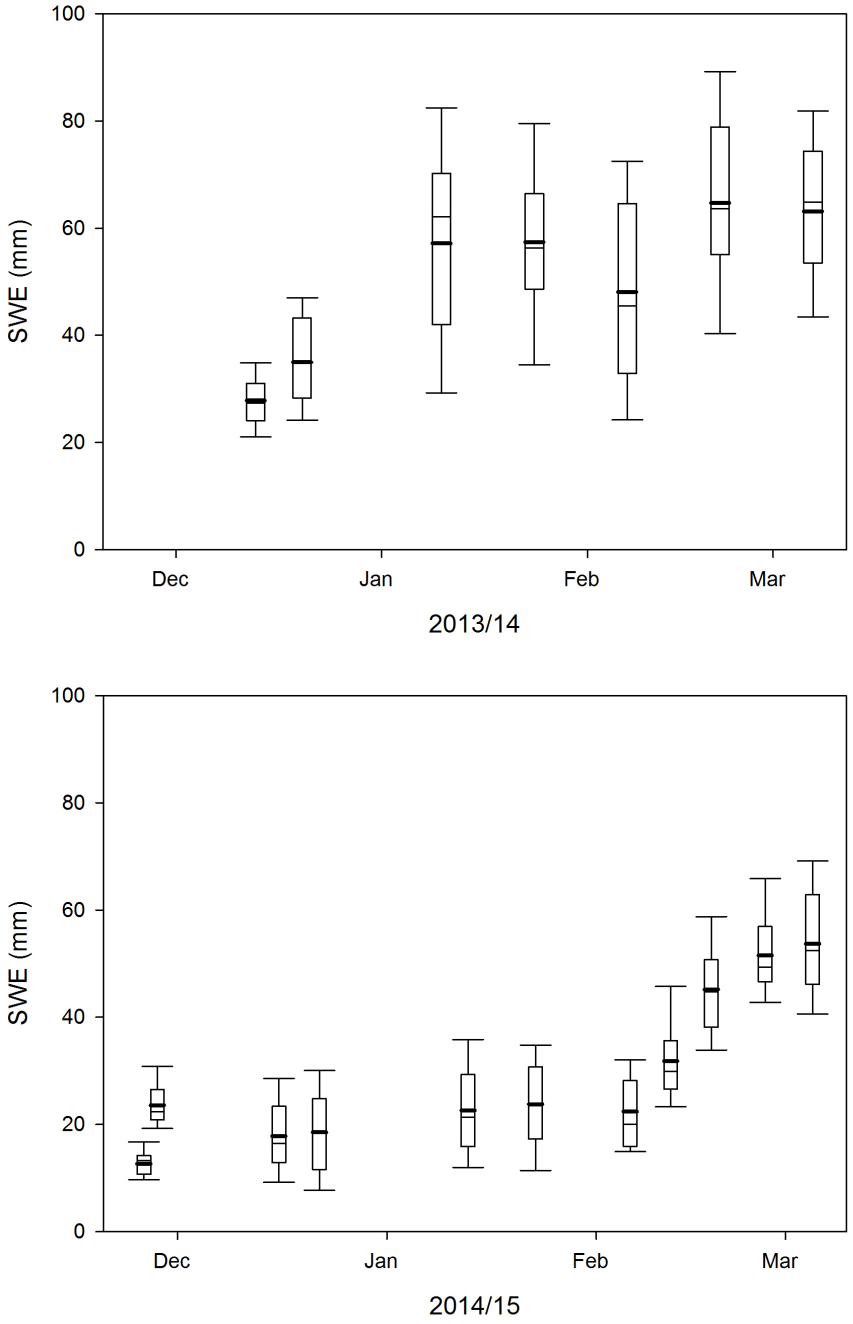

Figure B.1. Box plots showing the variability of SWE during the snow surveys for the 2013/14 and 2014/15 winters at the agriculture study site in Saskatoon, SK. Snow cores were taken along radials 25, 75, and 200 m away from the CRP located in the center of the field. The bold lines represent the mean SWE.

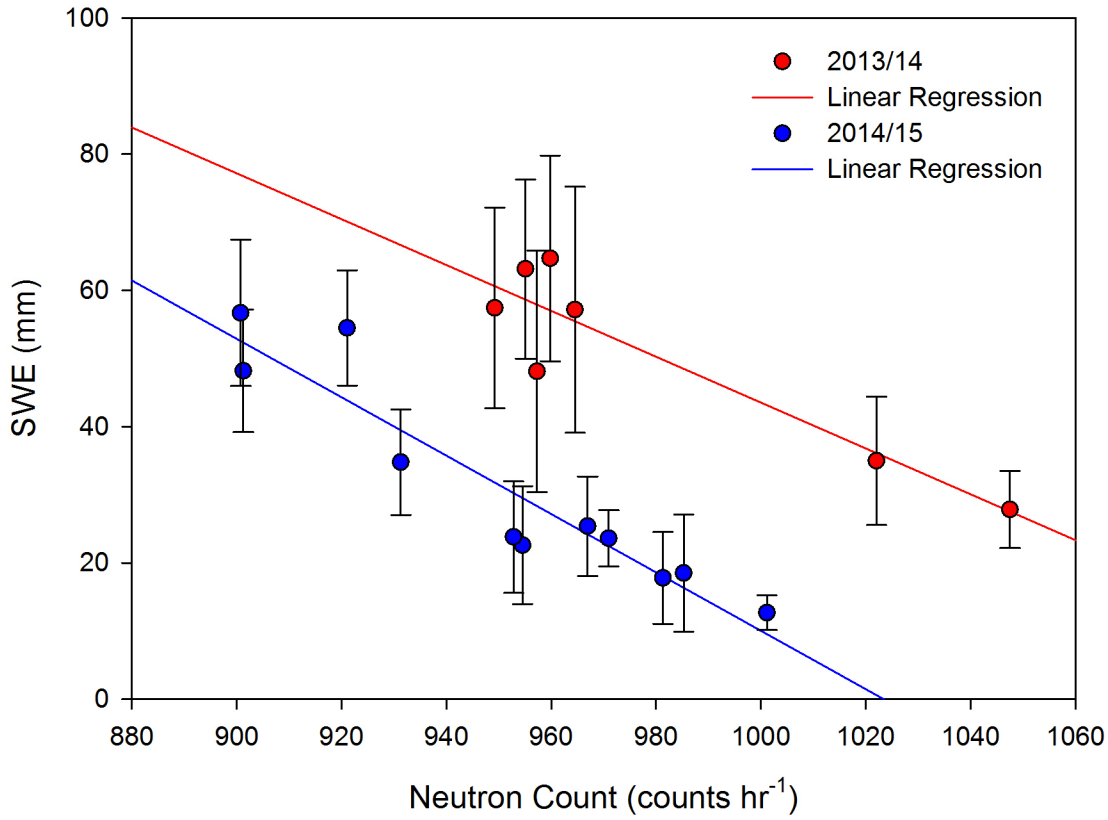

Figure B.2. Linear regression of mean SWE (no offset for soil water storage differences) and moderated neutron intensity for 2013/14 and 2014/15 winters. Errors bars represent standard deviation of SWE.

APPENDIX C. CALCULATION OF ABSOLUTE HUMIDITY FROM MEASUREMENTS OF AIR TEMPERATURE AND RELATIVE HUMIDITY

The method proposed by Rosolem et al. (2013) was used to calculate absolute humidity (p_v, g m^3) from surface measurements in of air temperature and relative humidity in Eq. 3.3 (Chapter 3). First the water vapor pressure at saturation (e_{s0}) is calculated using the method described by Bolton (1980):

$$e_{s0} = 6.112\exp\left(\frac{17.67T_0}{243.5+T_0}\right) \quad \text{(C.1)}$$

where air temperature (T_0) is in ˚C and e_{s0} is in hPa. The actual water vapor pressure (e_0) can then be calculated using the definition of relative humidity (RH_0):

$$e_0 = RH_0 \cdot e_{s0} \quad \text{(C.2)}$$

where RH_0 is in fraction form and e_0 is in hPa.

Finally, absolute humidity (p_v) can be calculated using the ideal gas law and the water vapor pressure:

$$p_v = \frac{e_0}{R_V T_0} \quad \text{(C.3)}$$

where e_0 is now in Pa and T_0 is in K. The parameter R_V is the gas constant for water vapor and is approximately 461.5 J K^{-1} kg^{-1}. The resulting units for p_v in Eq. C.3 are kg m^{-3}. In order to use p_v in Eq. 3.3 the units must be converted to g m^{-3} (i.e. multiply p_v by 1000).

APPENDIX D. INPUTS FOR HYDRUS-1D SIMULATIONS

Table D.1. Set up for HYDRUS-1D simulations of Peat and SSM columns.

HYDRUS-1D Conditions	Peat Column	SSM Column
Main Processes	Simulate: Water Flow	Simulate: Water Flow
Geometry Information	Length Units: cm Number of Soil Materials: 2 Number of Layers for Mass Balances: 2 Decline from Vertical Axes: 1 Depth of Soil Profile (cm): 100	Length Units: cm Number of Soil Materials: 2 Number of Layers for Mass Balances: 2 Decline from Vertical Axes: 1 Depth of Soil Profile (cm): 100
Time Information	Time Units: Days **Time Discretization** Initial Time (day): 0 Final Time (day): 147 Initial Time Step (day): 0.001 Minimum Time Step (day): 0.00005 Maximum Time Step (day): 1 **Time-Variable Boundary Conditions** Number of Time-Variable Boundary Records: 147 **Meteorological Data** Number of Meteorological Records: 147 Hargreaves Formula	Time Units: Days **Time Discretization** Initial Time (day): 0 Final Time (day): 147 Initial Time Step (day): 0.001 Minimum Time Step (day): 0.00005 Maximum Time Step (day): 1 **Time-Variable Boundary Conditions** Number of Time-Variable Boundary Records: 147 **Meteorological Data** Number of Meteorological Records: 147 Hargreaves Formula
Print Information	**Print Options** Print at Regular Time Interval Time Interval (day): 1 Screen Output Print Fluxes (instead of Temp) for Observation Nodes Number of Print Times: 147	**Print Options** Print at Regular Time Interval Time Interval (day): 1 Screen Output Print Fluxes (instead of Temp) for Observation Nodes Number of Print Times: 147
Iteration Criteria	Maximum Number of Iterations: 10 Water Content Tolerance: 0.001 Pressure Head Tolerance (cm): 1 Lower Optimal Iteration Range: 3 Upper Optimal Iteration Range: 7 Lower Time Step Multiplication Factor: 1.3 Upper Time Step Multiplication Factor: 0.7 Lower Limit of the Tension Interval: 0.000001 Upper Limit of the Tension Interval: 10000	Maximum Number of Iterations: 10 Water Content Tolerance: 0.001 Pressure Head Tolerance (cm): 1 Lower Optimal Iteration Range: 3 Upper Optimal Iteration Range: 7 Lower Time Step Multiplication Factor: 1.3 Upper Time Step Multiplication Factor: 0.7 Lower Limit of the Tension Interval: 0.000001 Upper Limit of the Tension Interval: 10000
Soil Hydraulic Model	**Hydraulic Model** Single Porosity Models: van Genuchten – Mualem **Hysteresis:** No hysteresis	**Hydraulic Model** Single Porosity Models: van Genuchten – Mualem **Hysteresis:** No hysteresis
Water Flow Parameters	**Mat 1:** Qr: 0.095	**Mat 1:** Qr: 0.05

	Qs: 0.7 Alpha: 0.042 n: 1.8 Ks (cm/day): 22 I: 0.5 **Mat 2:** Qr: 0.052 Qs: 0.38 Alpha: 0.034 n: 3.98 Ks (cm/day): 500 I: 0.5	Qs: 0.38 Alpha: 0.043 n: 3.03 Ks (cm/day): 200 I: 0.5 **Mat 2:** Qr: 0.052 Qs: 0.38 Alpha: 0.034 n: 3.98 Ks (cm/day): 500 I: 0.5
Water Flow Boundary Conditions	Upper Boundary Condition: Atmospheric BC with Surface Layer Lower Boundary Condition: Free Drainage Initial Condition: In Water Contents	Upper Boundary Condition: Atmospheric BC with Surface Layer Lower Boundary Condition: Free Drainage Initial Condition: In Water Contents
Time Variable Boundary Conditions	See Table D.2	See Table D.2
Meteorological Parameters	Radiation: Potential Radiation Latitude: 57˚N Crop Data: No Crop	Radiation: Potential Radiation Latitude: 57˚N Crop Data: No Crop
Meteorological Conditions	See Table D.2	See Table D.2
Soil Profile Graphical Editor	Peat: 0 – 30 cm Subsoil: 31 – 100 cm Observation node at 8 cm	SSM: 0 – 20 cm Subsoil: 21 – 100 cm Observation node at 8 cm
Soil Profile Summary	Peat: 0.45 cm^3 cm^{-3} (0-30 cm) Subsoil: 0.13 cm^3 cm^{-3} (31-100 cm)	SSM: 0.15 cm^3 cm^{-3} (0-20 cm) Subsoil: 0.13 cm^3 cm^{-3} (31-100 cm)

Table D.2. Meteorological conditions used in HYDRUS-1D simulations.

Time (day)	Precipitation (cm/day)	Temperature Max (˚C)	Temperature Min (˚C)
1	0.0	11.2	7.9
2	3.4	9.6	5.6
3	0.7	15.6	7.6
4	0.0	18.7	6.3
5	0.3	20	8.1
6	0.1	25.1	9.3
7	0.7	18.4	7.9
8	0.1	11.5	6.8
9	0.0	12	4.7
10	0.0	14.8	3.8
11	0.0	16.8	5.2
12	0.0	21.8	4
13	1.0	15.5	9.6
14	0.0	21.9	7.8
15	0.6	21.7	7.4
16	0.0	22.1	7.4
17	0.0	24.8	8.7
18	0.0	28.4	11.7
19	0.0	28.1	11.7
20	0.0	26.7	10.6
21	0.0	22.6	12.8
22	0.0	27.2	11.4
23	0.0	22.1	13.7

24	0.1	22.4	15.9
25	1.0	20.1	14.8
26	0.2	23.6	15.1
27	0.0	24.9	15.1
28	0.3	29.4	15.4
29	0.1	29.7	16.3
30	0.0	26.5	16.4
31	0.2	28	15.5
32	0.0	28.4	12.7
33	0.0	28.4	16.9
34	0.0	26.1	16.8
35	0.2	27.6	13
36	0.0	30.7	13.9
37	0.3	30.9	17.8
38	0.1	28.8	15.5
39	0.0	29	11.8
40	1.8	28.4	13.4
41	0.3	22.8	13.4
42	0.6	27.7	11.6
43	0.5	29.1	15.9
44	0.7	22.6	11.7
45	0.0	23.9	10.2
46	0.0	22.2	9.4
47	0.0	27	9.5
48	0.0	32.7	14.2
49	0.0	31.6	17.7
50	0.1	24.4	16.7
51	0.0	26.2	12.2
52	0.0	27.1	12.5
53	0.5	22.6	13
54	0.0	22.8	11
55	0.0	25.7	7.7
56	0.0	30.2	11.6
57	0.0	29.7	13.5
58	0.0	29.1	17.2
59	2.1	29.4	16.8
60	1.0	28.3	15.1
61	0.0	28.3	16.1
62	0.0	29.6	15.2
63	0.0	32.2	15.2
64	0.3	34.5	15.5
65	0.2	25.2	15
66	0.0	22.6	10.2
67	0.0	29.2	11.1
68	0.0	31.6	13.1
69	0.0	31.6	14.3
70	0.0	32.1	15.5
71	0.5	31.5	17.3
72	0.0	25.9	13.9
73	0.0	23.2	11.6
74	0.8	22.4	11
75	0.0	26.8	10
76	0.0	30.5	12.2
77	0.0	30.1	12.9
78	0.0	31.8	16.4
79	0.0	31.4	18.3
80	0.0	32.9	14.3
81	0.0	31.9	16.4
82	0.0	31.3	17.4
83	0.0	23.7	12.3
84	2.3	26.8	13.5
85	0.0	15.6	9.8
86	0.0	16.6	4.9
87	0.0	18.5	2.5
88	0.0	19.7	5.4
89	0.0	21.8	6.3

90	0.0	24	10.9
91	0.7	26.7	12.3
92	0.1	22.8	12.3
93	0.0	15.7	7.4
94	0.0	23.1	5.2
95	1.7	18.3	10.7
96	0.9	23.1	9.3
97	0.8	21.9	8.9
98	0.0	19.4	5.8
99	0.0	21.3	5.8
100	0.2	19.6	8.2
101	0.0	12.6	3.4
102	0.3	8.9	4.4
103	0.1	7.8	2.4
104	0.0	7.6	-0.3
105	0.0	9.2	0.9
106	0.0	10.1	1.1
107	0.0	15.6	-1.4
108	0.0	14.8	4.6
109	0.0	13.4	-1.2
110	0.0	20.4	1.4
111	0.0	22.6	4.5
112	0.0	16.8	4.8
113	0.0	14.9	4.4
114	0.0	22.9	6
115	0.1	23	9.7
116	0.3	21.4	9.1
117	0.0	27.8	8
118	0.0	29.2	11.2
119	0.1	26	12.1
120	0.0	19.3	7.8
121	0.1	14.5	8.1
122	2.0	8.4	3.2
123	0.1	13.8	3.3
124	0.0	14.4	0.9
125	0.0	18.1	4.8
126	0.2	15.4	6.8
127	0.3	7.9	0.8
128	0.1	4.7	-0.6
129	0.0	6.4	-4
130	0.0	7.3	0.8
131	0.0	16.8	4.4
132	0.0	8.1	4.5
133	0.0	11.2	1.2
134	0.0	9.3	-2.1
135	0.0	15	0
136	0.0	19.2	2.6
137	0.0	18.2	7.7
138	0.0	18.8	3.2
139	0.0	11.5	1.6
140	0.0	9.3	4.2
141	0.0	9.1	0.3
142	0.0	3.8	-0.1
143	0.0	12.8	0
144	0.0	11.4	5.8
145	0.0	19.1	3.5
146	0.0	13.5	3.3
147	0.0	12.1	4.2